

THE UNIVERSITY OF MANITOBA

EXCITER STRESSES IN CAPACITIVELY LOADED
SYNCHRONOUS GENERATORS

BY

ANIRUDDHA M. GOLE

A THESIS

SUBMITTED TO THE FACULTY OF GRADUATE STUDIES
IN PARTIAL FULFILLMENT OF THE REQUIREMENTS
FOR THE DEGREE OF DOCTOR OF PHILOSOPHY

DEPARTMENT OF ELECTRICAL ENGINEERING

WINNIPEG, MANITOBA, CANADA

AUGUST 1982

EXCITER STRESSES IN CAPACITIVELY LOADED
SYNCHRONOUS GENERATORS

BY

ANIRUDDHA M. GOLE

A thesis submitted to the Faculty of Graduate Studies of
the University of Manitoba in partial fulfillment of the requirements
of the degree of

DOCTOR OF PHILOSOPHY

© 1982

Permission has been granted to the LIBRARY OF THE UNIVER-
SITY OF MANITOBA to lend or sell copies of this thesis, to
the NATIONAL LIBRARY OF CANADA to microfilm this
thesis and to lend or sell copies of the film, and UNIVERSITY
MICROFILMS to publish an abstract of this thesis.

The author reserves other publication rights, and neither the
thesis nor extensive extracts from it may be printed or other-
wise reproduced without the author's written permission.

ABSTRACT

This thesis examines overvoltage stresses in the field circuits of synchronous machines connected to predominantly capacitive loads. It is shown that violent field current oscillations can be produced by resonances between the machine inductances and the terminal capacitance. As most static exciters do not allow reverse current, any attempt of the field current to reverse due to these oscillations causes severe field overvoltages.

In order to study this problem, a detailed synchronous machine model to be used with an Electromagnetic Transients Program is developed, with a novel interfacing technique which renders the simulation very stable and accurate. This simulation program is used to model complex situations in which the above mentioned overvoltages would occur, and also to explain a hitherto unexplained situation of exciter damage due to these overvoltages in Manitoba Hydro's Northern Collector System.

It is shown that the most severe overvoltage stresses occur to the exciter of the last machine to trip off a large capacitive load. It is also shown that if such stresses damage the exciter thyristors, these fail in the short circuited mode and thereby limit the rate of rise of terminal voltage during conditions of self excitation. Apart from these simulations, the nature (magnitude and frequencies) of the field transients is explained mathematically.

Methods to protect against such overvoltages and the speed requirements on field voltage surge suppressors have also been outlined. These methods are much the same as have been suggested by

others for exciter protection against field overvoltages due to other causes.

The field overvoltage phenomenon is also demonstrated on a laboratory setup, and the agreement with the predictions from simulations of such a case is excellent.

ACKNOWLEDGEMENTS

The author is grateful to the Manitoba Hydro Research Committee for funding this project. The author also wishes to thank Dr. J. Chand and Mr. R.W. Haywood of the staff of the System Performance Section (System Operating Department) where the bulk of this work was carried out.

Professor R.W. Menzies, the author's thesis supervisor, provided many useful suggestions, and did a considerable amount of work in the laboratory, and always lent support, for which the author is in his debt.

And, of course, special thanks to Dennis Woodford of Transmission Planning (System Planning), Manitoba Hydro, with whom the author collaborated on the modelling aspects, which proved to be extremely exciting and stimulating.

TABLE OF CONTENTS

	<u>Page</u>
ABSTRACT -----	i
ACKNOWLEDGEMENTS -----	iii
TABLE OF CONTENTS -----	iv
LIST OF FIGURES -----	vi
LIST OF SYMBOLS -----	xi
CHAPTER	
1. INTRODUCTION -----	1
1.1 The Problem -----	1
1.2 The Background -----	2
1.3 The Cause -----	4
1.4 The Scope of the Thesis -----	6
2. THE SYNCHRONOUS MACHINE ON CAPACITOR LOADS -----	10
2.1 Introduction -----	10
2.2 Field Current on Sudden Capacitive Loading	
Due to Load Rejection -----	11
2.3 Field Current Response Due to Machines	
Tripping on Capacitive Loading — Non-	
Self Excited Case -----	17
2.4 Field Current Response Due to Machines	
Tripping on Capacitive Load — Self	
Excited Case -----	20
2.5 Effect of Exciter Thyristor Failure -----	23

	<u>Page</u>
2.6 Analysis of Field Transients -----	25
2.7 The Field Time Constants -----	34
2.8 Tests on Laboratory Machine -----	39
2.9 Overall Conclusions for Chapter 2 -----	48
3. MODELLING -----	50
3.1 General -----	50
3.2 MH-EMTDC: The Programming Environment -----	50
3.3 Modelling the Machine -----	55
3.3.1 Machine Equivalent Circuit and Mechanical Dynamics -----	55
3.3.2 Interfacing with EMTDC -----	62
3.3.3 Starting Up -----	68
3.4 Modelling of Exciters and Governors -----	71
3.5 Modelling of the DC Bridge -----	73
3.6 Model Capabilities -----	77
3.7 Chapter Summary -----	83
4. REALISTIC CAPACITIVE LOADS -----	84
4.1 Introduction -----	84
4.2 Tripping of Machines with Different Kinds of VAR Loadings -----	86
4.2.1 Machines on a Long Line -----	86
4.2.2 VAR Loading with Machine Type VAR Sources -----	89
4.2.3 Effect of VARs Due to AC Filters -----	93

	<u>Page</u>
4.3 Machines Connected to DC Converters -----	97
4.3.1 Comparison of Actual DC Load Rejection	
With R-L Load Type DC Load Approximation --	97
4.3.2 Inclusion of Delta-Star Transformers -----	100
4.3.3 Inclusion of the Proper Opening of the	
Machine Breaker -----	101
4.4 Summary -----	103
5. SIMULATION OF AN ACTUAL DISTURBANCE -----	106
5.1 Introduction -----	106
5.2 Modelling Details -----	109
5.3 Simulation Results -----	112
5.4 Chapter Summary -----	120
6. PROTECTION METHODS -----	121
6.1 Introduction -----	121
6.2 Desired Speed of Response of Surge Arrestor -----	124
6.3 Effect of Different Reverse Resistances -----	128
6.4 Other Protection Methods -----	130
6.5 Chapter Summary -----	134
7. CONCLUSIONS AND RECOMMENDATIONS -----	136
7.1 Conclusions -----	136
7.2 Recommendations -----	141
APPENDIX I: The Per-Unit System for Synchronous Machines ---	142
APPENDIX II: Data Used in the Various Simulations -----	147
LIST OF REFERENCES -----	151

LIST OF FIGURES

	<u>Page</u>
CHAPTER 1	
1.2.1 Single Line Diagram of Collector System at 9:21:46.930 on September 30, 1978 -----	2
1.3.7 Schematic of Solid State Exciter -----	4
CHAPTER 2	
2.1.1 The Machine Equivalent Circuits -----	11
2.2.1 Rejection of R-L Load -----	12
2.2.2 Waveforms for Load Rejection of R-L Load -----	13
2.2.3 Overvoltages Due to ℓ - ℓ Short Circuits -----	14
2.2.4 Post Rejection System Model -----	15
2.3.1 Tripping of Machines Isolated onto a Capacitor ---	17
2.3.2 Waveforms for Tripping of Machines Isolated Onto a Capacitor (Non-self excited case) -----	19
2.4.1 Waveforms for Tripping of Machines Isolated Onto a Capacitor (Self excited case) -----	21
2.4.2 Waveforms for Cascaded Tripping of Machines -----	22
2.5.1 Waveforms with Thyristor Failure Modelled -----	24
2.6.1 Equivalent Circuit for Sudden Capacitive Loading -----	25
2.6.2 One Out of Two Machines Trips -----	27
2.6.3 The Prefault Phasor Diagram -----	30
2.6.4 Equivalent Induction Machine Circuit at Frequency f -----	31
2.6.5 Components of the Field Current -----	33
2.7.1 Simulated and Theoretical Variations in Field Time Constant with X_c -----	38
2.8.1 Three Phase Symmetrical Short Circuit on Laboratory Machine -----	40
2.8.2 Time Constant on Capacitive Loading -----	41
2.8.3 Test Setup for Machine Tripping -----	42

	<u>Page</u>
2.8.4 Observed and Simulated Waveforms for One Out of Two Machines Tripping -----	44
2.8.5 One Out of Two Machines Tripping: Self Excited Case, with Reverse Current Capability -----	45
2.8.6 Waveforms for Self Excited Case Without Reverse Current Capability -----	46
2.8.7 Effect of Not Modelling Machine Saturation -----	47
CHAPTER 3	
3.2.1 Equivalent Resistive Circuit Model for Inductor --	53
3.3.1 Equivalent Circuits -----	56
3.3.2 Kettle Machine Saturation Characteristics -----	60
3.3.3 Modelling Scheme for AC Machine -----	65
3.3.4 Terminal Interface -----	66
3.3.5 Obtaining the Machine Angle -----	71
3.4.1 Exciter Model -----	72
3.4.2 Governor Model -----	72
3.5.1 Interfacing the Valve Group Model -----	74
3.5.2 Equivalencing and Reduction of Convertor Models --	74
3.5.3 Six Pulse Valve Group Subnetwork Equivalent Circuit -----	75
3.5.4 Basic Pole Controller -----	78
3.5.5 Basic Valve Group Controller for Rectifiers and Inverters -----	78
3.6.1 Test DC Link Model -----	79
3.6.2 Simulated Recovery of DC Current After AC Fault For Alternative Representations of X_d , X_d' , And Full Machine Models -----	81
3.6.3 Comparisons of Simulator Performance with Real System for Inverter AC Fault -----	82
CHAPTER 4	
4.2.1 Machines Tripping on Long Line -----	87

	<u>Page</u>
4.2.2	Waveforms for Machines Tripping on Long Line ----- 88
4.2.3	Machines Tripping with VARs from Other Machines -- 89
4.2.4	Waveforms for Machines Tripping with VARs from Other Machines ----- 91
4.2.5	Machines Isolated Onto AC Filters ----- 94
4.2.6	Typical Impedance Plots of Machines and Filters With 5 th and 7 th AC Filters ----- 95
4.2.7	Tripping of Three Out of Two Machines with 5 th , 7 th , 11 th and 13 th Filters of 0.86 pu MVAR -- 96
4.3.1	Comparison of Waveforms for DC R-L Load Approximation, and Full Bridge Modelling ----- 99
4.3.2	To Study the Effect of Δ -Y Transformer Windings 100
4.3.3	Waveforms With and Without Δ -Y Transformer Representation ----- 102
4.3.4	Waveforms With Breaker Opening Phase-by-Phase --- 104
 CHAPTER 5	
5.1.1	Manitoba Hydro Collector System on September 30, 1978 at 09:22 hrs. ----- 107
5.2.1	Collector System Single Line Diagram as used in Study ----- 110
5.2.2	Comparisons of Load Flow and EMTDC Steady State Solutions ----- 112
5.3.1	Waveforms for Events 1-4 ----- 113
5.3.2	Waveforms for Events 4-6 ----- 117
5.3.3	Expanded Plot of Highest Overvoltage ----- 118
 CHAPTER 6	
6.1.1	One Out of Two Kettle Machines Tripping On 132 MVAR Filter Load ----- 122
6.2.1	Surge Arrestor Model ----- 125
6.2.2	Effect of Delay in Arrestor Breakdown ----- 127
6.3.1	Dependance of Field Overvoltage on Reverse Resistance ----- 129

	<u>Page</u>
6.4.1 Possible Automatic Switching Scheme -----	130
6.4.2 Waveforms for R2 = RF Switched in with U _{fo} = 15 × o.c. field volts -----	132
6.4.3 RREV = 1000 × R _f , Arrestor Breakdown (with delay) at 15 × o.c. field volts -----	133

LIST OF SYMBOLS

Tabulated below are some of the more frequently occurring symbols used in the text. Other symbols, which occur say only once, have been explained where used.

D	per unit damping constant for synchronous machine
E_f	voltage behind synchronous impedance
E'', E_0	voltage behind subtransient reactance
$f_0(\omega_0)$	power system normal frequency (angular frequency) (usually 60 Hz, 377 rad/s)
$f_r(\omega_r)$	resonant frequency (angular resonant frequency) of machine-capacitor oscillations
f^+	frequency induced in field due to positive sequence
f^-	frequency induced in field due to negative sequence
I_{dc}	dc current
i_d, i_{kd}, i_f	d-axis, q-axis ammortessieur and field currents
i_q, i_{kq}	q-axis and q-axis ammortessieur currents
i_m	magnetizing current
I^+, I^-	positive and negative sequence stator currents
$L_a, (X_a)$	armature leakage inductance (reactance)
$L_{md}, (X_{md})$	d-axis magnetizing inductance (reactance)
$L_{kd}, (X_{kd})$	Amortesseur (d-axis) inductance (reactance)
$L_f, (X_f)$	Field inductance (reactance)
$L_{mq}, (X_{mq})$	q-axis magnetizing inductance (reactance)
$L_{kq}, (X_{kq})$	q-axis amortesseur inductance (reactance)
L_{kf}	inductance representing mutual flux linking only the amortesseur and field windings

P, Q	real and reactive powers
p	Heaviside operator (d/dt)
r_a, r_{kd}, r_f	armature, d-amortisseur and field winding resistances
r_{kq}	q-amortisseur resistance
R_{rev}	field reverse resistance
s	Laplace Transform Variable (functionally, the same as p)
T_e, T_m	electrical and mechanical machine torques
u_d, u_q, u_f	d-axis, q-axis and field applied voltages
V_t, E_t	terminal voltage
V_{rev}	reverse voltage in field (i.e., U_f when $I_f \leq 0$)
V_{ref}	reference voltage on exciter
X_c	capacitive reactance
X_{com}	dc commutating reactance
X_d'', X_q''	d; q-axes subtransient reactances
α	converter bridge firing angle
β	$180^\circ - \alpha$
$\gamma, (\gamma_{min})$	extinction angle (minimum extinction angle)
δ	machine angle
$\theta(t)$	rotor position in time
ψ_d, ψ_q	d- and q-axes fluxes
ω	angular frequency ($d\theta/dt$)
ω_{ref}	governor reference frequency (usually ω_0)

CHAPTER 1

INTRODUCTION

1.1 The Problem

A synchronous machine with a predominantly capacitive (leading power factor) load behaves quite differently from the more usual case of a machine loaded with a lagging power factor load. Some of the phenomena that occur with excessive terminal capacitance are self-excitation (in which the machine flux rapidly builds up and results in excessive terminal voltage), and subsynchronous oscillations. These phenomena have been studied before in some detail [1, 2, 3, 4, 5]. However, the effect of the terminal capacitance on the field circuit of the synchronous machine is relatively unknown. This thesis examines this problem, and shows that violent oscillations can result in the field current of the machine when it is suddenly made to pick up capacitive load. If these oscillations are not allowed to continue, as for example when the thyristors of the excitation system prevent reverse current, very high voltages can result across the field terminals, which can cause damage to the thyristors of the excitation system. The primary objective of this thesis was therefore to determine the cause of and to construct a mathematical model for the study of these field transients, and to suggest ways of preventing such damage that they might cause.

As adequate tools for a detailed study were unavailable at the beginning of this study, a considerable effort was spent towards the modelling of the phenomena on the digital computer, and this too forms a topic covered in some detail in this thesis.

1.2 The Background

The northern end of the Manitoba Hydro HVDC system consists of two generating stations (Kettle and Long Spruce) feeding two HVDC transmission circuits which transmit the power to the south. The rectifier buses at Radisson and Henday converter stations (Figure 1.2.1) convert the generated ac power to dc for transmission. A certain

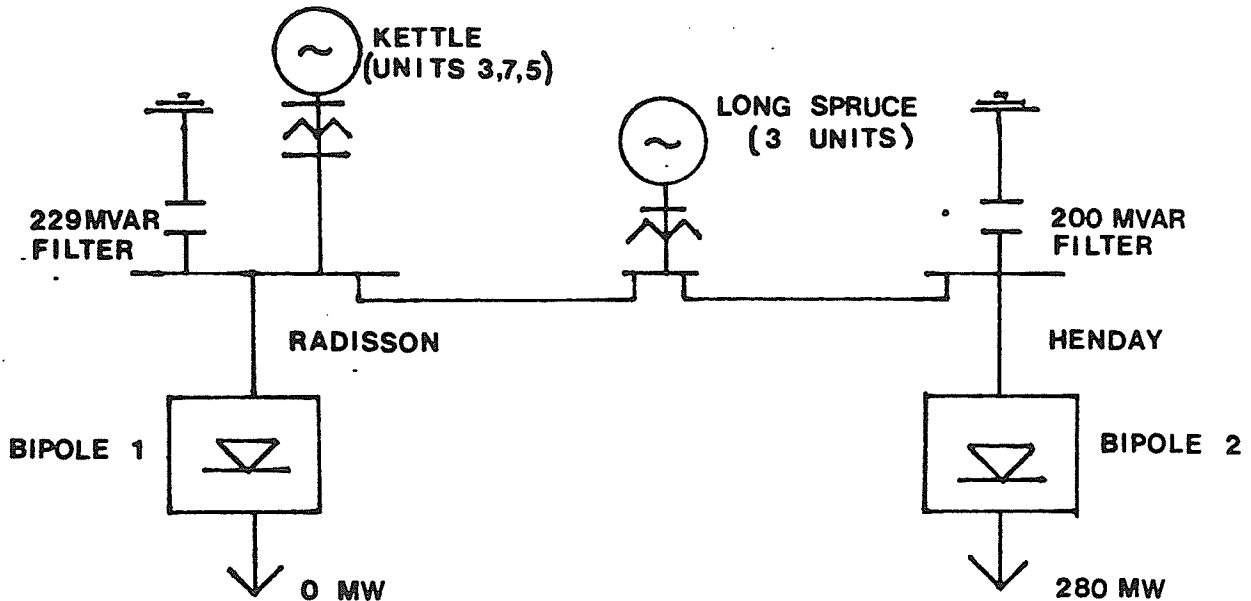


Figure 1.2.1: Single line diagram of collector system at 9:21:46.930 on September 30, 1978.

number of filters are thus necessary at the converter stations to filter out harmonic currents generated by the converters. Typically, on the ac side of the system, filters for the 5th, 7th, 11th and 13th harmonics, and high pass filters for higher harmonics, are provided. At fundamental frequency though (about 60 Hz - since the system is completely asynchronous with the receiving ac system, and hence fundamental frequency may vary transiently from 54 to 80 Hz), the filters appear capacitive. When the bipoles (rectifiers) block, increased

capacitance is suddenly felt by the machines because with the bipole operating, the filter capacitance is somewhat cancelled by the lagging power factor of the rectifier, which is no longer the case after the rectifiers block.

In the past, with the system operating with blocked bipoles (i.e., with high VAR inflow into the machines) as discussed above, and with a small number of machines operating at Kettle and Long Spruce, the tripping of some Kettle machines seems to have caused extensive damage to the exciters of those remaining on line. Typically, the last unit to trip suffered the most damage. The worst incident is one which occurred on September 30, 1978 [6, 7].

Due to a prior disturbance, at 9:22 on September 30, 1978, the Northern Collector System of Manitoba Hydro found itself in the configuration of Figure 1.2.1, with the three machines at the Kettle Generating Station (Units 3, 7 and 5) absorbing a large amount of reactive power (VARs). At this instant, the dc rectifier (Bipole 2) blocked, and the machines felt a sudden increase in VAR loading, and this disturbance caused the machines at Kettle to trip in the sequence 7, 3, 5. The thyristors in the exciter of the last unit to trip (Unit 5) were damaged and had failed in the short-circuited mode, while the exciters of Units 7 and 3 showed marks of flashover due to high voltage, but had no thyristor failures [7, 8]. It is believed that these failures were due to transients in the field current due to the predominantly capacitive load on the machine terminals.

1.3 The Cause

(i) The reason given previously was that pole slipping occurred and the consequent rotor induced voltage could not properly be limited by the surge arrester. (Figure 1.3.1 shows a schematic of the excitation arrangement, where each thyristor actually stands for seven

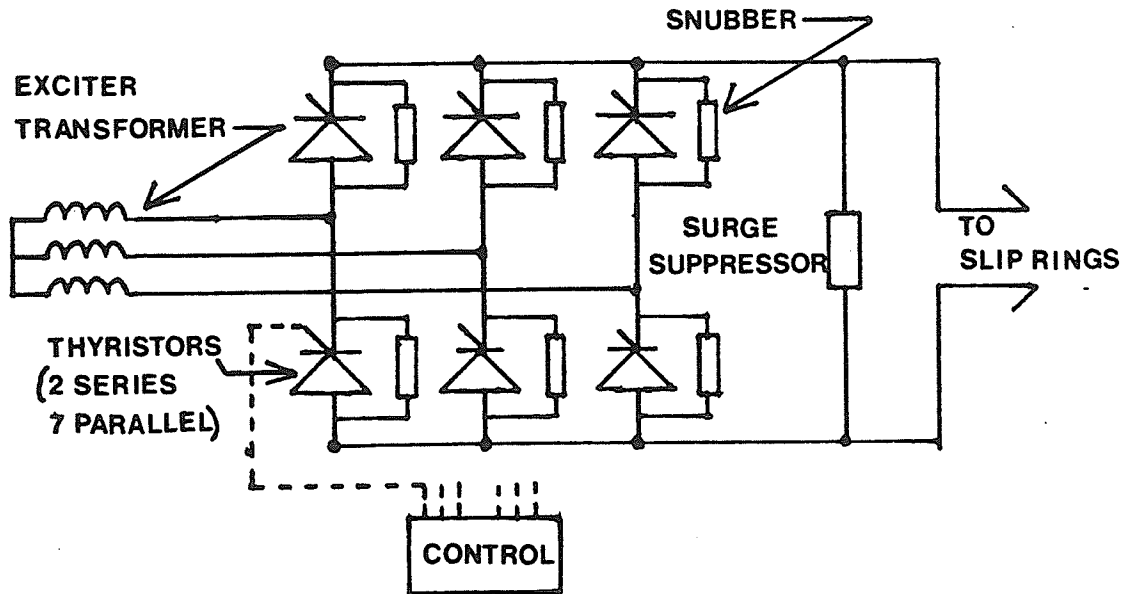


Figure 1.3.1: Schematic of the solid state exciter.

strings of two series thyristors each.) Previous literature [9, 10, 11] shows that for the pole slipping case, the maximum overvoltages induced are of the order of 20 - 30 times the nominal field voltage. As under maximum excitation conditions, the exciter has an output of about ± 5 times nominal, the pole slipping overvoltage is only about 5 times higher. In fact, much higher overvoltages occur in the field circuit for line-to-line short circuits on the generator, and the surge arrestors are presumably able to withstand some of these [9, 12].

In fact, sustained pole slipping has been observed [11], without any damage reported.

Hence, pole slipping does not appear to be the primary cause of the exciter damage, though, as machines started to trip, the unequally loaded Long Spruce and Kettle systems might have stepped out of synchronism with each other later on.

(ii) Another reason advanced arose from the fact that the exciter feeder transformer overcurrent relay operated. This seems to imply that stator side overvoltage forced extra current through the exciter, especially because of possible spurious (due to dV/dt) turn on of a thyristor. While this could have happened, it could not be the cause for thyristor damage because: (1) the current was not high enough to damage the exciter transformer; and (2) the terminal voltage on the exciter would have to rise abnormally high to cause reverse breakdown of the thyristors.

(iii) In going through the literature [9, 10, 12, 13], one comes across exciter stresses caused by negative going transients induced in the rotor circuits, when the exciters feeding the rotor do not have negative current capability (exactly as it is at Kettle). Such transients can occur, for example, for a line-to-line short circuit. Under these conditions, the stator field which was previously rotating at an electrical frequency of 60 Hz, now has an additional stationary (or dc) component due to the short circuit (terminal) conditions of the machine. As the rotor, which is still rotating nominally at 60 Hz, sweeps past the stationary component of the magnetic field, 60 Hz transients are induced in it, and may cause the current to cross zero, and attempt to reverse. Because the thyristors prohibit the current from

going negative, a very high overvoltage results, due to the sudden interruption of energy flow in the rotor circuit.

The situation with a capacitive load (i.e., filters), is similar. With many machines feeding a capacitive load, the tripping of a few of them effectively puts increased capacitance on the others. The capacitor forms an oscillatory circuit with the inductive elements of the machine, and the resulting ringing of frequency f_r sets up rotating fields (either positive sequence or negative sequence) in the machine, which induce currents of frequencies $f_r \pm 60$ Hz in the rotor. If the resultant current now goes negative, overvoltages result.

Normally, the surge arrester across the winding should limit the overvoltage, but if it is slow-acting, or has insufficient energy absorption capability, thyristor damage may still result. This appears to be the case with the Kettle surge arrestors.

This third reason for the damage seems most probable (though pole slipping could have occurred at a later stage, as machines at Long Spruce and Kettle sped up unequally). A computer program was developed which simulated the machine. The machine model was incorporated into a transients simulation program called MH-EMTDC, developed by D. Woodford [14] at Manitoba Hydro. Results of the simulation do indeed show these field overvoltages.

1.4 The Scope of the Thesis:

The study was organized into the following sections:

- (1) A theoretical explanation of the field current transients based on a pure capacitance connected to an

ideal synchronous machine. The behaviour of the field current time constant was also investigated. The results are substantiated by comparison with an actual laboratory machine [Chapter 2].

- (2) Modelling details of the machine model, and its host programming environment are discussed. Modelling formed quite an important part of the study, as time domain simulation of machines, filters and dc converters was carried out [Chapter 3]. A novel way of interconnecting the machine model to EMTDC was developed, which resulted in a very stable simulation. It also got rid of drawbacks such as the requirement to separate two different machines by distributed parameter transmission lines, as in the case of other models [15].
- (3) Analysis of an actual case of such exciter damage, i.e., the problem on Manitoba Hydro's Northern Collector System as described in Section 1.2 [Chapter 4] is included.
- (4) Methods for protection against such overvoltages [Chapter 5] are suggested.

The major conclusions of this thesis can be stated as follows:

- (1) Overvoltages occur in the field circuits of machines that are made to suddenly pick up capacitive load, from either inductive load rejection or tripping of some of many machines connected to capacitive loads.

These overvoltages are due to field current transients attempting to go negative, the transients being due to L-C type oscillations between the machine reactances and the terminal capacitance. Needless to say, no such overvoltages exist in exciters with negative field current capability. The exciter overvoltage is most severe in the case of a machine in or near self-excitation.

- (2) Excitation control is ineffective in controlling these overvoltages because the machine's field time constant is extremely large when the machine is on capacitive load; and so the exciters cannot change field current very rapidly.
- (3) Different kinds of capacitor loads give different kinds of overvoltages (in magnitude and frequency). No overvoltage is induced when, say, one of two machines absorbing reactive power generated by another generating plant trips. Likewise, proper modelling of the dc converter is required in order to obtain the proper load rejection overvoltage in the field of a machine connected to a dc converter station.
- (4) Protection schemes using surge arrestors with fast breakdown or a reduced reverse field resistance, may help in curtailing these overvoltages.

- (5) The machine model, with its unique type of interface with EMTDC, results in a very stable simulation, without restrictions such as are present in other models that operate in programs such as the Bonneville Power Administration's EMTP program.

CHAPTER 2

The Synchronous Machine on Capacitor Loads

2.1 Introduction

Leading Power factor loads are amongst the worst types of loads possible on a synchronous machine. Under fault conditions, the field circuit of a machine with such a load may be unduly stressed. If the load is too capacitive, a form of instability known as self excitation may result, in which the terminal voltage and current in the machine keep growing, to be limited only by machine saturation. Added to all this is the fact that the field circuit time constant increases with more capacitive load and hence the response of the field becomes more sluggish which could prove detrimental if some rapid control is desired. It should be noted that excitation control of the terminal voltage may still be rapid as the gain of the function $\Delta V_t / \Delta U_f$ also changes. In this chapter we shall discuss certain types of transients seen by the field circuit on sudden load rejection, and on tripping of machines connected to a purely capacitive load. Other phenomena such as short circuits on capacitive loads [9, 12, 17] and self excitation [1, 2, 3, 5, 16] have been investigated in detail previously.

As algebraic manipulation is quite difficult in many cases, digital computer solutions have been used to augment the algebraic analysis. The machine is represented by the two axis model [20, 21] with three windings on the direct axis and two windings on the quadrature axis, as shown in Fig. 2.1.1. Modelling details are discussed in the next chapter. In this chapter the effects of the excitation and governor systems have been neglected as only the very basic effects are to be studied.

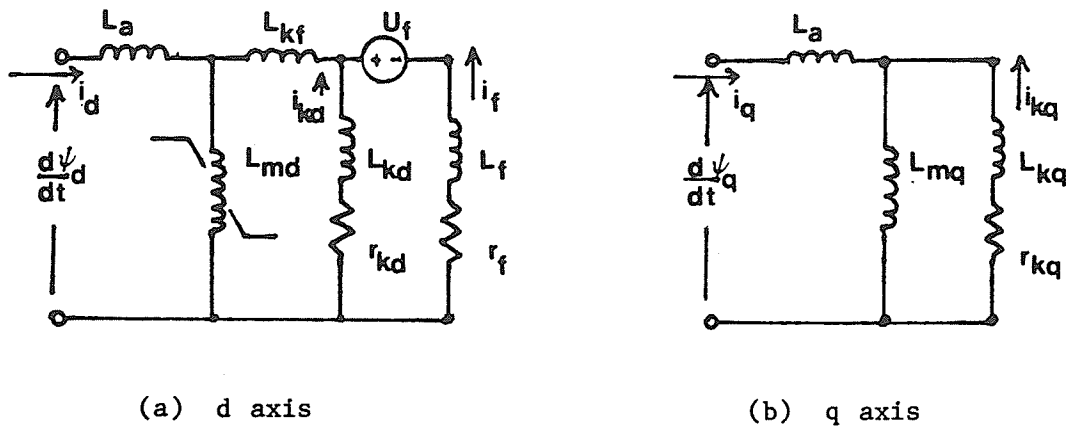


Figure 2.1.1: The machine equivalent circuits

The following sections examine the effects of capacitive loading using the parameters of Manitoba Hydro's Kettle Generating Station machine (Appendix II, Table 2.1) without considering the effects of saturation. The chapter concludes with a demonstration of some of these effects on a 15 kVA laboratory machine with saturation modelled in some cases. The data for both machines is given in Tables A 2.1 and A 2.2 in Appendix II.

2.2 Field Current on Sudden Capacitive Loading Due to Load Rejection

Figure 2.2.1 shows the situation under study. The R-L load might represent, for example, the load due to an HVDC converter, and the capacitor might represent an ac filter connected to the converter. Tripping the bipole causes an oscillation between the capacitor and machine, similar to subsynchronous oscillations [16].

The R and L values have been selected to represent 1 pu loading on the machine so that the simulation represents a full load rejection. The field current waveform is shown in Figure 2.2.2 a.

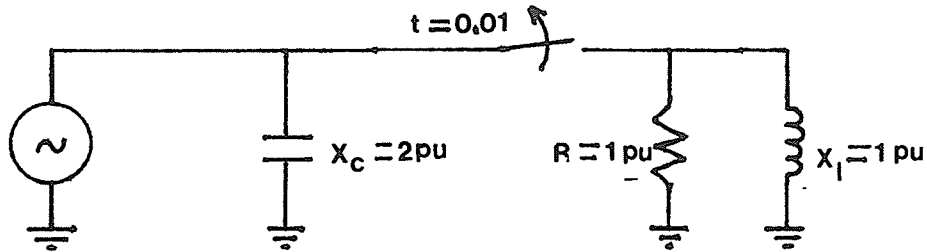


Figure 2.2.1: Single Line Diagram for Load Rejection Simulation.

The machine data corresponds to that of one of Manitoba Hydro's 120 MVA Kettle Station generators. One notices that the waveform of field current has a number of spikes of various frequencies present in it. If the field current were to come sufficiently low in value, so that some of these spikes reached the zero axis, this would mean a transient reversal of current in the field circuit. If the exciter does not allow a negative current, as is indeed the case with most static exciters, a large overvoltage appears across the field slip rings. This is similar to the case of an asymmetric short circuit on a capacitively loaded machine [9, 10, 12] in which the field current goes transiently negative (Figure 2.2.3) causing overvoltage spikes of substantial magnitude (up to ~120 times open circuit field voltage). The mechanism that causes a field current reversal, though, is different in the two cases.

From the waveform of Figure 2.2.2 a, one notices that the spikes do not extend very much below the dc component of the field cur-

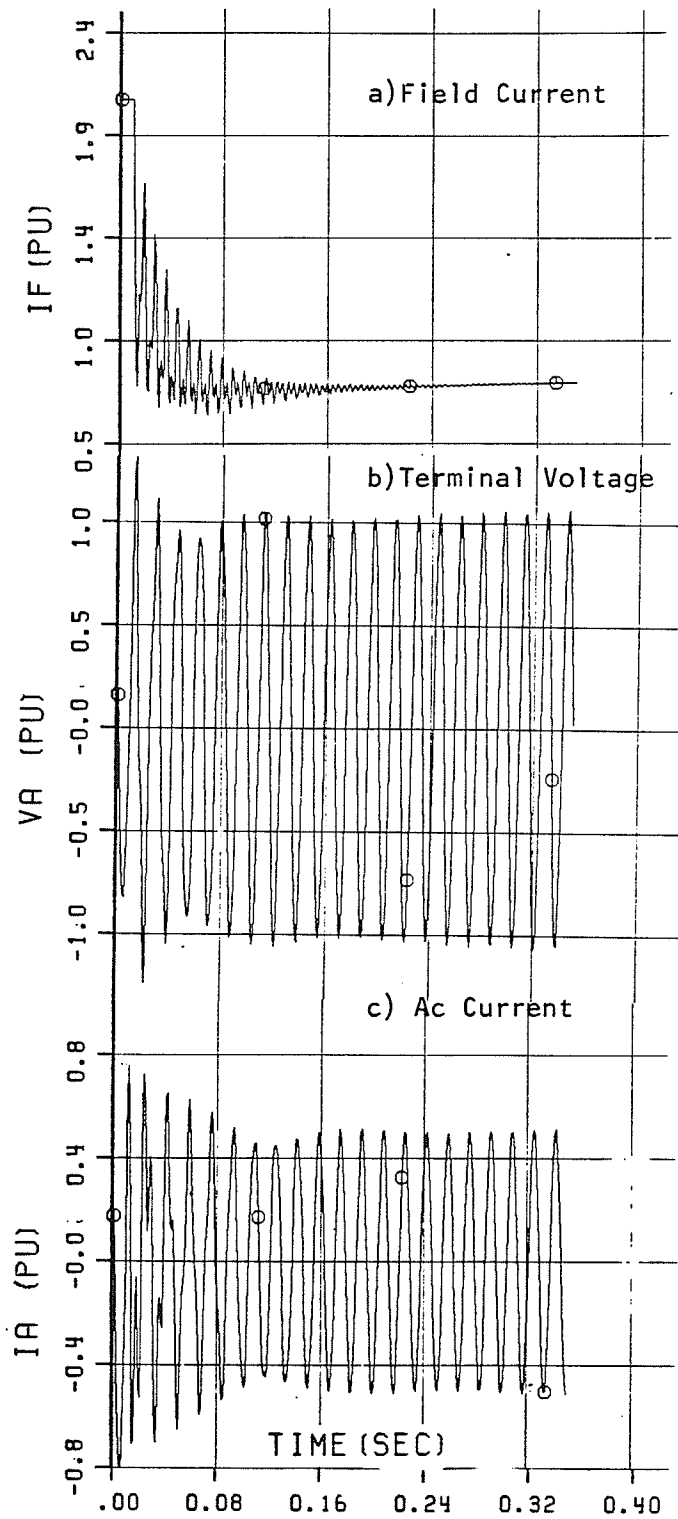
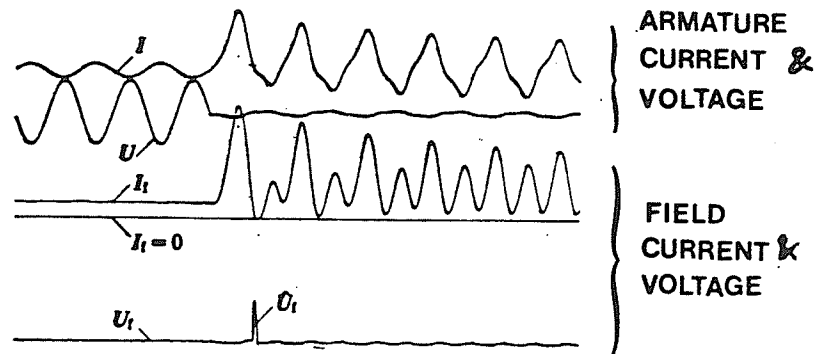


Figure 2.2.2: Waveforms for Load Rejection of R-L Load
 $(X_1=1.0\text{pu}; R=1.0\text{pu}; X_c=2.0\text{pu})$

rent. Thus, for the spikes to cross zero, the field current dc value itself must come very close to zero, i.e., the machine must get very near self excitation.



: Line-to-line short circuit, generator mode, p.u. values:
 $i = 1.16$ $p = 0.97$ $q = -0.63$
 $i_f = 1.14$
 $\dot{u}_f = 139$

Figure 2.2.3: Overvoltages due to 1 - 1 short circuits by Canay [12].

Usual magnitudes of real and reactive powers consumed by an HVDC converter and the magnitude of the filter capacitance are such, that a load rejection of the above sort seldom leads close to self excitation, and hence, as shown in Figure 2.2.2 a the field current never reaches low values. Hence, there is little probability of field overvoltage in the above case. However, the field current can go lower than that shown in Figure 2.2.2 a if there are other factors in the

power system such as machines at another plant, which begin supplying VARs (to the other plant) due to a change in the load flow on account of the load rejection. This factor will be considered in a later chapter. Also, if other machines at the generating station trip, then the machines remaining behind are forced to have a lower field current, which can make the superposed spikes touch the zero axis.

On closer inspection of Figure 2.2.2 a, one notices that it has three components. There is a dc component, and two ac components: the two ac frequencies differ by 120 Hz. (In Figure 2.2.2 a the frequencies are approximately 113 Hz and 233 Hz, respectively). The presence of these components of current can be explained as follows:

- (i) The dc component is due to a sudden increase in magnetizing armature current on account of the increased capacitive loading. The field current decreases in order to maintain constant flux linkage.
- (ii) The presence of the ac components can be explained with the help of Figure 2.2.4 which shows the subtransient model of the machine. (For the sake of this argument, the subtransient reactances x_d'' and x_q'' have been assumed equal.)

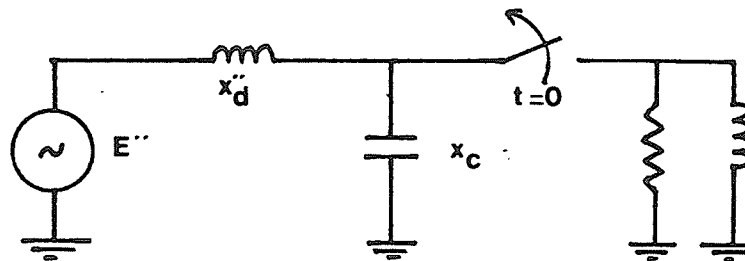


Figure 2.2.4: Post-Rejection system model

The opening of switch S excites the natural frequency of the circuit to its left which is

$$f_r = f_o \sqrt{\frac{x_c}{x_d''}} \quad \dots \quad 2.2.1$$

where f_o is the system frequency).

An armature current of this frequency produces a magnetic field in the machine air gap which may be decomposed into its sequence components, i.e., two rotating magnetic fields in the air gap rotating in opposite directions with natural frequency f_r . With respect to the rotor, which is rotating synchronously, these fields appear to have frequencies $f_r + f_o$ and $f_r - f_o$ for the negative and positive sequence rotating fields respectively. Thus rotor currents are induced at each of these frequencies. Note that the difference of the two frequencies is $2f_o$, which in this case is 120 Hz as observed. Also, in the example, $x_c = 2$ pu, $x_d'' = 0.25$ pu, so that

$$f_r = f_o \sqrt{\frac{x_c}{x_d''}} = 170 \text{ Hz} \quad \text{--- a}$$

$$f^- = f_r + f_o = 230 \text{ Hz} \quad \text{--- b} \quad \dots \quad 2.2.2$$

$$f^+ = f_r - f_o = 110 \text{ Hz} \quad \text{--- c}$$

which is in close agreement with the observations of Figure 2.2.2 a. The additional frequency f_r in the armature current is also visible

in Figure 2.2.2 c.

2.3 Field Current Response Due to Machines Tripping on Capacitive Load -- Non Self Excited Case

Figure 2.3.1 shows three machines left isolated onto a large capacitive load, after their real power load has been rejected. This situation corresponds to the case of the blocking of an HVDC converter and the subsequent isolation of the machines at the generating station onto the converter's ac side filters. Now if for some reason some relay operation causes the machines to trip and they do not do so simultaneously, the machines to trip last see a sudden increase in VARs transiently, after the earlier machines are tripped.

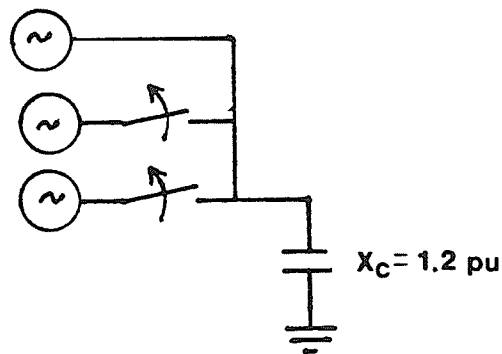


Figure 2.3.1: Machines Tripping on a Purely Capacitive Load.

Figure 2.3.2 shows the field current, field voltage and terminal voltage waveforms for the remaining machine of Figure 2.3.1 following the simultaneous tripping of the other two machines. Note that the field current falls quite low, and some of the ac transient spikes actually touch zero. If the exciter on the machine does not have negative field current capability (which is the case with most of the modern thyristorized solid state exciters), a large voltage appears

across the field slip-rings as the field circuit loop is interrupted because the thyristors do not conduct in reverse. This field overvoltage is shown in Figure 2.3.2 b, and it should be noted that unlike pole slipping and short circuit induced field overvoltages [9, 10, 12], it has an extremely sharp rate of rise (though a smaller duration per peak) on account of the higher frequencies in the field current. If the surge arrestors across the field circuit are not fast enough to quench the leading edges of these overvoltage spikes, the thyristors of the excitation system can be damaged.

It can be seen from Figure 2.3.2 b that for the case under consideration, the overvoltage was about 50 times the open circuit field voltage (eg., voltage on the field circuit required to produce rated terminal voltage on the open circuited machine). It will be seen from later chapters that the overvoltage can be even higher if the load is modelled not just as a capacitor, but as a tuned circuit, such as a filter. The observed terminal voltage is seen in Figure 2.3.2 c, and shows an overvoltage on account of the sudden increase in VARs into the machine. (In an actual generator, the exciter would try to bring this voltage down, but for the purposes of this simulation, the exciter has not been modelled.)

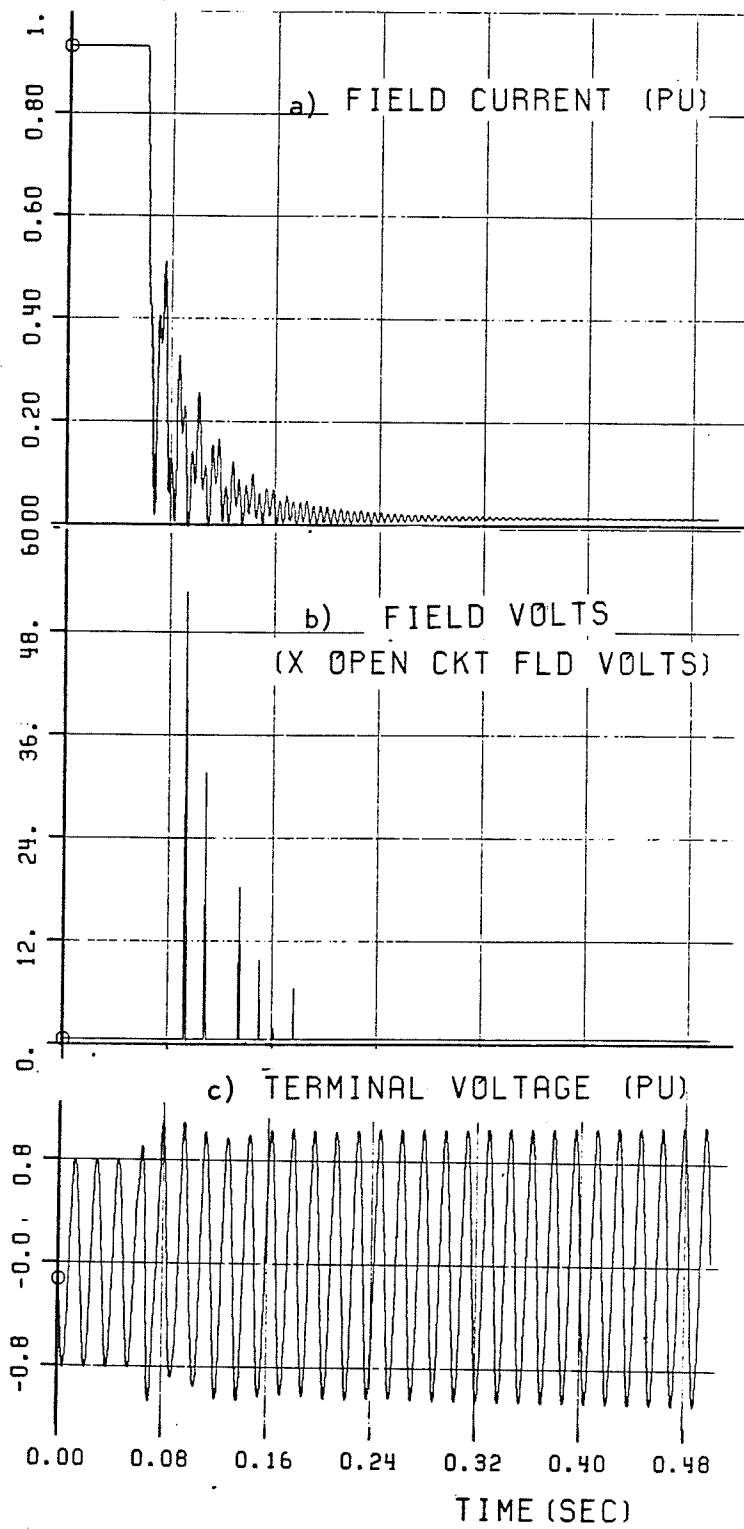


Figure 2.3.2:2 out of 3 Machines Tripping on Capacitor Load ($X_c = 1.2$ pu)

2.4 Field Current Response of Machines Tripping on Capacitive Load - Self Excited Case

This case is similar to that of the previous section, except that when two machines trip, the third one sees a capacitive load, $x_c = 0.83$ pu, which is large enough to cause self excitation, in the final moments before it too trips. This interval, for which the machine sees this excessively large capacitive load, may be of too short a duration to cause any excessive voltage rise on its terminals. The field current, however, would immediately be affected and very large overvoltages could occur. The waveforms for this case are shown in Figure 2.4.1.

Note that the field current goes to zero immediately (Figure 2.4.1 a) and overvoltage spikes appear in the field voltage (Figure 2.4.1 b). If for any reason the machine breaker fails to operate, the machine can suffer severe overvoltage on its terminals (Figure 2.4.1 c). The field voltage shows initial spikes of large magnitude due to the ac component of field current. The sustained field overvoltage later on, which rises exponentially, is due to the continuing self excitation. Note that the field voltage spikes are in excess of 160 times the open circuit field voltage. Later simulations will show that the terminal voltage does not rise continuously as in Figure 2.4.1 c, but is limited by machine saturation.

Cascaded Tripping. In reality, when machines trip, they would trip in some sequence, and not two at the same time as suggested in Figure 2.3.1. The graphs of Figure 2.4.2 show the case of first one and then the second of the three machines of Figure 2.3.1 tripping with

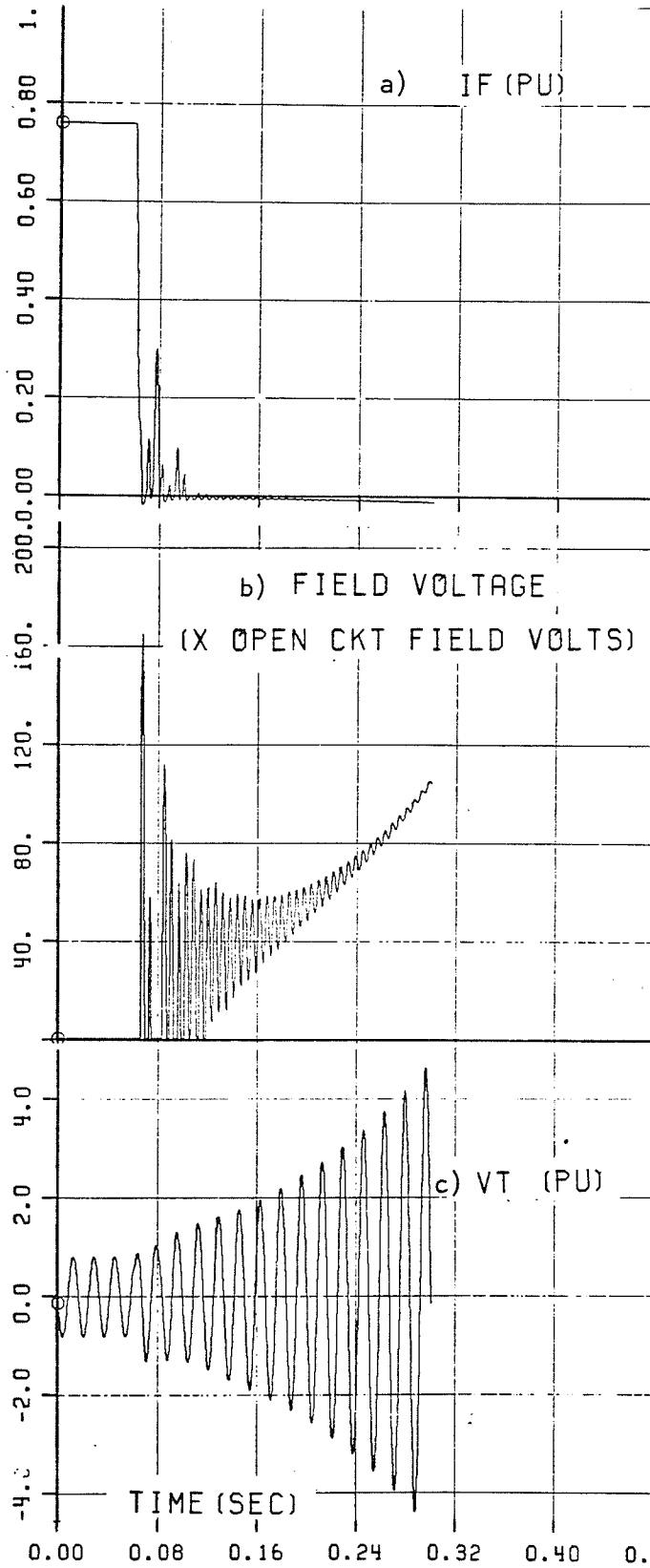


Figure 2.4.1: 2 out of 3 Machines Tripping on Capacitive Load-Self Excited Case. ($X_c = 0.85pu$)

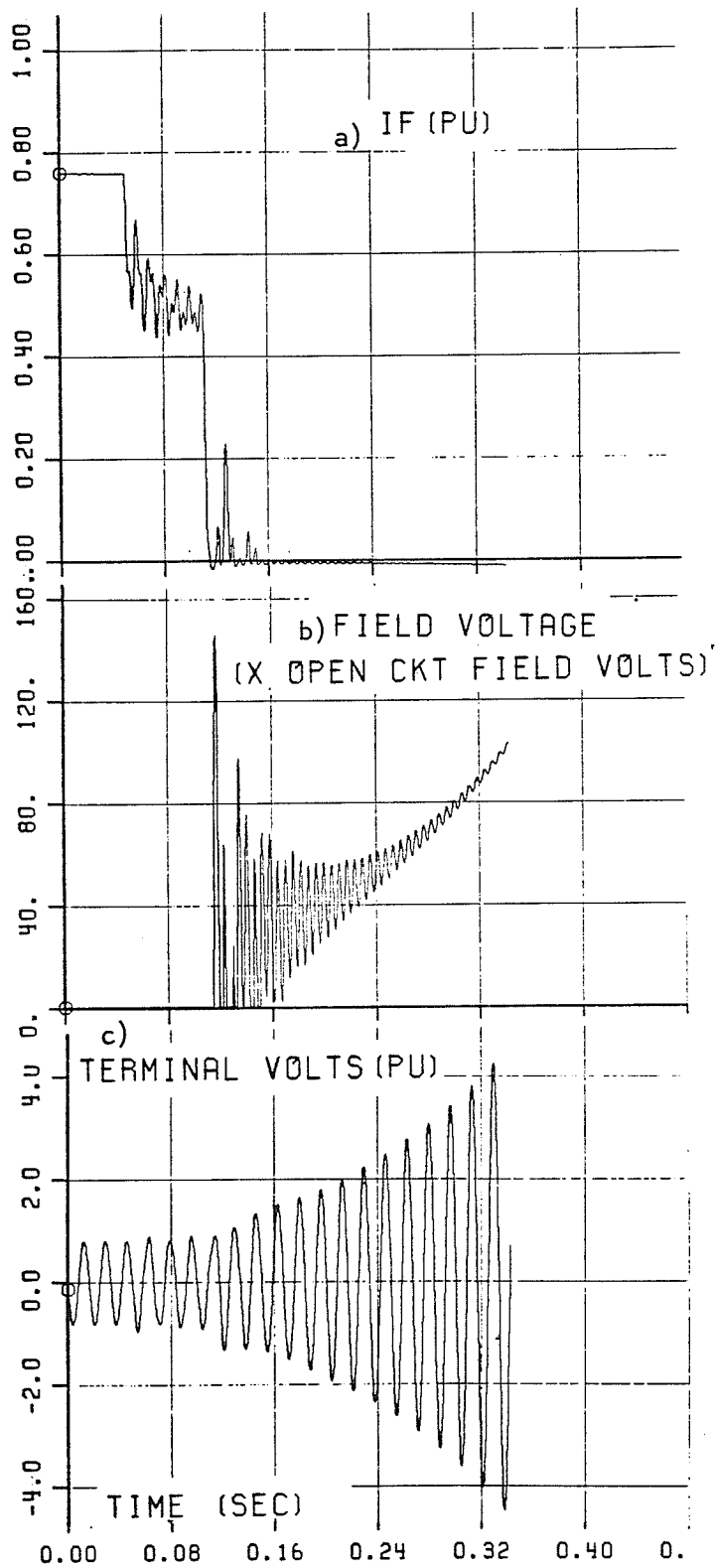


Figure 2.4.2: Cascaded Tripping of Machines

about a 50 ms delay between them. There is no overvoltage in the field circuit after the tripping of the first machine, but there is considerable overvoltage after the tripping of the second machine. This explains why the last machine to remain usually suffers the greatest damage to its exciter thyristors on account of such capacitor induced transients.

2.5 Effect of Exciter Thyristor Failure

In this study, the exciter thyristors were made to fail in the short-circuit mode if the following condition occurred (with reverse field current induced field voltage V_{rev}):

$$\int |V_{rev}| dt > BD \text{ for } V_{rev} > V_{bd}$$

where V_{bd} is the peak reverse voltage of the thyristor string, and BD is a specified quantity representing an energy absorption capability. The integration was used to simulate the fact that the surge arrester and smaller circuits cushion the thyristors against some of the overvoltage. Figure 2.5.1 a shows the field current. Note the negative field current after the breakdown has occurred. Figure 2.5.1 b shows the field overvoltage (which exists before the thyristors breakdown). Comparing Figures 2.4.2 c and 2.5.1 c, one sees that the thyristor breakdown curtails the stator overvoltage, giving time for the machine to trip safely. (de Mello et al. have established [1] that negative current capability in the exciter slows down self excitation. Thyristors that have failed shorted, in fact, introduce this capability.)

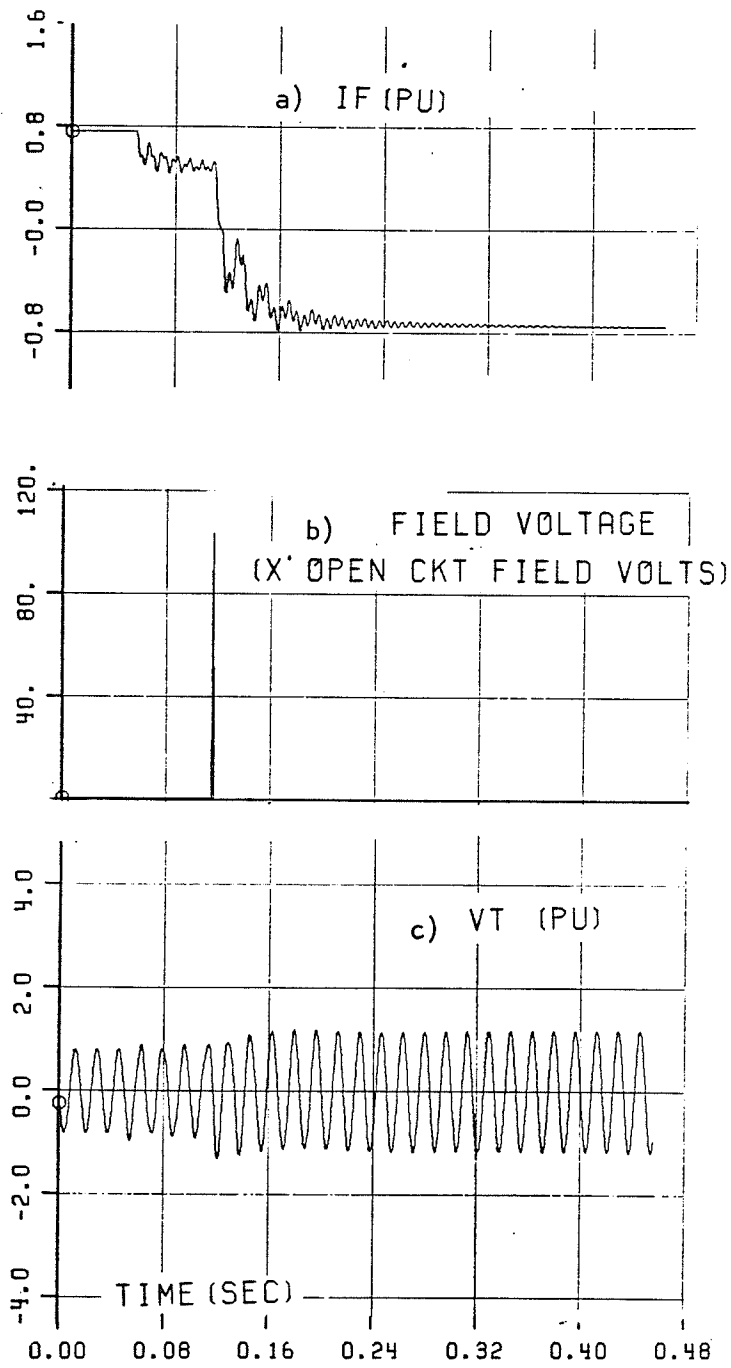


Figure 2.5.1 : Waveforms with Thyristor Failure Modelled.

2.6 Analysis of the Field Transients

In Section 2.2, a preliminary analysis of induced field currents was given. In this section, a more detailed analysis of transients in the field circuit will be provided.

Figure 2.6.1 shows the equivalent circuit of a synchronous machine in a time period immediately following a sudden change in capacitive loading. As the voltages behind the subtransient reactances x_d'' and x_q'' remain essentially unchanged, and as $x_d'' \approx x_q'' = x''$, then subtransiently, the machine may be regarded as of the cylindrical rotor type.

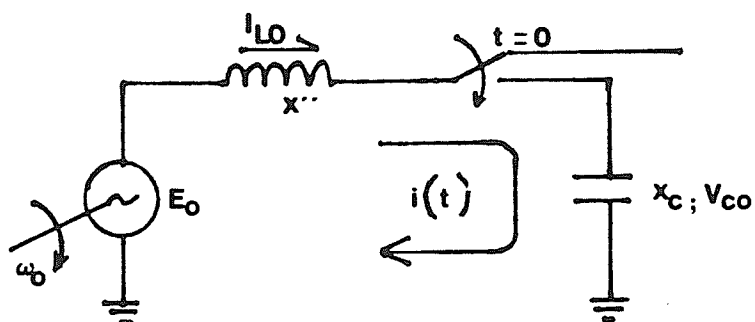


Figure 2.6.1: Equivalent circuit for sudden capacitive loading

The resulting current oscillations may now be written as:

$$\begin{aligned}
i(t) &= \frac{-E_0}{x_c - x''} \sin(\omega_0 t - \phi_0) \\
&+ \left[\frac{E_0 \omega_r \cos \phi_0}{(\omega_r^2 - \omega_0^2) \ell''} - \frac{V_{CO}}{x_r} \right] \sin \omega_r t \quad \dots 2.6.1 \\
&+ \left[I_{LO} - \frac{E_0 \omega_0 \sin \phi_0}{(\omega_r^2 - \omega_0^2) \ell''} \right] \cos \omega_r t
\end{aligned}$$

where $\ell'' = x''/\omega_0$, $x_r = \omega_r \ell''$, $\omega_r = \frac{1}{\sqrt{\ell''} c}$; ω_0 is the fundamental frequency, $E_0 \cos(\omega_0 t - \phi_0)$ being the voltage behind subtransient reactance, V_{CO} and I_{LO} being initial capacitor voltage and inductor current, respectively.

Note that equation 2.6.1 has two components, one at 60 Hz frequency, and the other at frequency $\omega_r = \omega_0 \sqrt{x_c/x''}$. Also note that the 60 Hz component in phasor form is:

$$\tilde{I}_{\omega_0}'' = \frac{\tilde{E}}{j(x_c - x'')} \quad \dots 2.6.2$$

as is to be expected, from a subtransient phasor solution of the system.

Now consider the situation of Figure 2.6.2, where one out of two machines feeding a capacitor load suddenly trips. Equations of the form 2.6.1 may be written for all three phase currents. Neglect for the time being the fundamental frequency component of the current, and

concentrate on the component of frequency ω_r (represented by i_{A_r}).

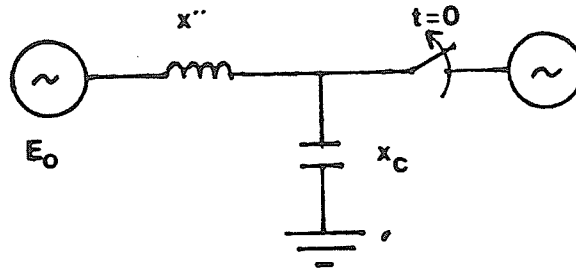


Figure 2.6.2: One out of two machines trips

Thus:

$$i_{A_r}(t) = \left[\frac{E_0 \omega_r \cos \phi_0}{(\omega_r^2 - \omega_0^2) l''} - \frac{V_{COA}}{x_r} \right] \sin \omega_r t$$

... 2.6.3

$$+ \left[I_{LOA} - \frac{\omega_0 E_0 \sin \phi_0}{(\omega_r^2 - \omega_0^2) l''} \right] \cos \omega_r t$$

and similarly for phases B and C.

Note that as the system was initially in steady-state

$$\phi_{OC} = \phi_{OB} + 2\pi/3, \quad \phi_{OB} = \phi_{OA} + 2\pi/3$$

... 2.6.4

$$\begin{aligned} I_{LOA} &= I_0 \cos \lambda, & I_{LOB} &= I_0 \cos (\lambda - 2\pi/3), \\ & & I_{LOC} &= I_0 \cos (\lambda - 4\pi/3); \text{ and} \end{aligned}$$

$$\begin{aligned} V_{COA} &= V_0 \cos \psi_0, & V_{COB} &= V_0 \cos (\psi_0 - 2\pi/3) \\ & & V_{COC} &= V_0 \cos (\psi_0 - 4\pi/3). \end{aligned}$$

Also, because of the absence of the neutral

$$\sum_{A,B,C} i_{A_r}(t) = 0 = \sum I_{A_r}(\omega_r) \quad \dots 2.6.5$$

where the capitals stand for phasors of frequency ω_r .

The vector of phasor currents $(I_{A_r}, I_{B_r}, I_{C_r})$, can be transformed by means of a well known [22, 23] symmetrical components transformation:

$$\begin{bmatrix} I^+ \\ I^- \\ I_0 \end{bmatrix} = \begin{pmatrix} 1 & a & a^2 \\ 1 & a^2 & a \\ 1 & 1 & 1 \end{pmatrix} \begin{bmatrix} I_{A_r} \\ I_{B_r} \\ I_{C_r} \end{bmatrix} \quad \dots 2.6.6$$

where $a = e^{j2\pi/3}$.

The positive sequence component I^+ sets up a rotating magnetic field in the air gap of frequency ω_r , rotating in the direction

of motion of the rotor. Consequently, rotor currents of frequency $\omega_r - \omega_0$ are induced. Likewise, due to the negative sequence rotating field of I^- , rotor currents of frequency $\omega_r + \omega_0$ are induced. Note that as I^+ and I^- have, in general, different magnitudes, the resultant rotor currents have different magnitudes as well, proportional to the magnitudes of I^+ and I^- .

Equation 2.6.3 may be written in phasor form as:

$$I_{A_r} = \left[I_{LOA} - \frac{\omega_0 E_0}{(\omega_r^2 - \omega_0^2) l''} \sin \phi_{0A} \right] \dots 2.6.7$$

$$- j \left[\frac{E_0 \omega_r \cos \phi_0}{(\omega_r^2 - \omega_0^2) l''} - \frac{V_{COA}}{x_r} \right]$$

and similarly for phases B and C.

Using transformation 2.6.6 on 2.6.7, and with identities 2.6.4 we obtain:

$$I^+ = I_{A_r} + I_{B_r} e^{j2\pi/3} + I_{C_r} e^{j4\pi/3}$$

$$= \frac{3}{2} I_0 e^{j\lambda} - \frac{\omega_0 E_0}{(\omega_r^2 - \omega_0^2) l''} e^{j(\phi_{0A} - \pi/2)} \dots 2.6.8$$

$$- j \frac{E_0 \omega_r}{(\omega_r^2 - \omega_0^2) l''} e^{j\phi_{0A}} + \frac{j}{x_r} V_0 e^{j\psi_{0A}}$$

where ϕ_{0A} , λ , ψ_{0A} are angles of prefault internal voltage, current and terminal voltage, respectively.

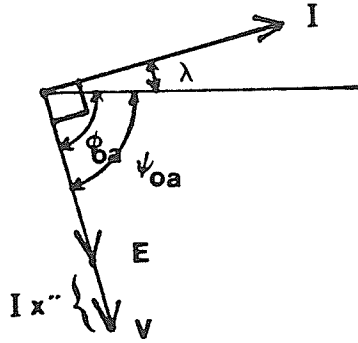


Figure 2.6.3: Prefault phasor diagram

From the Prefault Phasor diagram (Figure 2.6.3), we have

$$\phi_{OA} = \psi_{OA} = \lambda - \pi/2 ,$$

and so choosing $\lambda = 0$ arbitrarily, without loss of generality, Equation 2.6.8 becomes

$$\begin{aligned} I^+ &= \frac{3}{2} \left[I_0 + \frac{V_0}{x_r} + \frac{E_0}{(\omega_r^2 - \omega_0^2)l''} [\omega_0 - \omega_r] \right] \\ &= \frac{3}{2} \left[I + \frac{V_0}{x_r} - \frac{E_0}{(\omega_r + \omega_0)l''} \right] \end{aligned} \quad \dots 2.6.9$$

likewise $I^- = \frac{3}{2} \left[I_0 - \frac{V_0}{x_r} + \frac{E_0}{(\omega_r - \omega_0)l''} \right]$

Neglecting for the moment the system frequency ω_0 in comparison with the natural frequency ω_r , Equation 2.6.9 becomes

$$I^+ \approx \frac{3}{2} \left[I_0 + \frac{V_0 - E_0}{x_r} \right] = I_0 \left[1 + \frac{x''}{x_r} \right] \cdot \frac{3}{2}$$

... 2.6.10

$$I^- \approx \frac{3}{2} \left[I_0 - \frac{V_0 - E_0}{x_r} \right] = I_0 \left[1 - \frac{x''}{x_r} \right] \cdot \frac{3}{2}$$

And so $\frac{I^+}{I^-} = \frac{x_r + x''}{x_r - x''}$, or for the case of Figure 4.1, I^+ is larger than I^- initially. (As is also seen from the field current plots in Figure 2.3.1 a.)

The fields due to I^+ and I^- are reflected into rotor currents of proportional magnitude. The equivalent induction motor circuit (employed in studying subsynchronous oscillations) of the machine at slip s is shown in Figure 2.6.4 [16, 18].

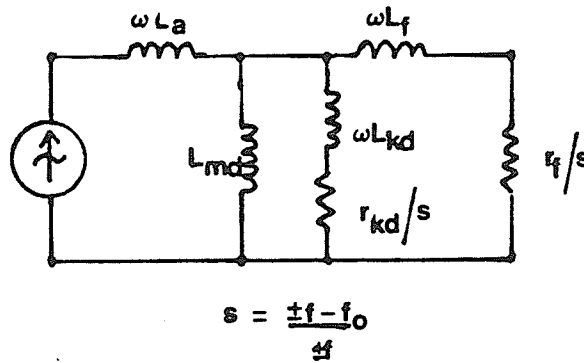


Figure 2.6.4: Equivalent induction motor circuit at frequency ω • ($f = \frac{\omega}{2\pi}$).

We see that the equivalent resistance in the circuit is larger at the frequency $|f - f_0|$ than at the frequency $|f + f_0|$ which is conse-

quently less damped. Hence, the lower frequency oscillations, although larger to start with, decay rapidly, as is evidenced from the rotor waveforms (Figure 2.3.1, etc.).

Figure 2.6.5 shows the three components of rotor current. On the tripping of a machine, there is a sudden change in the dc component of field current, corresponding to the subtransient flux linkages remaining constant, followed by a more gradual one. The dc component of Figure 2.6.5 a gradually comes up to its pre-fault value, with a modified field time constant (discussed in the next section). Superposed on this dc component are the two ac components of Figures 2.6.5 b and c, which are of different magnitudes and have different decay time constants. The total waveform of Figure 2.6.5 d is obtained by summing the waveforms a, b and c. Comparison should be made between this waveform and those in Figures 2.2.2 and 2.3.2 where the correlation is obvious.

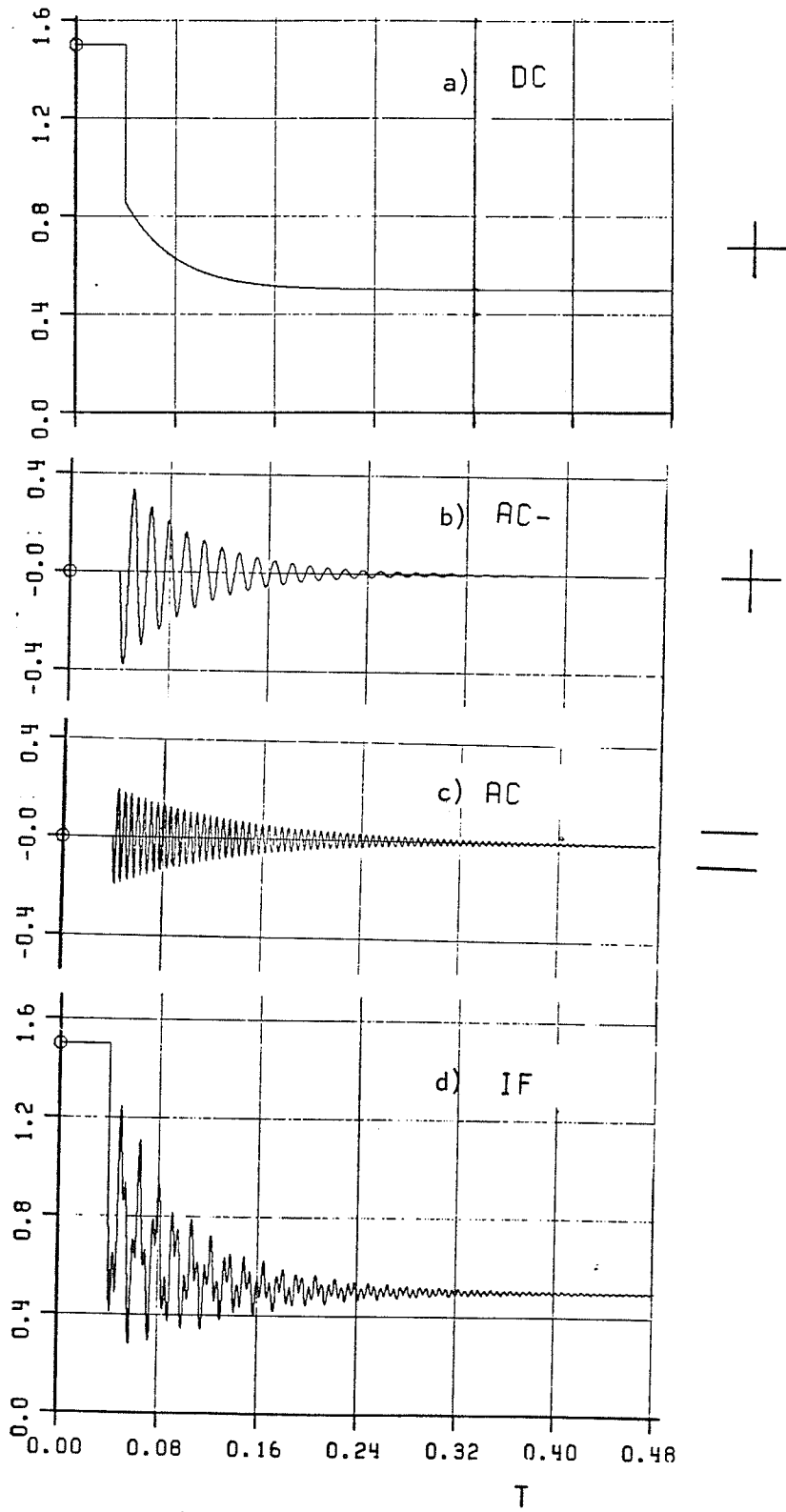


Figure 2.6.5 : The Components of the Field Current.

2.7 The Field Time Constants

The cases considered so far were with constant field excitation. It is interesting to study what a machine with an exciter would do under these circumstances of sudden capacitive loading. The following is an analysis of the field circuit response time. It is shown that as the machine is loaded with increasing capacitance, the time constant of the field circuit keeps increasing, until, finally at the onset of self excitation, it is infinitely large. (This is on the assumption of a linear machine. With saturation, of course, as the voltage at the terminals increases, the magnetizing impedance X_{md} of the machine decreases, thereby reducing the time constant.) Thus, on account of the increased time constants, the exciter's capability of controlling the field current is lessened and the exciter is incapable of maintaining the field current positive.

The machine equations can be written in operational form as

$$\psi_d(p) = \frac{X_d(p)}{\omega_0} I_d + \frac{G(p)}{\omega_0} U_f(p)$$

$$\psi_q(p) = \frac{X_q(p)}{\omega_0} \cdot I_q$$

... 2.7.1

$$U_d = p \psi_d + \omega \psi_q + r_a I_d$$

$$U_q = p \psi_q - \omega \psi_d + r_a I_q$$

with $p = d/dt$, the differential operator.

The terminal equations with capacitor load can be written as

$$\begin{bmatrix} I_d \\ I_q \end{bmatrix} = \begin{pmatrix} -pC & -\omega C \\ \omega C & -pC \end{pmatrix} \begin{bmatrix} U_d \\ U_q \end{bmatrix} \quad 2.7.2$$

where the ψ s stand for fluxes, the U s for axis voltages, with subscripts d and q denoting the respective axes, and U_f the field voltage. X_d, X_q are the d and q axis operational impedances, ω is the instantaneous radian frequency, ω_0 the base frequency (i.e., $2\pi f_0$ radians/sec) and r_a the armature resistance.

The off diagonal terms in Equation 2.7.2 arise due to the fact that the transformation matrix from a, b, c to dqo coordinates itself is a time function, and has to be differentiated when \underline{V}_{abc} is converted to \underline{U}_{dqo} in the expression $\underline{I}_{abc} = [C] \frac{d}{dt} \underline{V}_{abc}$, where \underline{V}_{abc} , \underline{I}_{abc} stand for phase voltages and currents, and \underline{U}_{dqo} , \underline{I}_{dqo} for the transformed vectors.

Using the first three equations of 2.7.1 with 2.7.2 and eliminating I_d, I_q , one obtained

$$U_d = \frac{N(p)}{D(p)} \cdot U_f \quad 2.7.3$$

The denominator $D(p)$ has been evaluated by Crary [19], though not in the same way as above, and is of the form:

$$D(p) = 1 + p(T_0 a_1 + a_2) + b p^2 + c p^3 + \dots \quad 2.7.4$$

The coefficient of p , $(T_0 a_1 + a_2)$, is then the approximate time constant. Crary has further neglected terms of the sort a_2 in Equation 2.7.4 and thus obtained a time constant (with T_0 as the open circuit time constant).

$$\tau(x_c) \approx \frac{(x'_d - x_c)(x_q - x_c) + r_a^2}{(x'_d - x_c)(x_q - x_c) + r_a^2} x T_0 \quad 2.7.5$$

Neglecting r_a^2 , Equation 2.7.5 yields

$$\tau \approx \frac{x'_d - x_c}{x'_d - x_c} T_0 \quad 2.7.6$$

Thus, one sees that as $x'_d \rightarrow x_c^+$, $\tau \rightarrow \infty^+$, i.e., the time constant becomes arbitrarily large. Also, for $x'_d < x_c < x_d$, τ is negative, i.e., the system is unstable. This corresponds to self excitation.

Another interesting fact is the form of the Equation 2.7.6. With a pure inductance in the output, lumping the inductance with the leakage reactance and then treating the machine as though on short circuit, one obtains [20, 21]

$$\tau_L = \frac{x'_d + x_l}{x'_d + x_l} T_0 \quad 2.7.7$$

Equation 2.7.6 is of the same form as 2.7.7, except with a sign change. Thus, the capacitance may be regarded as a pure reactance which subtracts from the leakage impedance, in deriving time constants. However, though very satisfying, this is a coincidence. Equation 2.7.6 is not exact, but comes about after neglecting terms of $D(p)$. It should be carefully remembered that the mechanisms which yield 2.7.6 and 2.7.7 are completely different, though the final forms are quite alike!

Figure 2.7.1 gives simulation results along with a plot of Equation 2.7.5 for the machines at Manitoba Hydro's Kettle Generating Station. As can be seen, the agreement is close, except in the region $0.1 < x_c < 0.5$, where the rate of self excitation is very large. For $x_c < x'_d$, Equation 2.7.5 shows that the system may be stable, with a small time constant, whereas actually, as seen from the simulation, it may not be so.

Other observations from the figure are:

(i) the worst self-excitation takes place around $x_c = x'_d$

where $\tau = -\delta$, where $\delta \approx 0$ and is positive.

(ii) $\lim_{x_c \rightarrow 0} \tau(x_c) = \frac{x'_d}{x_d} T_0 = T'_d$ — the short circuit time constant. This is as expected.

(iii) $\lim_{x_c \rightarrow \infty} \tau(x_c) = T_0$ — the open circuit time constant, again, as expected.

KETTLE GENERATOR TIME CONSTANT WITH XC

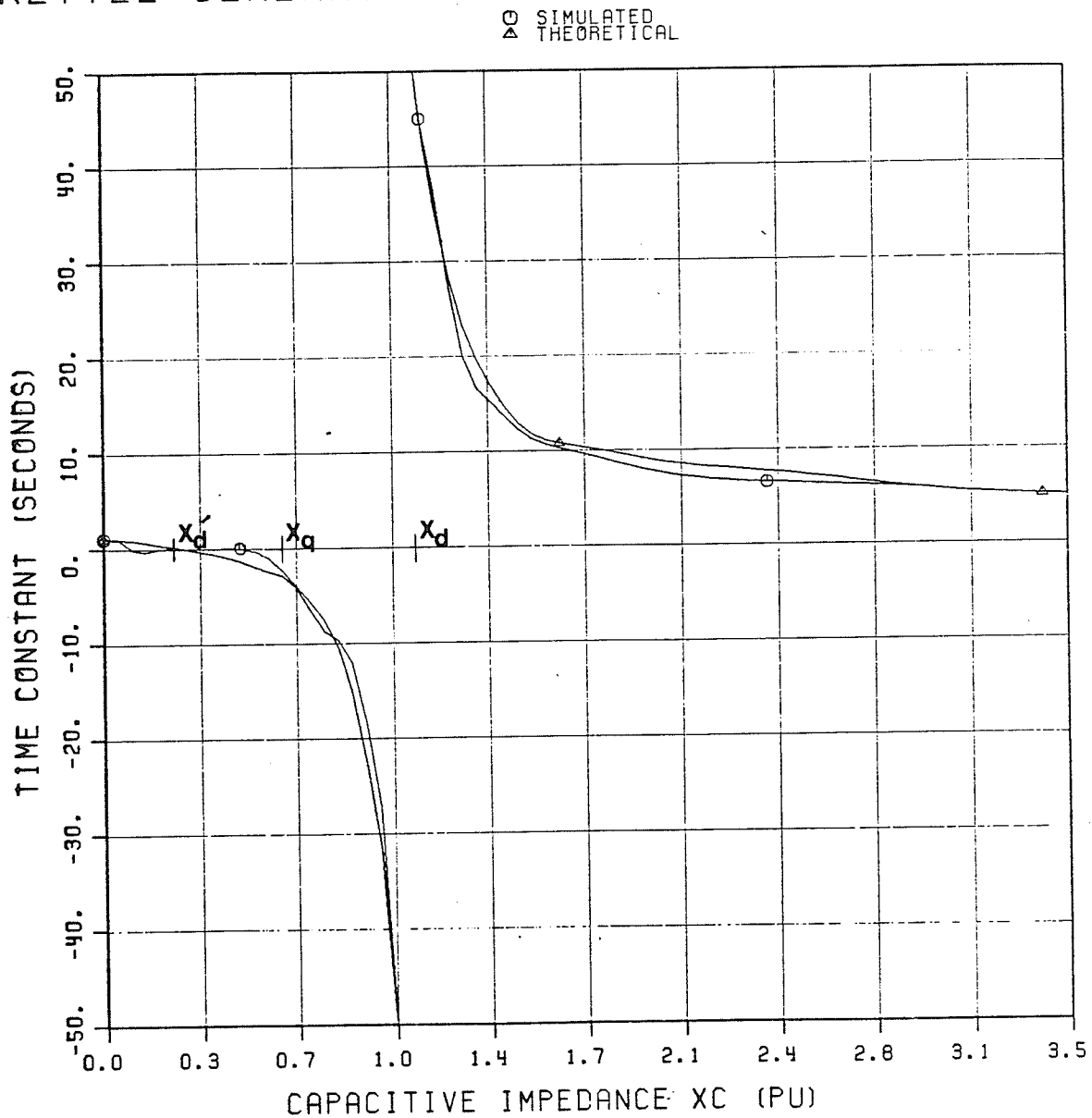


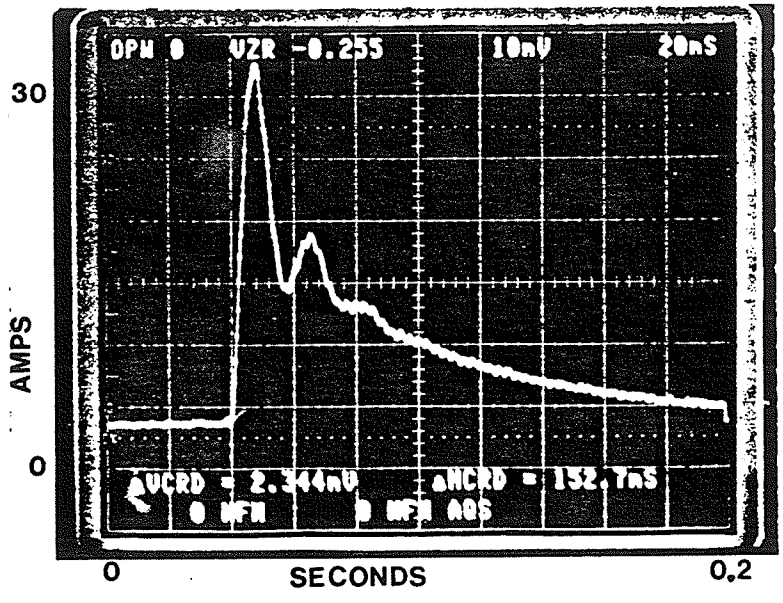
Figure 2.7.1: Simulated and Theoretical Variations in Field Time Constant with Varying X_c

2.8 Tests on Laboratory Machine

As tests on Manitoba Hydro's Kettle Generating Station machines could not be scheduled, tests were carried out on a 15 kVA machine in the laboratory to verify some of the phenomena discussed in earlier sections, and to determine the accuracy of the computer model by comparison. In general, the agreement was excellent. The data for the machine under consideration is available in Table 2.1 of Appendix 2.

(i) Short Circuit Tests. In order to verify the validity of the computer simulation, standard tests like the short circuit test were simulated and compared. Figure 2.8.1 shows the observed and simulated field current waveforms. Saturation in the machine has been modelled. As can be seen, the agreement is close, except for more damping in the simulated waveform, probably due to the improper armature resistance value. Exact values of armature resistance were difficult to determine because of the sliding brass contacts used in the laboratory which introduced a considerable contact resistance in some instances.

(ii) Time Constant Tests. In order to demonstrate the variation in the field time constant as discussed in Section 2.7, the machine was run at synchronous speed with zero field current while connected to a balanced three-phase capacitor load. The field voltage was then suddenly impressed, and the field time constant observed. Figure 2.8.2 shows the field current responses for open circuit and for a 1.84 pu capacitive load. As can be seen, the field time constant has increased. Table 2.8 gives observed and simulated time constants for various capacitor loads.



a) Observed

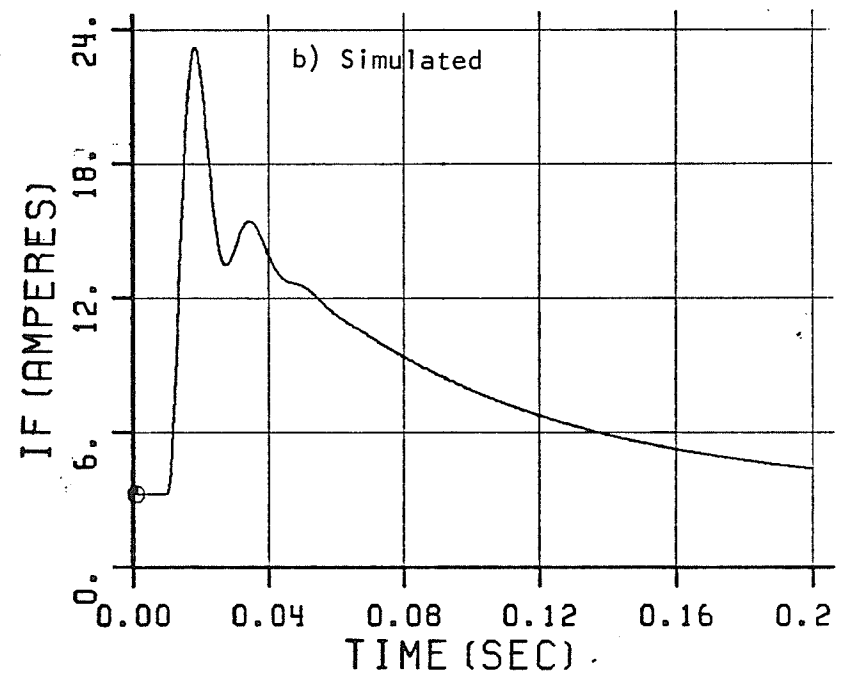
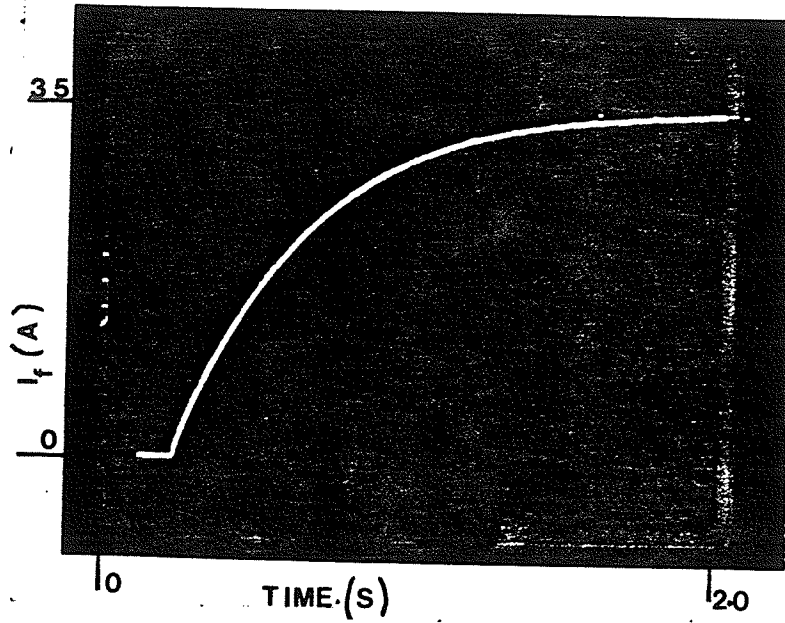
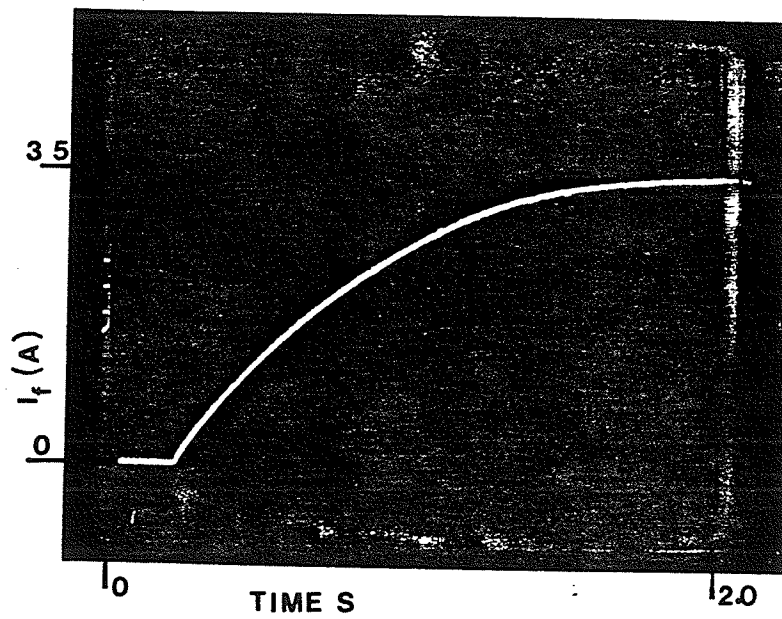


Figure 2.8.1 : Three Phase Symmetrical Short Circuit on Lab Machine;



a) $X_c = \text{infinity}$ (open cct) $\tau = 0.42$ s



$X_c = 1.84$ pu, $\tau = 0.63$ s

Figure 2.8.2: Time Constants on Capacitive Loading (Lab Machine)

x_c (pu)	τ (sec), actual	τ (sec), simulated
∞ (o.c.)	0.42	0.42
1.84	0.63	0.58
0.92	1.2	1.2
0.66	4.5	4.8

Table 2.8: Observed and Simulated Machine Time Constants

(iii) Tripping of Machines. The effect of tripping of machines connected to a capacitive load was verified with the setup shown in Figure 2.8.3. With the synchronizing switch, S_1 open, the capacitors were connected to an infinite bus by closing switch S_2 .

The machine was then brought up to speed and synchronized to the infinite bus - capacitor system. The prime mover input power was then left untouched. This ensured that the machine was loaded with zero real power. By weakening the field of the machine, both the machine and infinite bus could be made to equally share the capacitive load current, so that when the switch S_2 was opened at time $t = t_0$, the

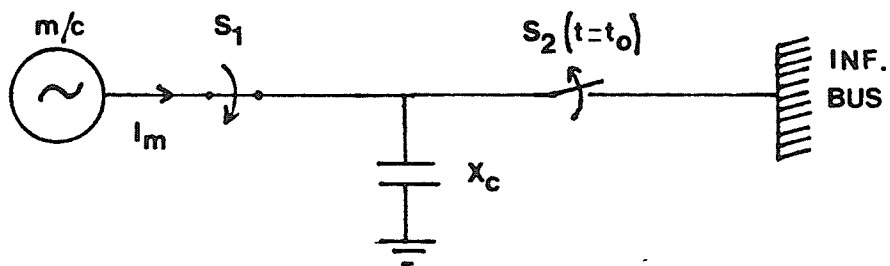


Figure 2.8.3: Test Setup for Machine Tripping

situation would simulate one out of two machines tripping. Figure 2.8.4 shows the resulting simulated and observed waveforms for $x_c =$

0.86 pu which is not sufficient capacitance to lead to self excitation.

This test was repeated for $x_c = 0.47$ pu which lead to field current reversal and self-excitation as shown in Figure 2.8.5.

As can be seen in both figures there is good agreement between the observed and simulated waveforms. The 120 Hz frequency in the field current was because the load was not exactly balanced (due to differences in values of the laboratory capacitors). This was taken into consideration while inputting data to the simulation model. Thus $x_c = 0.47$ pu mentioned earlier is only the average capacitance value in the three phases. Individual phase capacitors varied from this by a small amount.

(iv) Field Overvoltage. The previous test with $x_c = 0.47$ pu was again repeated, except that a rectifier was installed in series with the field circuit to prevent reverse current. The resulting field current, field voltage and terminal voltage waveforms are shown in Figure 2.8.6.

Again, the agreement between simulation and observation is very good. As can be seen there are very fast rising reverse voltage spikes across the exciter of about ten times the field voltage required for rated open circuit terminal voltage.

Comparison of Figures 2.8.5 and 2.8.6 clearly indicates that negative current capability in the exciter does limit the rate of rise of terminal voltage.

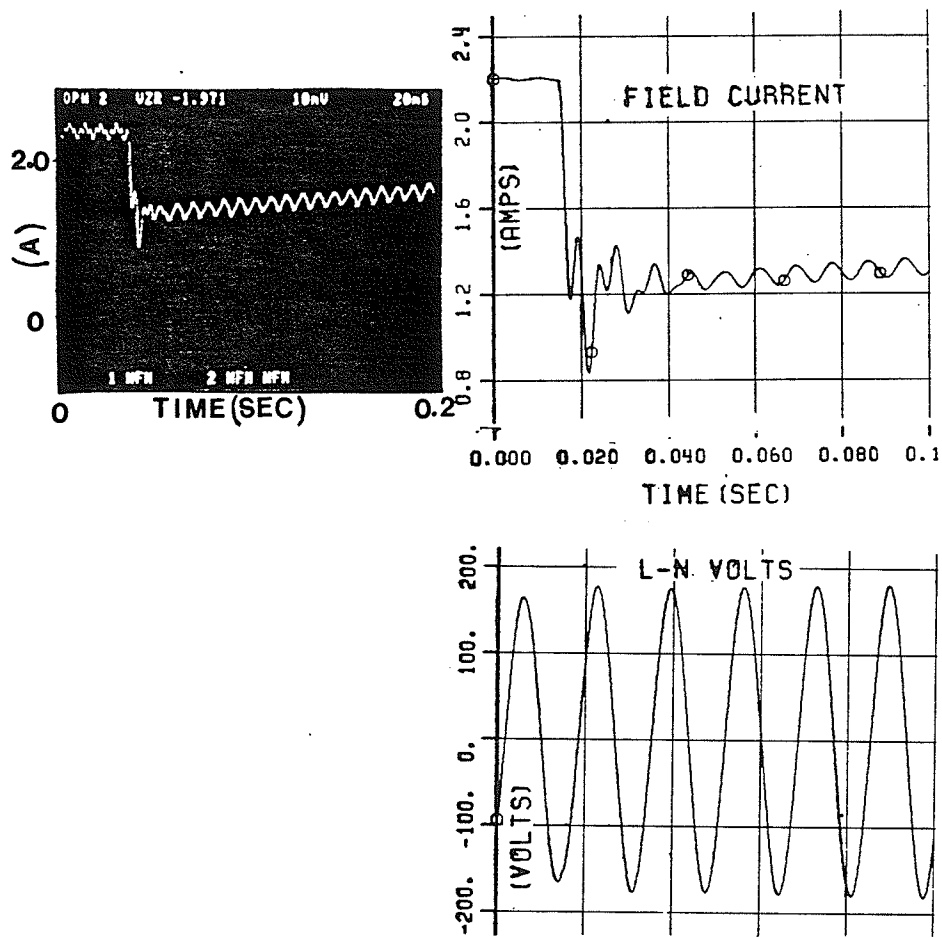


Figure 2.8.4: Observed and Simulated Waveforms for 1 out of 2 Lab Machines Tripping. ($X_c = 0.86$ pu)

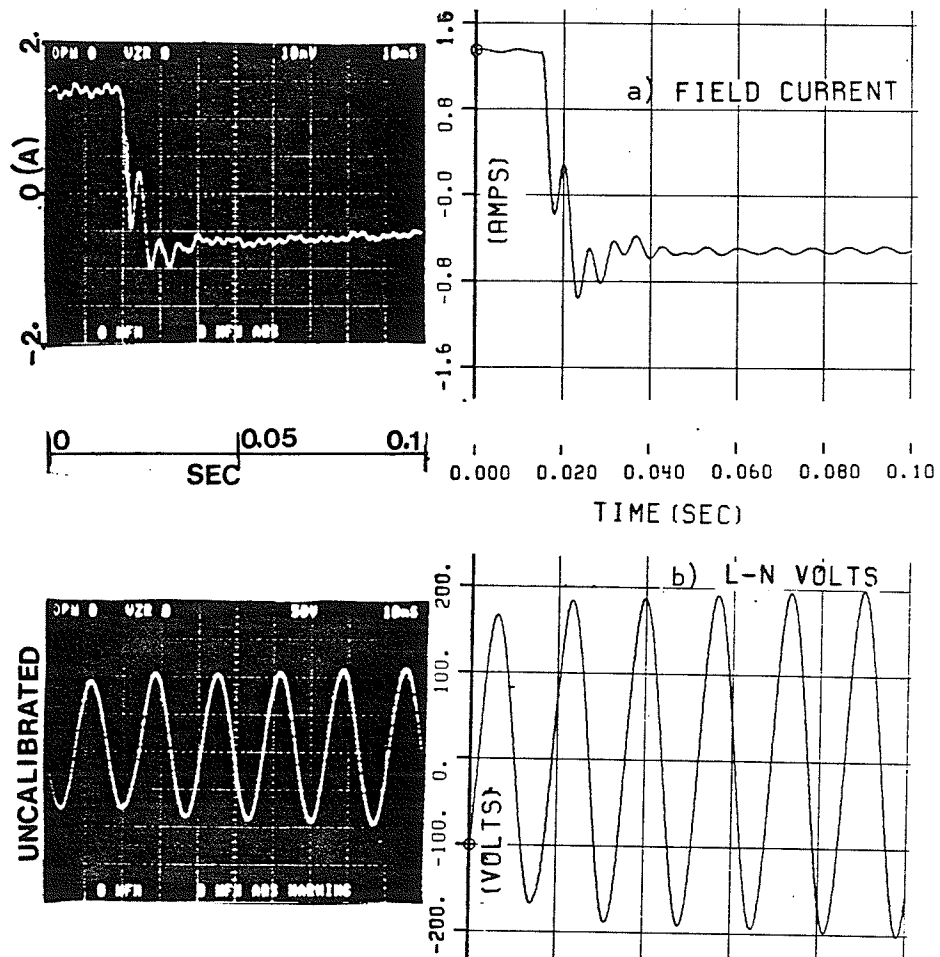


Figure 2.8.5: 1 out of 2 Machines Tripping, Self-Excited Case ($X_c = 0.47$ pu), Observed and Simulated Waveforms (With Reverse Current Capability)

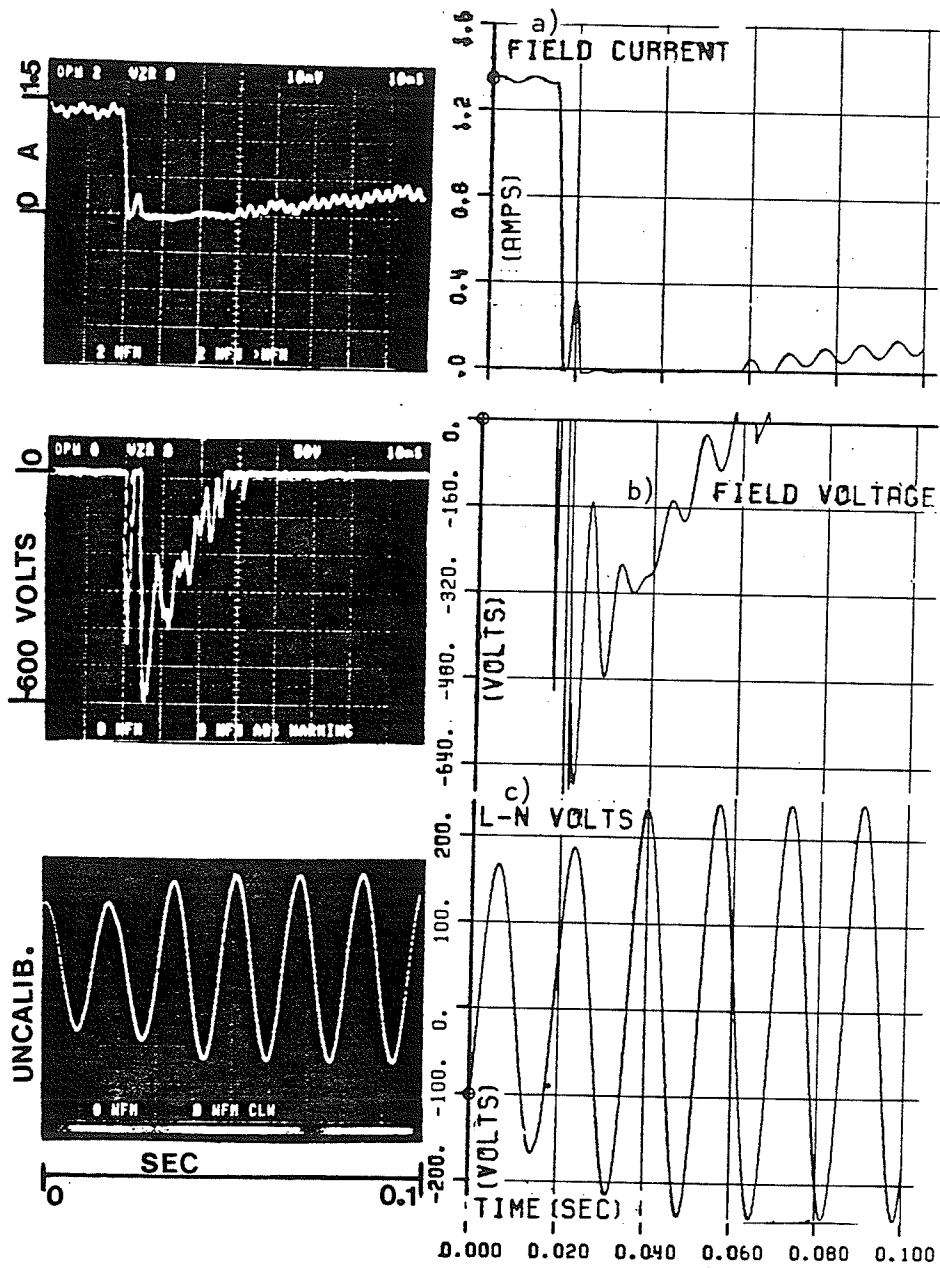


Figure 2.8.6: Waveforms (Observed and Simulated) for 1 out of 2 Machines Tripping, Self-Excited Case (Without Reverse Current Capability)

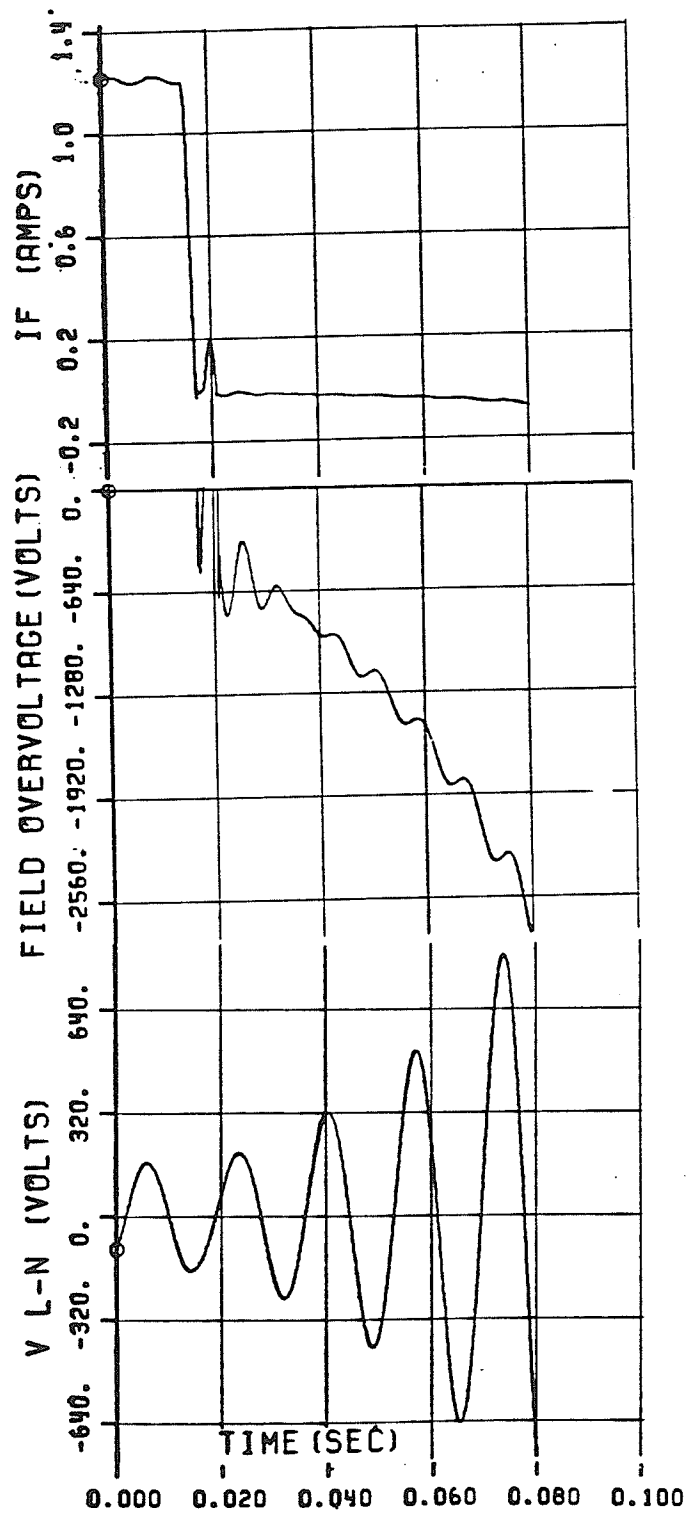


Figure 2.8.7: Effect of not Modelling Saturation

(v) Effect of Saturation. In order to determine the effect of neglecting saturation as was done in the previous sections, the simulation of the above test was repeated without modelling saturation of the magnetizing reactance. As shown in Figure 2.8.7, the field current does not rise above zero later, and the terminal voltage continues to increase exponentially. The reason for this is that the magnetizing branch impedance X_{md} keeps decreasing (in the saturated case) with increased saturation until a point is reached when X_d equals x_c , and the machine comes out of self excitation, and stabilizes in an overvoltage condition. This does not happen in the unsaturated case, because X_{md} never decreases. It must be noticed however that the first couple of overvoltage spikes in the field are not affected in magnitude by the modelling of saturation, and as it is these that cause the exciter thyristors to fail, it is expected that results obtained from the unsaturated modelling can be used to determine the overvoltage, if study beyond the initial few spikes is unimportant.

2.9 Overall Conclusions for Chapter 2

This chapter concerned itself with simulation of field current responses when machines connected to a capacitive load were subjected to a load rejection or a tripping. If without negative current capability in the exciters, the machines' field voltages were shown to reach considerable magnitudes with a very fast rise time. This effect was found to be especially severe in machines near the self excitation condition, where the field currents were very low, and hence any tran-

sients would push the field current to zero thereby causing field and thus exciter overvoltage.

In the case where machines actually got into a self-excited condition on account of the tripping of other machines, it was found that this field overvoltage could cause the thyristors to fail in the short circuit mode, thereby introducing negative field current capability where there was ordinarily none. This would prevent a rapid rise of machine terminal voltage.

The nature of the field current response was explained in terms of transferred harmonics to the field circuit from L-C oscillations resulting from the x'' , terminal x_c . It was also pointed out that under low field current conditions, the field current's value could not be kept positive by rapid exciter action, as the field current time constant became large although the time constant of field voltage to terminal voltage may still be small).

Finally some of these factors were observed from experiments on a small (15 kVA) laboratory synchronous machine. Agreement between modelling and observation was good. The effect of saturation on the field current was also simulated.

The next chapter discusses the modelling schemes in detail. It is followed by other chapters in which the modelling is increased to greater detail in order to study the phenomena more completely.

CHAPTER 3

Modelling

3.1 General

The problem at hand required a considerable amount of simulation on a digital computer, on account of the complexity of the equations resulting from the situations studied. For this purpose, a machine model of considerable detail was developed, as mentioned in Chapter 2, and this shall be mainly discussed in this chapter.

As, in some cases, the machines being studied were connected to dc systems, it was also important to accurately model the dc converter, and the ac network quite completely. For this reason, a digital network analyzer program called MH-EMTDC, which was developed at Manitoba Hydro, was utilized [14]. This program is particularly suited for simulation of ac-dc systems. The interfacing of the machine model with this program shall also be discussed in this chapter. Lastly the modelling of exciters and governors required with the machine model for a complete simulation is described.

The combined package of digital network analyzer/converter model/machine model, etc., proved to be a very powerful and user-friendly transients simulation package, far easier to use than other contemporary simulation packages such as the BPA Electromagnetic Transients Modelling Program (EMTP) [24].

3.2 MH-EMTDC: The Programming Environment

The Electromagnetic Transient Analysis Program (EMTP) developed at the Bonneville Power Administration (BPA) based on the algor-

ithm by Professor Dommel [24] has been a powerful transients simulation tool for a long time. MH-EMTDC developed by D. Woodford [14] at Manitoba Hydro retains Dommel's algorithm for modelling transmission system elements, but has the following additional features (this program was not developed by the author, but used as a means of modelling transmission systems and networks for the machine model developed by him, so that system studies could be made):

- (i) Easy interfacing with user developed subroutines, such as valve group models, machine models, etc., which are not part of the EMTDC program; that is, they do not interface as elements of the system matrix.
- (ii) Disconnected subnetworks are allowed; thus, the power system under study can judiciously be divided into many subsystems, for example, the ac and dc sides of a converter may be regarded as disconnected subsystems, as can be two ac systems connected by a distributed parameter transmission line.
- (iii) Functions such as are available on IBM's CSMP (Continuous System Modelling Program [25]), to simulate integrators, leadlag functions, real poles, complex poles, etc., are available.

The greatest power of MH-EMTDC lies in the concept of disconnected subnetworks. As each subnetwork is independently solved (and matched with the solution across boundaries with other subnetworks), the matrix sizes handled are small. For example a 40 node network would require an inversion of a 40×40 matrix, whereas if modelled as two 20 node subnetworks, it requires inversion of only two 20×20

matrices, which is an easier task. Modelled as four subnetworks of 10×10 size matrices, it is even easier.

Another advantage of this approach is that it is directly amenable to processing on a parallel processor system. Each subsystem model can be allocated to its own processor, and could interface with other subsystems through a common interface bus. The externally imposed models such as machines and valve groups can also reside in their own processors.

Knowledge of FORTRAN is necessary for using MH-EMTDC, as the machines, valve groups, switching functions, sequence of actions are written in a FORTRAN subroutine. Network interconnections and passive network elements are specified in the data file.

Variables to be plotted/printplotted are specified, likewise, in a FORTRAN subroutine. MH-EMTDC, like BPA's EMTF, uses the trapezoidal rule for integration, which is known to be a fairly stable and accurate integration method. Furthermore, this integration procedure has a direct physical analog. For example, the differential equations for inductors and capacitors yield resistors and current sources, as is shown below for inductors [24]:

$$i(t) = \frac{1}{L} \int_0^t V(z) dz \quad \text{gives}$$

$$i(t) = \frac{1}{L} \int_{t-\Delta t}^t V(z) dz + i(t - \Delta t) \quad 3.2.1$$

Using the trapezoidal integration rule:

$$i(t) = \frac{1}{L} \left[\frac{V(t) + V(t - \Delta t)}{2} \right] \Delta t + i(t - \Delta t)$$

$$\text{or } i(t) = \frac{V(t)}{R_L} + J_L(t - \Delta t)$$

3.2.2

$$\text{where } R_L = \frac{2L}{\Delta t} \text{ and } J_L(t - \Delta t) = \frac{V(t - \Delta t)}{R_L} + i(t - \Delta t)$$

The resulting circuit model is shown in Figure 3.2.1.

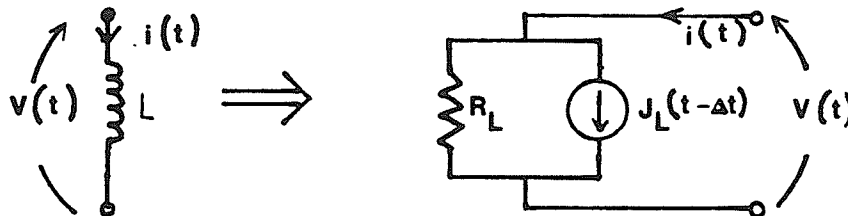


Figure 3.2.1: Equivalent resistive circuit model for the inductor.

The same procedure can be applied for models of distributed transmission lines, coupled branches and so on. Thus, using the trapezoidal rule, the entire network reduces to a resistive network with current source excitations, which can be easily solved, just by writing all the equations such as 3.2.2 in matrix form

$$[Y] \underline{V} = \underline{I} \quad 3.2.3$$

and then inverting Y by an efficient inversion procedure. Saturable branches and other network nonlinearities can be modelled by including

these in the form of additional (dependent) current sources in parallel with the corresponding resistive element, as is done utilizing the well-known Compensation Theorem [26].

Interfacing subprograms with EMTDC is fairly straightforward. All quantities calculated within the subprogram are stored in one large array (called STORE, that is presently dimensioned to a maximum of 5000 entries). Base-Indexed addressing is used, in which each call of a subprogram has associated with it a starting location (called NEXC), and all the quantities of interest for this subprogram are stored sequentially and starting at location STORE(NEXC+1). For example, the machine model requires 100 storage locations, and hence is called MAC100; the 100 standing for the number of storage locations required. Thus, suppose an entry to MAC100, the value of NEXC is, say 30, then MAC100 utilizes locations STORE(NEXC+1) to STORE(NEXC+100) or STORE(31) to STORE(131). The last statement in the subprogram updates NEXC as follows:

$$\text{NEXC} \leftarrow \text{NEXC} + 100.$$

Thus, the next subprogram (which could well be another call to MAC100), starts off with NEXC = 131, and thus the location STORE(NEXC+1), which is the first storage location in the new subprogram becomes STORE(132). This approach results in compact packing of all the storage required in all the subprograms called. It also automatically assigns a unique storage area for any subroutines called.

3.3 Modelling the Machine

In the past, a number of machine simulation programs have been written. Programs written for transient stability studies usually use phasor models [11], which assume that the terminal voltage and current of the machine are phasor quantities. Thus for rapid changes with time these do not provide accurate solutions for the fastest transients. Programs used in time domain simulations (such as EMTP), use more detailed machine representations. A comparison between such programs and the one developed here will be made in subsection 3.3.2, because the basic machine equations used by the author and listed in subsection 3.3.1, are almost the same for all these methods belonging to the time domain simulation class.

3.3.1 Machine Equivalent Circuit and Mechanical Dynamics

A two axis equivalent circuit model for the machine is utilized. In this approach, the machine equations written in terms of the phase variables for the three phases, are transformed by a nonsingular transformation into two sets of equations, each set having the minimum amount of interaction with the other. This utilizes the well-known dqo transformation [20], and the resultant equations are known as the d (or direct) axis and the q (or quadrature) axis equations.

The main advantage of this approach is that the axis voltages and currents come out as dc quantities during steady state, fundamental frequency machine operation, thereby considerably simplifying the analysis. As the physical interpretation of the d and q axes are axes rotating with the machine rotor, at the speed of the machine rotor, they contain the rotor coils (such as field and amortisseur coils), and the transformed stator coils. A number of requirements exist in

order for a proper d-q equivalent to exist, the most important being the sinusoidal distribution of windings on the stator [20].

Unlike the phasor model discussed earlier, this model includes the effects of rapidly changing d and q axes fluxes (i.e., includes terms such as $d\psi_d/dt$ and $d\psi_q/dt$, where ψ_d and ψ_q are the axes fluxes) which are not normally neglected in the phasor solution. Also conventionally assumed in machine modelling that whatever flux links the amortisseur and field coils on the direct axis, also links the d axis coil; this is tantamount to assuming equal mutual inductances between field, direct axis and dampers. However, since the amortisseur (damper) and field are on the same iron, which is separated from the stator iron, it is conceivable that some of the flux links the field and damper without linking the stator coil. This flux has been identified as the culprit [13, 27] in many discrepancies between the model and actual machine when studying rotor transients. Thus it was

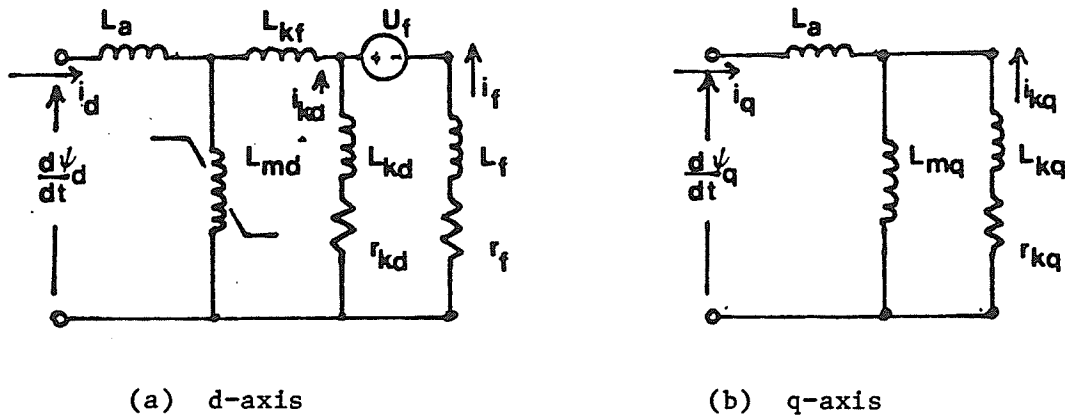


Figure 3.3.1: Equivalent Circuits

felt important to include this flux, and the resulting d and q axis equivalent circuits are shown in Figure 3.3.1, which is the same as

Figure 2.1.1, but has been repeated here for the sake of convenience.

The per-unit system is explained in Appendix I, and utilizes rms ℓ -n voltage and current as base quantities on the stator side. The circuits give the relations between the axis fluxes (ψ_d, ψ_q) , and the field, damper, and d, q axis currents (i_f, i_{kd}, i_d, i_q) . With machine (electrical) speed ω , and d, q axis voltages u_d, u_q , the equations obtained are [20]:

$$\begin{array}{c}
 \text{d axis} \\
 \left[\begin{array}{c} u_d - \omega \psi_q - r_a i_d \\ u_f - r_f i_f \\ -r_{kd} i_{kd} \end{array} \right] = \left[\begin{array}{ccc} (L_{md} + L_a) & (L_{md}) & (L_{md}) \\ (L_{md}) & (L_{md} + L_{kf} + L_f) & (L_{md} + L_{kf}) \\ (L_{md}) & (L_{md} + L_{kf}) & (L_{md} + L_{kf} + L_{kd}) \end{array} \right] \left[\begin{array}{c} i_d \\ \frac{d}{dt} i_f \\ i_{kd} \end{array} \right] \\
 \\
 = [L_d] \frac{d}{dt} \left[\begin{array}{c} i_d \\ i_f \\ i_{kd} \end{array} \right]
 \end{array}
 \tag{3.3.1}$$

q axis

$$\begin{bmatrix} u_q + \omega\psi_d - r_a i_q \\ -r_{kq} i_{kq} \end{bmatrix} = \begin{bmatrix} (L_{mq} + L_a) & L_{mq} \\ L_{mq} & (L_{mq} + L_{kq}) \end{bmatrix} \frac{d}{dt} \begin{bmatrix} i_q \\ i_{kq} \end{bmatrix} = \mathcal{L}_q \frac{d}{dt} \begin{bmatrix} i_q \\ i_{kq} \end{bmatrix}$$

3.3.2

Additional windings on the axes may, of course, be incorporated by suitably modifying equations 3.3.1 and 3.3.2.

Note that the current directions are chosen positive into the machine, and thus would be positive for motor operation. The i_d would reverse and be negative for generator operation. The motor convention has been used in order to make the resultant equations symmetrical (otherwise the matrix would have terms like $L_a + L_{kd} - L_{md}$, etc., which do not treat all the machine coils identically).

Equations 3.3.1 and 3.3.2 may be written as:

$$\frac{d}{dt} \begin{bmatrix} i_d \\ i_f \\ i_{kd} \end{bmatrix} = \mathcal{L}_d^{-1} \begin{bmatrix} -\omega\psi_q - r_a i_d \\ -r_f i_f \\ -r_{kd} i_{kd} \end{bmatrix} + \mathcal{L}_d^{-1} \begin{bmatrix} u_d \\ u_f \\ 0 \end{bmatrix} \quad 3.3.3$$

$$\frac{d}{dt} \begin{bmatrix} i_q \\ i_{kq} \end{bmatrix} = \mathcal{L}_q^{-1} \begin{bmatrix} \omega\psi_d - r_a i_q \\ -r_{kq} i_{kq} \end{bmatrix} + \mathcal{L}_q^{-1} \begin{bmatrix} u_q \\ 0 \end{bmatrix} \quad 3.3.4$$

Noting that ψ_d, ψ_q are linear combinations of the currents, Equations 3.3.3 and 3.3.4 therefore are in the classical state variable form [28],

$$\dot{\underline{x}}_m = A \underline{x}_m + B \underline{u}_m$$

with

$$\underline{x}_m = \begin{bmatrix} i_d \\ i_f \\ i_{kd} \\ i_q \\ i_{kq} \end{bmatrix}, \quad \underline{u}_m = \begin{bmatrix} u_d \\ u_q \\ u_f \end{bmatrix} \quad 3.3.5$$

Saturation is included by making L_{md} and L_f as functions of the net magnetizing current $i_m = (i_d + i_f + i_{kd})$. Thus

$$L_{md} = L_{md0} k(i_m) \quad 3.3.6$$

where L_{md0} is the unsaturated magnetizing reactance, and $k(i_m)$ is the factor obtained by taking the ratio of ordinate to abscissa in the open circuit characteristic (Figure 3.3.2).

Modelling of the mechanical dynamics of the rotor and shaft was not required in much detail for this study, and so only a single

▽ DC SATURATION CURVE
 ○ XMD/XMDO

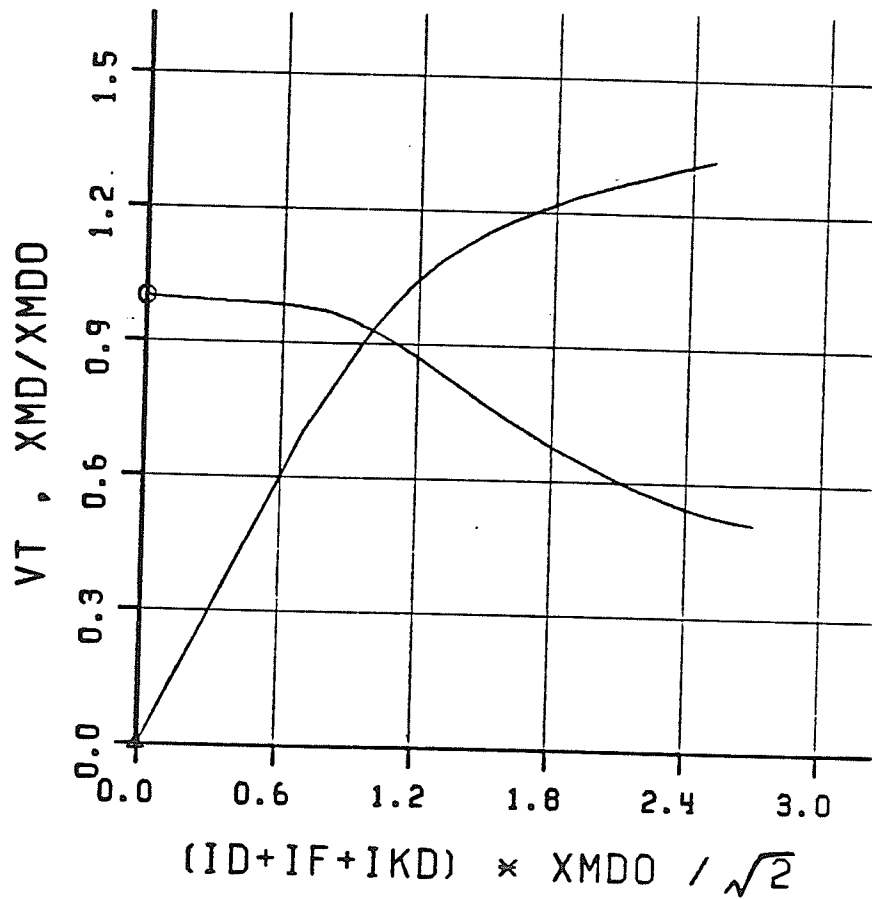


Figure 3.3.2: Kettle Machine Saturation Characteristics

lumped inertia with damping was included. With machine inertia constant H , rotor position θ , angular (electrical) speed ω , the relevant equation is (see Appendix 1 for per-unit system used):

$$\frac{2H}{\omega_0} \frac{d\omega}{dt} + \frac{D}{\omega_0} (\omega - \omega_0) = T_m - T_e$$

3.3.7

$$\frac{d\theta}{dt} = \omega$$

where ω_0 is the base angular frequency in rad/sec., H the p.u. inertia constant in (pu MW - sec) and D the frequency damping constant in pu MW/pu Hz (the $1/\omega_0$ multiplier ensures fractional angular speed instead of plain angular speed).

Equation 3.3.7 can be rewritten as:

$$\frac{d}{dt} \begin{pmatrix} \theta \\ \omega \end{pmatrix} = \begin{pmatrix} 0 & 1 \\ 0 & \frac{D}{2H} \end{pmatrix} \begin{pmatrix} \theta \\ \omega \end{pmatrix} + \begin{pmatrix} 0 \\ \frac{\omega_0}{2H} (T_m - T_e) - D \end{pmatrix}$$

3.3.8

which is, again, in the classical state variable form. Here, $T_m - T_e$, the difference between applied torque T_m and output torque T_e , is the accelerating torque, which causes change of angular speed. T_m is

accepted as input, and T_e is calculated from the flux linkage and currents as:

$$T_e = (\psi_d i_q - \psi_q i_d)/2 \quad 3.3.9$$

Equations 3.3.3, 3.3.4 and 3.3.8, when solved, yield all the state variables of the machine, from which any other quantity of interest, i.e. power, flux, etc., can be determined.

Although in this field overvoltage study a single lumped inertia has been considered, it may be necessary to include multiple lumped inertias in studies such as subsynchronous resonance. Then several equations of the sort 3.3.8 and 3.3.9 result, and can be added on to the machine model in a straightforward manner.

Also to be noted is that \mathbf{l}_d^{-1} and \mathbf{l}_q^{-1} in Equations 3.3.3 and 3.3.4 do not have to be evaluated by any numerical inversion procedure on \mathbf{l}_d and \mathbf{l}_q . Formulae for every element for \mathbf{l}_d^{-1} and \mathbf{l}_q^{-1} are readily precalculated by hand, and their numerical values easily evaluated during the run.

3.3.2 Interfacing with EMTDC

Digital machine models have been previously developed for transients simulation programs such as BPA's EMTP. They generally fall into two categories: (1) in which the machine is represented by a current source (utilizing the well-known 'compensation theorem' [26]); and (2) in which the machine is modelled as a Thevenin equivalent voltage source and impedance.

The present Universal Machine model (UM) available in EMTF [15] and others [19] fall into the first class of program, in which the machine is represented as a current source. There is a theorem in network theory, called the Compensation Theorem [26], which allows such a representation. The approach used by the author (described in section 3.3.1) utilizes terminal voltages to calculate currents to be injected, and hence falls in this class. This class of models has the drawback, that for stable solution, each machine has to be computationally 'far' from other machines or nonlinear sources. This is achieved by separating subsystems containing machines from other such subsystems by distributed parameter transmission lines [29], which are essentially time delays. Since the machine is represented by a current source which is dependent on past voltages (in the previous time-step), any sudden change in voltage causes a current response only in the next timestep. Thus, for the previous timestep, the machine looks like an open circuit (as it does not respond with new current till later). The cumulative effect of many machines causing this error in the same subsystem simultaneously can be de-stabilizing, and hence the reason for the above-mentioned restriction. The author has overcome this drawback by one solution to be discussed later, and hence the EMTDC machine program (called MAC100) does not have the restriction of the BPA-EMTF models discussed above.

The second approach of modelling the machine as a Thevenin equivalent, due to Brandwajn et. al. [30], does not suffer from the drawback because the machine impedance is included in the Y matrix (see equation 3.2.3) of the main system, and the system current response (solution of 3.2.3) calculated in the same time-step. However, since

the machine impedance changes with rotor position, a straightforward solution would involve a changing system Y matrix which would have to be inverted each time the rotor position changed. Brandwajn has overcome this problem by modelling this changing impedance with a fixed and a variable part, with the variable part approximately included in the Thevenin voltage source.

The method used here utilizes terminal voltage values of the machine in previous time intervals, and calculates (using equations 3.3.3 and 3.3.4) the new machine currents, and hence belongs to the first class. The integration method used is the trapezoidal rule, but any other method could be used, as could be any integral or subintegral timestep of the timestep used in the main (EMTDC) program. Here lies the advantage of this approach (type 1), in that the machine model interfaces with EMTDC as a controlled current source, and is never a part of the EMTDC main matrix. Therefore machine parameters can even be changed in the middle of a run (if so desired), without affecting the main EMTDC matrix in any way. Figure 3.3.3 explains the interfacing with the use of a block diagram.

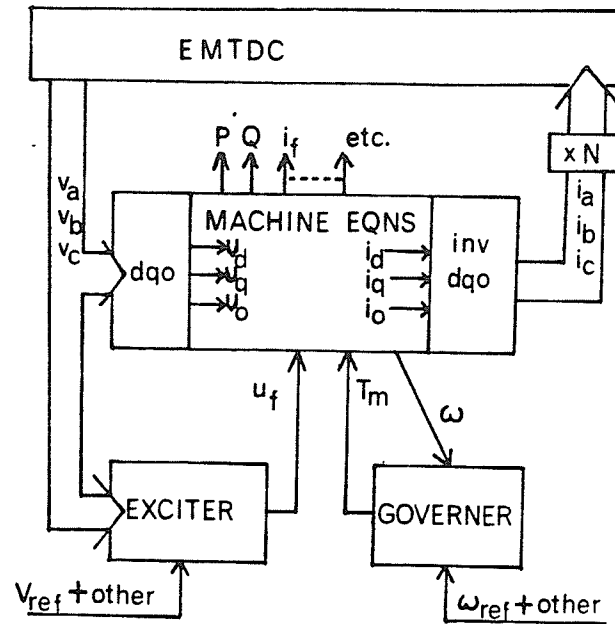


Figure 3.3.3: Modelling scheme for the ac machine.

A number of machines operating in coherence (such as all the machines at one plant) can be modelled as one machine, by utilizing a multiplying factor 'N' as shown in Figure 3.3.3. This 'N' can be changed any time during program execution. Another advantage of this approach over others which include the machine as electrical branches in the main program, is the fact that it does not increase the complexity of the main system matrix.

Figure 3.3.3 also shows how other system components such as governors and exciters can readily be interfaced with the machine and main system.

The approach described so far (in Figure 3.3.3), at first glance seems to have the drawback of the type (1) models mentioned earlier, which approaches incorporating the machine as a part of the main matrix (type 2) do not. This is, that the machine current to be

injected into the network is calculated only in the next time step in response to the machine terminal voltage of the previous step. Thus, if there is a step change in machine terminal voltage, say due to a lightning surge, the machine will not respond with current till a time-step later, and consequently appears as an open circuit for the duration of the first timestep. Thus, spurious spikes may appear in the machine terminal voltage. This drawback is overcome in the following way:

- (i) A resistance $r'' = 2\ell''/\Delta t$ is calculated, where ℓ'' is the subtransient machine inductance, and is placed from each node of the machine terminal to neutral as in Figure 3.3.4. This resistance becomes a part of the main (EMTDC) network

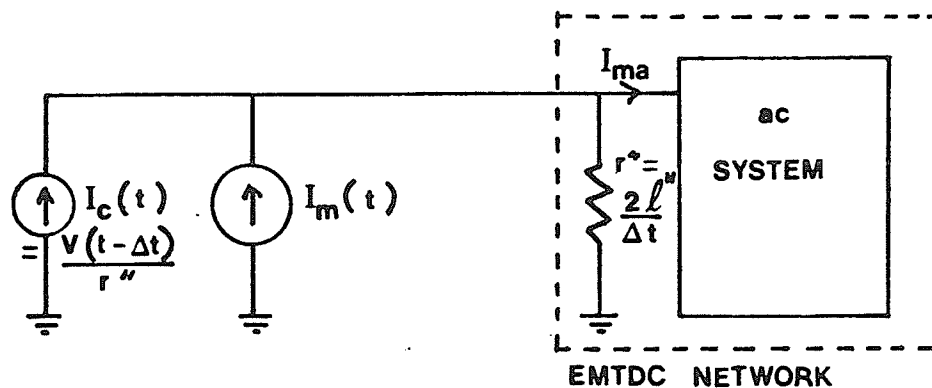


Figure 3.3.4: Terminal interface.

- (ii) Then, instead of injecting the calculated current $I_m(t)$, a compensated current $I_m(t) + I_c(t)$ where

$$I_c(t) = V(t - \Delta t)/r''$$

is injected, where $V(t - \Delta t)$ is the terminal voltage

in the previous timestep. Thus, the actual current injected into the network is not the calculated current

$I_m(t)$, but $I_{ma}(t)$ where

$$I_{ma}(t) = I_m(t) + \frac{(V(t - \Delta t) - V(t))}{r''}$$

Now r'' is quite large, because of the Δt in its denominator. Also, for a small timestep $V(t - \Delta t) \approx V(t)$, and thus $I_{ma}(t) \approx I_m(t)$, and the error introduced vanishes in the limit with a small Δt .

- (iii) However, for a sudden change, as $I_m + I_c$ is not calculated until the next time step, the network sees an impedance r'' for this instant, instead of the open circuit discussed earlier. This is exactly the instantaneous impedance it would have seen had the machine been represented by its subtransient reactance ℓ'' in EMTDC. Therefore, the network current calculated in this instant is more accurate, and the spurious spikes discussed earlier do not arise. Thus this concept of terminating the machine with its 'characteristic impedance' and then compensating for this in the current injection, is a convenient way for assuring accurate solutions.

This feature was introduced into the model later. In earlier simulations, the machine terminals were required to be connected to ground through a capacitor to prevent spurious spikes. Also, with nothing connected at the machine terminals, the solution would go unstable (i.e., for the open circuit condition). With the above-introdu-

ced modification however, the behaviour of the machine model has been uniformly good. There is also no restriction on having more than one separately modelled machine in the same subsystem, which is a restriction in other models of this type [15].

3.3.3 Starting Up

Time domain simulation of networks on the computer is extremely time consuming. Hence, it becomes necessary to 'plug-in' steady state solutions into the machine model. Such steady state solutions could be obtained for example, from a load flow. This is easily accomplished because the storage locations (discussed in Sec. 3.3.2) of the machine model include the state variables -- the axis currents and rotor angle, which may be loaded with their steady state values, before commencing the run. However, it is difficult to specify initial values on all network elements in EMTDC, especially when dc bridges are involved, which generate harmonic currents that significantly affect the steady state (60 Hz) values calculated from the load flow.

The following techniques have been used in starting up the system:

- (a) For systems involving machine models only as sources:
 - (i) From a load flow, obtain the steady state voltage magnitudes and angles all over the network.
 - (ii) Obtain machine internal angles from real and reactive power and terminal voltages of the machines. Figure 3.3.5 shows how this is done graphically, the procedure is actually carried out on the computer, however. The diagram is drawn

for the generator convention, i.e. current out of the machine is considered positive.

First calculate the armature current $I_a = \frac{P-jQ}{V_t}$.

Then locate the quadrature axis q by taking the phasor voltage: $V_t + jX_q I_a$. The angle δ thus formed between V_t and the q axis is the machine load angle with respect to the terminal bus angle. This is strictly true only in the case of a machine without saturation, but δ obtained in this way when plugged into the machine with saturation, does not give significant errors.

- (iii) Start the system up, with all machine rotors running exactly at synchronous speed, with the above calculated angular differences. Let the exciters control the machine terminal voltages to those obtained from the load flows. Soon, the steady state will be reached, at which time the inertias are released, and the machine torques are now controlled by the governors. It is not wise to include governor dynamics up to this point on account of the large time constants involved. Initial conditions on governors are however continually being updated during the run-up period, so the governor is ready-to-go the instant it is released.

(b) For systems involving machine models as well as Thevenin equivalent sources:

(i) The machine model allows specifying the number of machines at one plant. If this number is specified as zero (0), then the machine model calculates its internal currents etc., for the given terminal voltage applied, but this is not injected back into the network. Thus, using the steps as in part (a) above, the machine is started up with the number of machines specified as zero. When the machine internal voltage (E_f in Figure 3.3.5) becomes equal to its desired value (again, calculated from load flow and Figure 3.3.5), the number ($N = 0$) of machines is now changed to the desired number ($N = n$). The solution then quickly settles to its desired value.

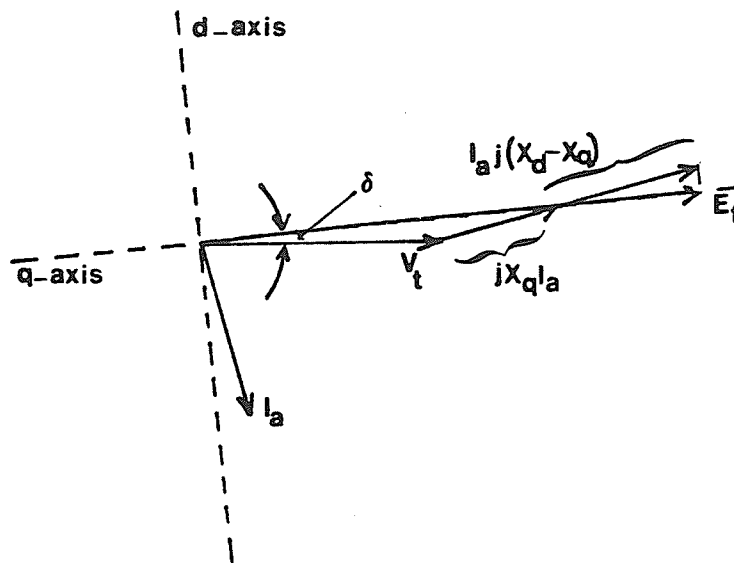


Figure 3.3.5: Obtaining the machine angle
(Figure in generator convention).

3.4 Modelling of Exciters and Governors

As mentioned in the introduction to this Chapter, functions such as $\frac{1}{1 + sT}$, $\frac{1}{s}$, $\frac{1 + sT_1}{1 + sT_2}$, are available to the user using EMTDC. These are analogous to the functions available in IBM's CSMP and the TACS feature of BPA's EMTD programs. Using these building blocks, any given control system may be modelled. The exciter and governor models used in this study are shown in Figures 3.4.1 and 3.4.2 respectively.

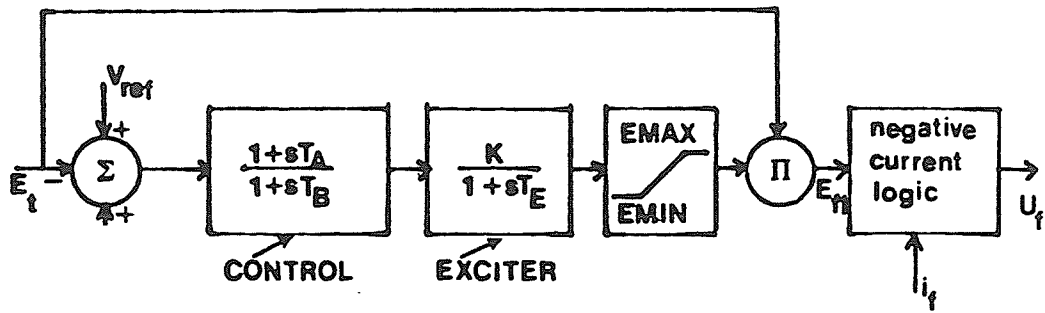


Figure 3.4.1: Exciter Model (Solid State Exciter)

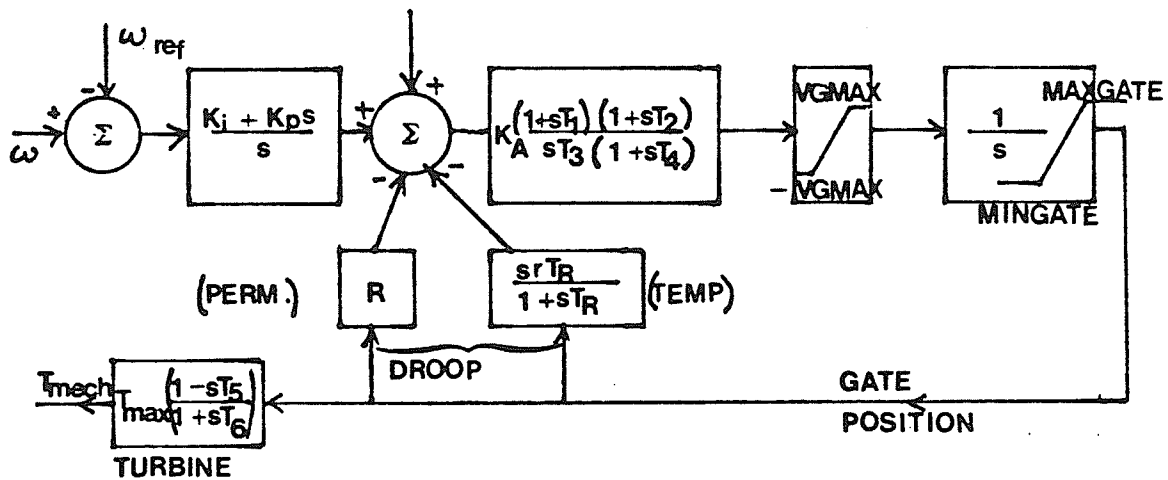


Figure 3.4.2: Typical Governor Model

The exciter model consists of a cascade of a reference voltage and actual voltage comparison block, followed by a control system representation, followed by an exciter time constant, with upper and lower limits. This is followed by a block which computes different field voltages at the output, depending on whether the exciter can or cannot carry reverse current. In the case of an exciter without reverse current capability, the voltage U_f of Figure 3.4.1 is either

equal to E_{fl} or equal to $R_{rev} \cdot I_f$ depending on whether the current is in a positive or a negative direction. (Here R_{rev} is the reverse resistance of the bridge.) Figure 3.4.2 shows the governor used, with a speed sensing circuit, a gate control circuit followed by a gate position integrator, and with a droop [22] in the characteristic. The hydro turbine is modelled as a non-minimum phase leadlag function, and mechanical torque is the output from this model. Typical values for the various block parameters are mentioned wherever used (i.e., Chapters 4 and 5) and Appendix II.

Both these models have the feature of being able to be kept dormant during program run-up (to steady state) conditions, in which all state variables are kept continuously updated, so that they may be switched on at any instant. For example, in the governor model, the machine is kept running at 377 rad/sec until the steady state solution is obtained. During this time, the mechanical torque T_{mech} required for the machine to be kept at this speed is calculated (i.e. $T_{mech} = T_{elec} + T_{loss}$, where T_{elec} and T_{loss} are electrical and loss torques), and the various integrators given the appropriate computed steady state values.

3.5 Modelling the dc Bridge [14]

This model was developed by D. Woodford at Manitoba Hydro, and is mentioned here only for completeness, as it was used in the author's simulations.

Just like the machine model the dc bridge interfaces with the ac system as a current injecting source. Onto the dc line, it interfaces as a dependent voltage source. This is shown in Figure 3.5.1.

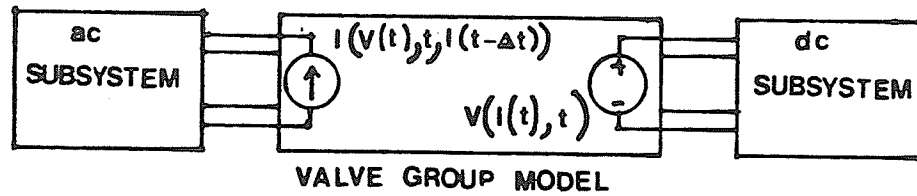


Figure 3.5.1: Interfacing the valve group model.

The ac injected current vector \underline{I} is calculated from the state equations of the valve group, and is dependent on previous time instant currents and present ac voltages. Likewise the applied dc voltage \underline{V} is similarly calculated. Internally, each thyristor valve with its RC snubber circuit is modelled as in Figure 3.5.2 (b). In the off state $R_v = R_d + \Delta t/2 C_d$ (R_d , C_d the snubber resistance and capacitance, and Δt the internal timestep respectively). In the on-state, R_v is replaced with the forward resistance of the thyristor, typically 1Ω .

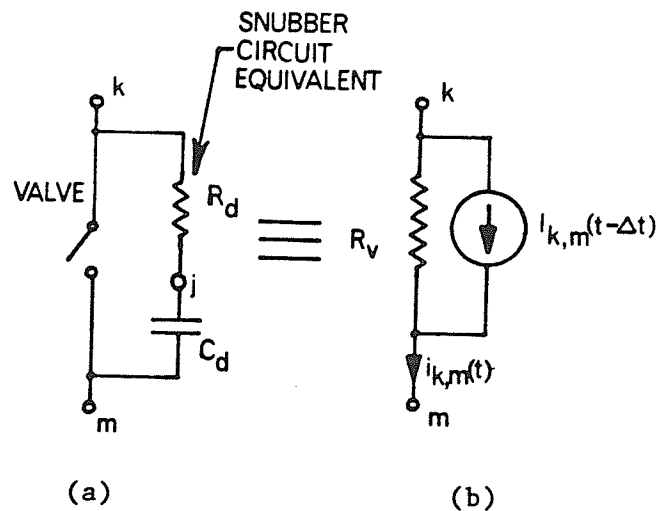


Figure 3.5.2: Equivalencing and reduction of converter valve.

Likewise, the internal current source $I_{km}(t - \Delta t)$, is suitably controlled by the proper switching logic to assume on and off state values. Thus, the internal valve group model remains unchanged, only the component values being variable, dependent on the thyristor states. Thus, there is no need to define separate modes of operation (i.e., different circuits), and switch from one mode to another as thyristors switch on and off. In this case, the algorithm is completely automatic, and thus commutation failure and other non-standard modes are automatically obtained if the conditions are proper for their occurrence.

The valve model of Figure 3.5.2 then replaces each valve in Figure 3.5.3, which shows the complete six pulse valve group. The ℓ 's are the commutating inductances, and the e 's the predicted commutating voltages (e 's are not the same as primary side converter transformer voltages, because the Y-Y or Y- Δ connections of the transformer windings are taken into account while calculating them).

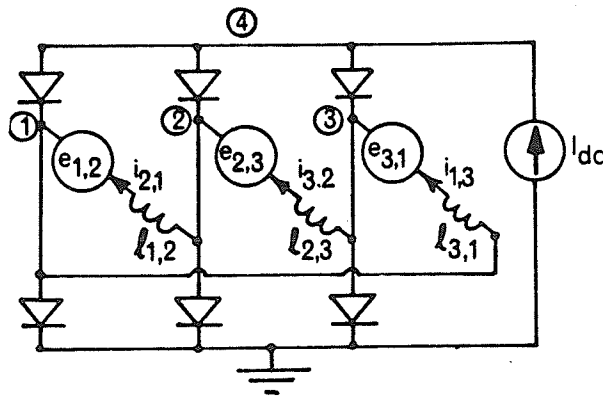


Figure 3.5.3: Six pulse valve group subnetwork equivalent circuit.

Converter saturation is taken into account by adding an additional flux dependent saturation current to the current computed by the linear part of the model.

Controls: DC link controls can be written in any desired form, using the CSMP type functions available under EMTDC.

In this program, the phase locked loop method of generation of firing pulses was used. In this scheme, a phase locked loop oscillator [31] tracks the commutating bus voltage frequency, and hence provides a timing reference for applying firing pulses. The actual firing angle desired is obtained from a pole controller which determines the firing angle for an entire HVDC pole (which may have more than one series valve group). This firing angle order is then processed by a valve group controller which somewhat modifies this order, and feeds it to the main valve group firing control (which uses the phase locked loop for timing reference, and computes elapsed angle based on its internal frequency which is locked with the commutating bus frequency).

Figure 3.5.4 shows a typical pole controller of the type used in these simulations. The controller, using proportional-integral control, generates a firing angle command α_{desired} , which controls the dc current to be equal to the desired current, or within a desired margin (if $I_m \neq 0$).

Figure 3.5.5 shows a valve group controller to which the α_{order} of Figure 3.5.4 is fed. If the valve group is in normal rectifier mode, the 'whichever is least' block selects the α_{order} from the pole controller and delivers it to the firing control electronics. If the valve group is in inverter operation with constant extinction angle

control [31], then the 'whichever is least' block selects the α_{order} from the upper circuit. This circuit monitors the extinction angle (γ measured), selects the lowest over a period of a cycle, and generates a γ_{desired} order. γ_{desired} is equal to γ_{min} if $\gamma_{\text{measured}} > \gamma_{\text{min}}$. However, if $\gamma_{\text{min}} > \gamma_{\text{measured}}$, the γ_{desired} is advanced to $\gamma_{\text{min}} + \gamma_{\text{measured}}$, to bring the extinction angle quickly back out of the dangerous area. The actual firing angle $\alpha = \pi - \beta$, is determined by solving the equation [31].

$$\cos \gamma \approx X_{\text{com}} I_d + \cos \beta \quad (3.6.1)$$

where X_{com} is the commutating impedance. These two are just the control blocks used by the author. EMTDC allows construction of any type of block diagrams for the firing order devices, by using the CSMP type functions.

3.6 Model Capabilities

A number of tests have been carried out to test the various models described above. The machine model has been compared to an actual laboratory machine, and the results have proved to be accurate, as seen by the tests of section 2.8. Ordinary phasor models of the machine (which exclude the rate of change of flux terms — see section 3.3) would not have shown the harmonics induced in the field circuit.

Some other simulations not directly related to the problem at hand, but which nevertheless demonstrate the versatility of the modeling scheme are briefly presented below:

(a) Modelling Manitoba Hydro's HVDC System

For this simulation, Manitoba Hydro's Nelson River Bipole I

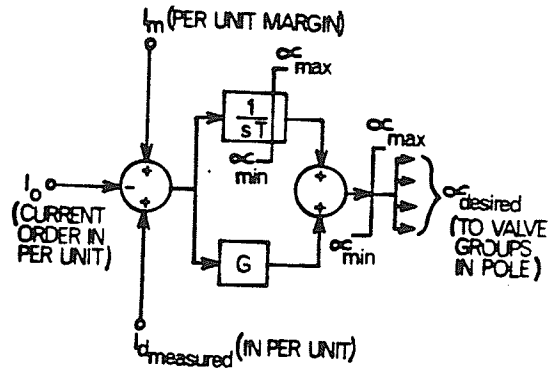


Figure 3.5.4: Basic Pole Controller (14)

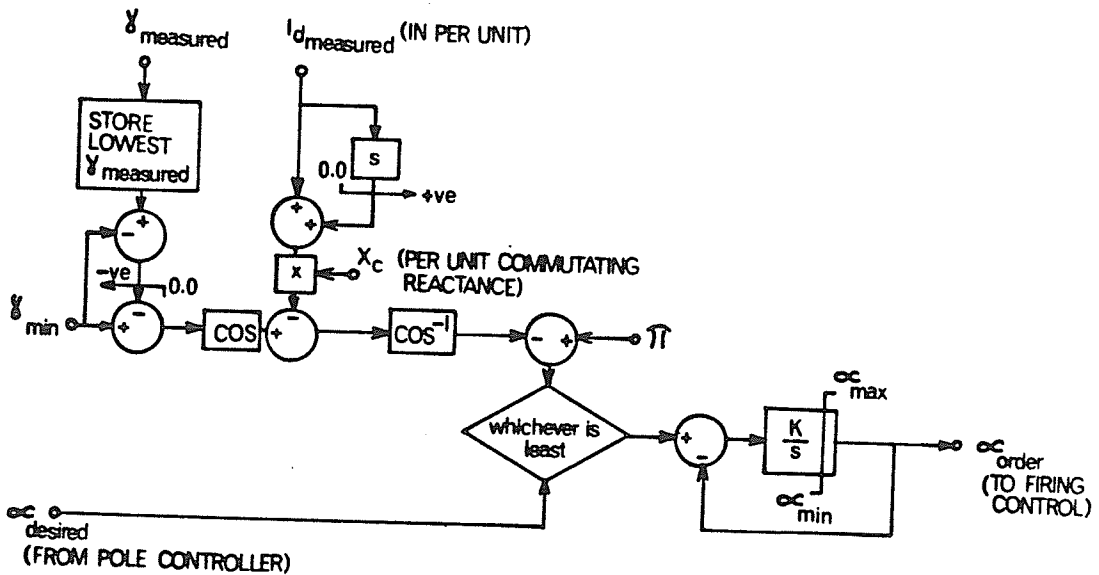


Figure 3.5.5: Basic Valve Group Converter for Rectifiers and Inverters (14)

HVDC transmission system was modelled as shown in the single line diagram (Figure 3.6.1). The sending end system was modelled with ac filters, and a Thevenin equivalent source representing the generating system. As the receiving end system was being studied, the synchronous condenser shown was modelled as a complete machine whereas the rest of the system was represented by a Thevenin Equivalent.

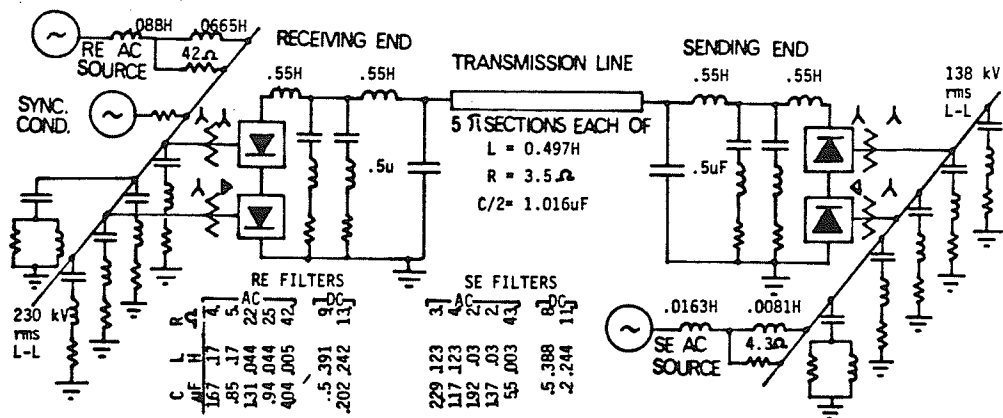


Figure 3.6.1: Test dc link model.

Because of interest in operation at low short circuit ratios, a value of 2.4 based on the synchronous condenser subtransient reactance X_d'' was selected for the inverter. For the purpose of this study, the short circuit ratio (SCR) is defined as:

$$SCR = \frac{2}{P_d \cdot Z} \quad (3.6.1)$$

where V = ac L-L rms commutating bus voltage in kV

P_d = dc power at the converter in MW

Z = ac system short circuit impedance at the commutating bus
in ohms per phase.

One test to demonstrate the use of EMTDC is to examine the question whether X'_d or X''_d [14] is the most significant parameter on which to base the calculation of short circuit ratios at the inverter bus, as it affects inverter performance during and after an ac fault. For this purpose, three models were used to represent the synchronous condenser in Figure 3.6.1:

- (a) a complete model including exciter and inertia
- (b) a simple Thevenin equivalent circuit with a fixed voltage source behind subtransient reactance X''_d
- (c) a simple Thevenin equivalent circuit with a fixed voltage behind transient reactance X'_d .

The simulations for each of the above cases representing the system of Figure 3.6.1 were carried out for a four cycle fault on the inverter ac bus. The dc current waveforms for these cases is shown in Figure 3.6.2. Figure 3.6.2 shows that the response of the system in which X''_d is used in the machine representation represents the fully modelled machine more closely than when X'_d is used.

This simple study using MH EMTDC indicates that X''_d rather than X'_d is the better representation for use in ac system short circuit ratio calculations so far as inverter performance during ac faults is concerned.

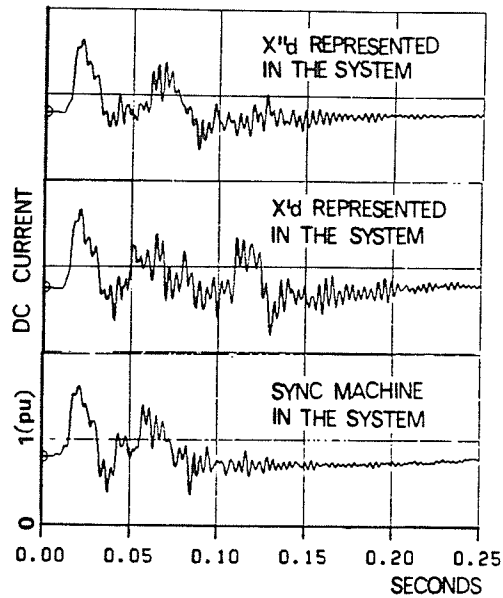


Figure 3.6.2: Simulated recovery of dc current after ac fault, for alternative representations of X''_d , X'_d and full machine model.

(b) Comparison With an Actual dc Link

A fault similar to one fault recorded for Bipole 2 of the Nelson River DC Transmission [7] was run for comparison with this model on MH EMTDC. The actual and simulated cases are shown on similar scale in Figure 3.6.3. It will be observed that there is more harmonic content in the simulated case compared with the actual. Since no attempt was made to provide any significant harmonic damping in the model, this case demonstrates the need for its consideration in digital simulation studies.

Taking the harmonic problem into account, it can be seen that the simulated model performance is reasonable and comparable when referenced to the performance of an actual dc link.

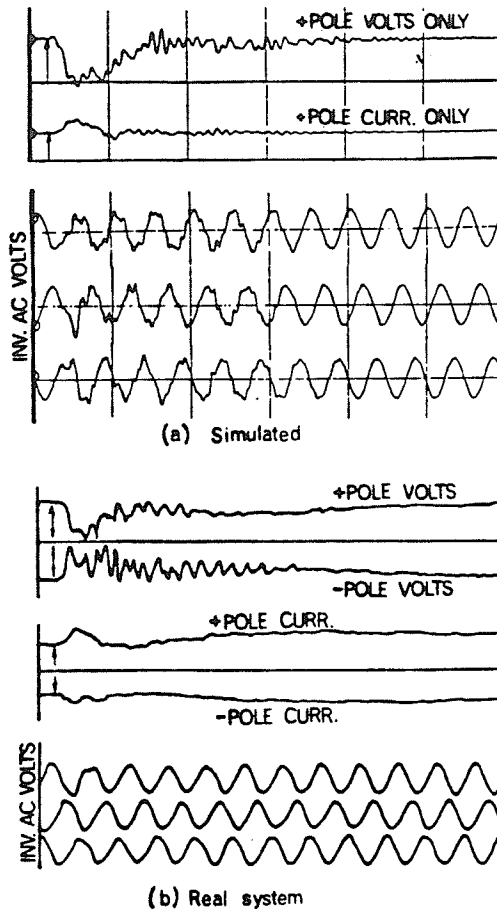


Figure 3.6.3: Comparison of Simulator Performance with a real system for an ac fault at the inverter.

Computer Running Times

With the system modelled in Figure 3.6.1 with synchronous condenser, represented fully, a one second simulation time with a twenty microsecond time step takes about twenty minutes of C.P.U. time on a PRIME 750 computer.

3.7 Chapter Summary

The EMTDC - modelling program developed at Manitoba Hydro provides a flexible base for easily doing a large number of transient solutions on various systems. Interfacing machine and valve group models, and their associated control circuits is also easily achieved. In particular, the machine model developed to interface with EMTDC is very well behaved as is evident from the fairly extensive testing and can do everything that can be done on sophisticated analog simulators (except, of course, the real time nature of the analog simulations) [33]. A fairly detailed system involving machines, valve groups, and transmission system also computes well and agreement with field observation is fairly close. In the following chapters, the models mentioned here are extensively used to study the exciter stress phenomenon, which is the main topic of this work.

CHAPTER 4

Realistic Capacitive Loads

4.1 Introduction

In Chapter 2, the basic phenomenon of exciter overvoltage on capacitively loaded machines was investigated with the load modelled as a capacitor. In this chapter, realistic capacitive loads are considered, and any deviation of the results from those of Chapter 2, recorded and explained. The different types of capacitive loads normally encountered in practice are the following:

- (i) Capacitor banks: these have been looked at in Chapter 2;
- (ii) Long transmission lines loaded below their surge impedance loading level;
- (iii) Machines at other plants being overexcited and hence pushing reactive power (VARs) into machines at the plant in question;
- (iv) Machines connected to dc converter stations, seeing the effect of the ac filters at the converter bus.

As was explained in Chapter 2, Section 6 the exciter overvoltage is caused by resonant L-C oscillations between the terminal capacitor load, and the machine's subtransient reactance x_d'' . Thus, the exact nature of the capacitive load has a bearing on this overvoltage, in that it changes the type of oscillation. For example, an ac filter, though capacitive at system operating frequency, can have many resonant frequencies when oscillations between machine and filter are

excited. Likewise, the capacitive loading due to long transmission lines could cause different frequencies of oscillation. In the simulations in this chapter, oscillations (and hence exciter overvoltage) due to long transmission lines was found to be similar to those in the purely capacitive case of Chapter 2. In the case of the filters, however, more than one frequency may exist in the post fault machine ac current, and consequently more frequencies may exist in the field circuit. Some of these frequencies are usually higher than those with a pure capacitor, and thus sharper overvoltage peaks might result in the field.

When VARs come into one plant from other machines, however, machine tripping at the plant causes no field overvoltage, because the internal voltages and angles change in a way so as not to cause the rapid negative field current transient.

Another aspect studied in this chapter is the effect of phase shifting due to machine terminal transformers, and the effect of a machine breaker opening phase by phase, as the current in the phase extinguishes. It is observed that the phase shift due to the star-delta machine transformer does not significantly affect the field transient. There is some difference observed when the breaker opening is modelled (instead of a sudden switching of all three phases, in which case the number of machines change instantaneously).

Also, comparison is made between the rejection of an actual dc converter load (thereby leaving the filter capacitance on the machine terminals), and the rejection of an R-L load simulating the actual dc converter at fundamental frequency. In the case of the actual dc load, harmonics caused by the dc converter injected into the

filters prior to the rejection cause a more severe field transient than is caused when the converter is modelled as a simple R-L load which cannot include the effect of these harmonics.

Again, as in Chapter 2, the effect of saturation is not modelled, so that comparison may be made with Figure 2.4.1.

4.2 Tripping of machines with different kinds of VAR loadings

In this section are considered the effects of one or more of several machines connected to purely reactive leading power factor (capacitive loads). These loads include long transmission line, ac filter and synchronous condenser type machine loads. In these studies, saturation has not been modelled so that comparison may be made with Figure 2.4.1, the case of the pure capacitance. As has been shown in Section 2.6, the modelling of saturation affects only the sustained field overvoltage, and not the initial one or two spikes of transient exciter overvoltage. The effect of exciters has also been considered. From the results of this section it appears that the long transmission line load is similar to a plain capacitor load but that an ac filter load causes different frequencies in the rotor field circuit. The machine load does not cause any rapid field transients. These cases are now discussed in detail.

4.2.1 Machines tripping on a long line

Figure 4.2.1 shows the case of three machines left connected to a long transmission line supplying approximately 130 MVAR.

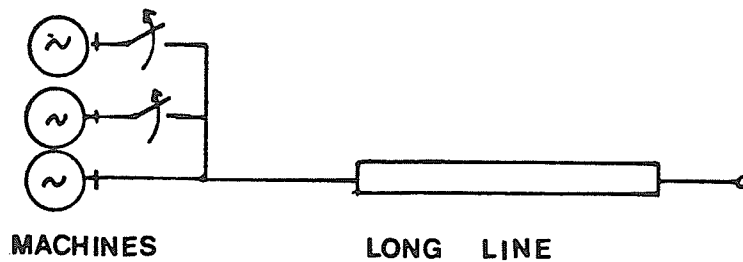


Figure 4.2.1: Machines tripping on long line.

The machine data is as in Table 2.1, Appendix II. Figure 4.2.2 shows the effect of two of these machines tripping off suddenly in a situation similar to Figure 2.4.1. The VAR loading in these two cases (i.e., that of Figure 2.4.1 and this one), are almost identical and after switching, sufficient to self-excite the machine. The machines are also identical. Comparison of Figures 2.4.1 and 4.2.2 show that the nature of the two responses is similar, except that because of the different resistive components of the two schemes, the self-excitation rates are somewhat different. (Originally it was desired to have the same resistance for a good comparison, but the transmission line chosen is a close approximation to Manitoba Hydro's Rosser-Dorsey line. Choosing too small a damping for the line would have realized unrealistic values for the line. Thus, values that were in the practical range were chosen, and contain more damping than just the pure capacitor case considered earlier.) Again, two frequencies can be noticed in the field current, corresponding to only one frequency in the rotor circuit. (These show clearly if negative current is allowed to flow in the exciter, but this is not shown in the figure.) Thus, for over-

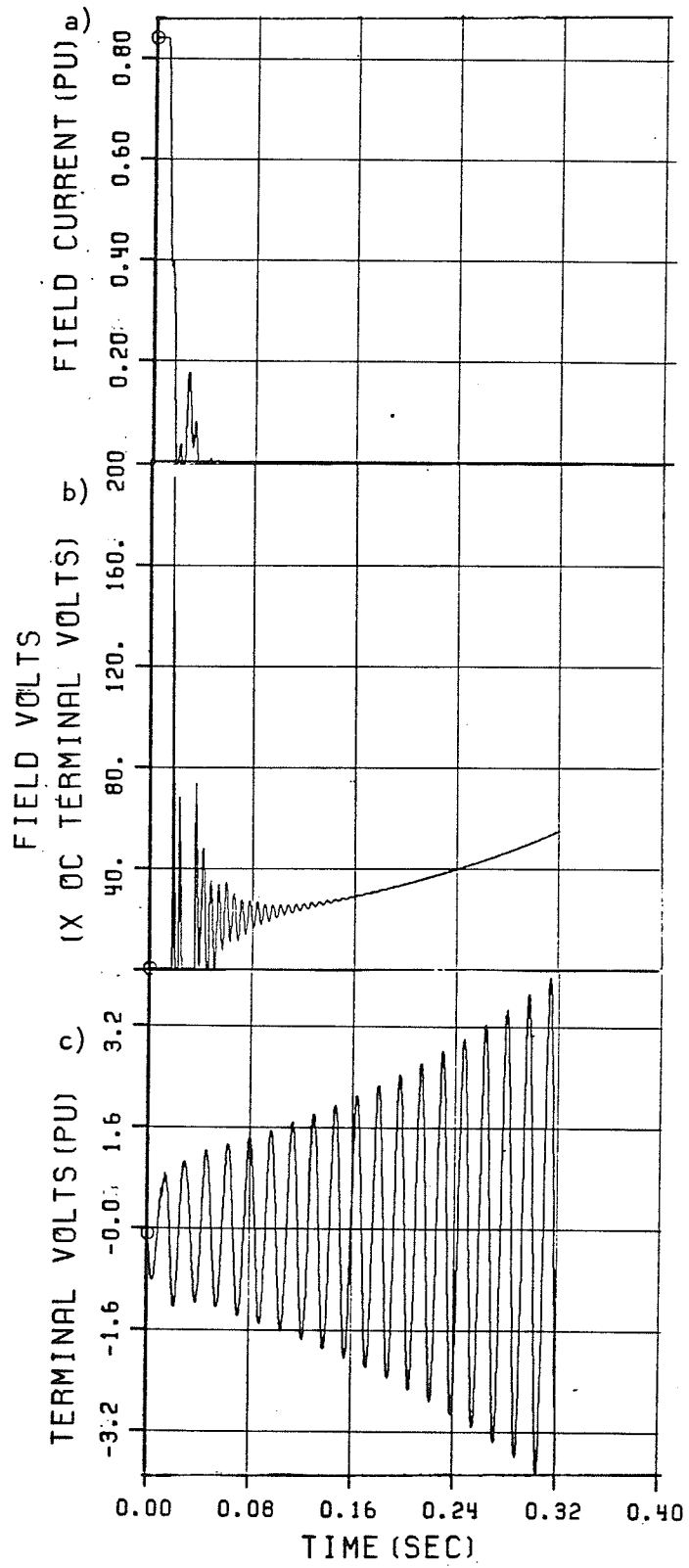


Figure 4.2.2 : Waveforms for Machines Tripping on Long Line.

for overvoltage calculation purposes, the long line may be treated as a pure capacitor. This is commensurate with the practice of considering the long line as a pure capacitor when calculating rotor currents and torques during studies of subsynchronous resonance [16].

4.2.2 VAR loading with machine (synchronous condenser) type VAR sources

Investigated now is the field current response when a group of machines absorbing VARs from other machines experiences the tripping of some of its machines. This situation is shown in Figure 4.2.3.

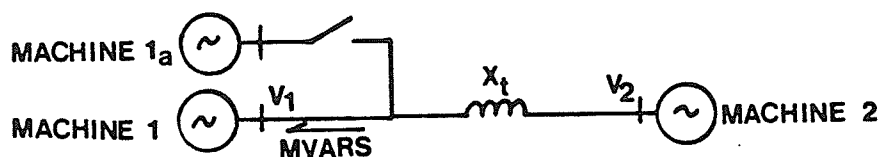


Figure 4.2.3: Machines tripping.

From here onwards, a slight correction is made to the machine data of Table A2.1 (Appendix II) in that $X_{md} = 0.94$ instead of 1.0.

(This was done as more accurate data became available.)

A simulation for a case such as in Figure 4.2.3 with the machines similar to those at the Kettle Generating Station, and the impedance $X_t = 0.15$ pu, was carried out. The two left-hand side machines were each loaded to 1.1 pu MVAR (into the machine), and 0.1 pu

real power. Governor dynamics were ignored, i.e. machine speeds were fixed to 377 radians/sec. This was done because the VAR loading effect was to be studied in isolation.

Figure 4.2.4 a shows the field current and MVAR responses of the machine remaining behind. As can be seen, though the original pair of machines was absorbing a total of 2.1 pu MVAR, the VARs suddenly adjust so that after one machine trips, the other machine (machine 1) absorbs only 0.95 MVAR. Consequently, it does not self-excite (as would be expected if the initial VAR loading were due to a capacitance), nor does the field current show any oscillations.

The above absence of self-excitation is explained by the fact that in the case of a pure capacitive load, the VAR absorption by the machine is (with machine voltage V_1 , capacitance C),

$$\text{VAR} = \frac{V_1^2}{\omega C}$$

and consequently

4.2.1

$$\frac{\partial(\text{VAR})}{\partial V_1} = \frac{2V_1}{\omega C}$$

i.e., as voltage increases, the VARs absorbed increase proportionately, causing a further buildup of voltage, this cycle, in the case of self excitation being a vicious spiral.

The VAR absorption by the left hand side machines (1 and 1a) of 4.2.3 is however [20],

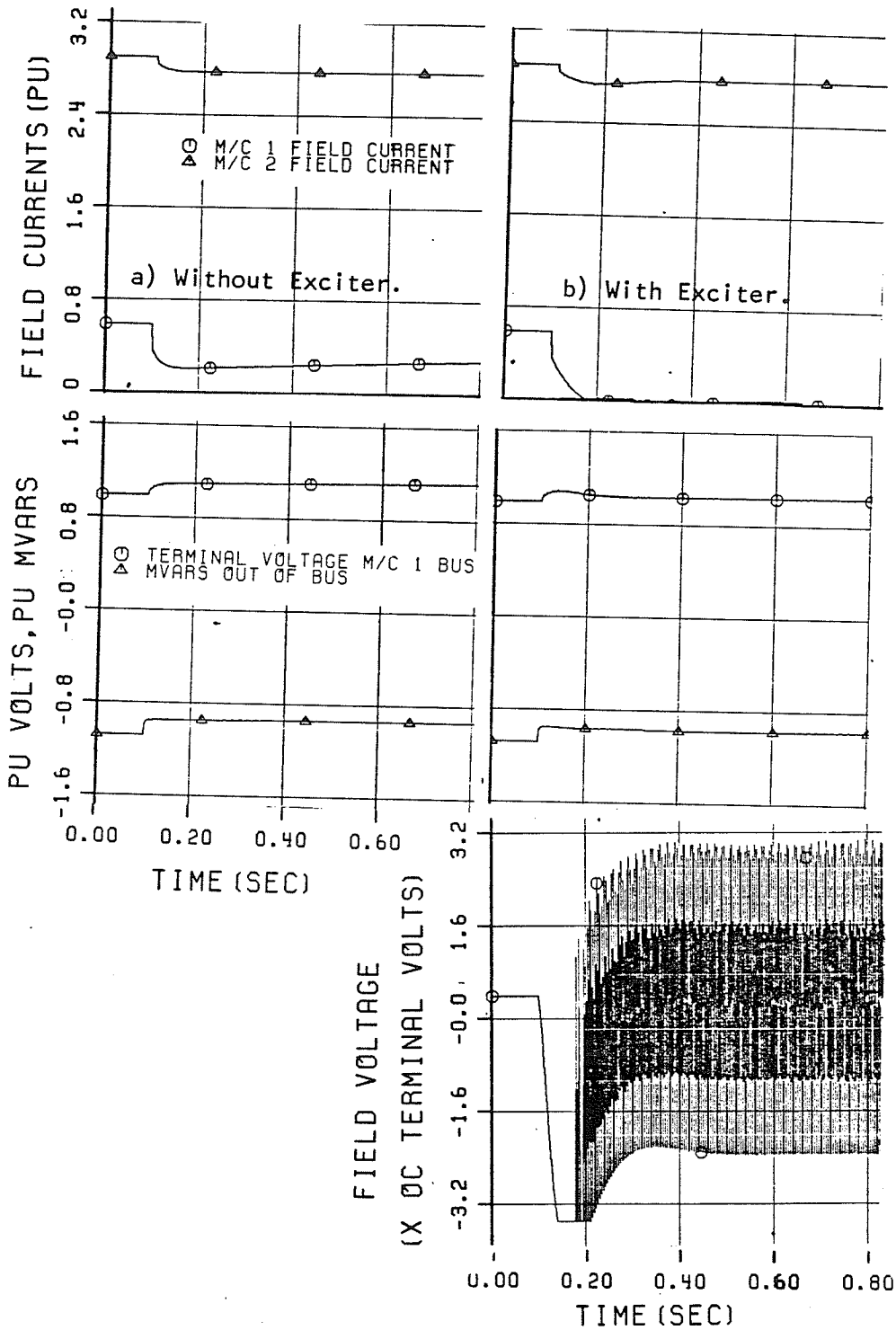


Figure 4.2.4: 1 of 2 Machines Tripping with 1.1 pu MVAR Loading From Other Machine

$$\text{VAR} = -\left[\frac{V_1^2 - V_1 V_2 \cos \delta}{X_t} \right] \approx -\frac{V_1(V_1 - V_2)}{X_t} \quad \text{for small } \delta$$

4.2.2

where V_1, V_2 are 1 and 2 bus voltage magnitudes, δ the phase angle difference, and X_t the line impedance between them.

Consequently,

$$\frac{\partial(\text{VAR})}{\partial V_1} \approx \frac{V_2 - 2V_1}{X_t} \quad . \quad 4.2.3$$

and thus, as the terminal voltage V_1 goes up, because $V_2 \approx V_1$, and hence $V_2 - 2V_1 < 0$, the VARs come down, and the self-excitation discussed above never occurs. Also, though the field current drops, it does not contain any L-C type oscillations as in the case of the capacitance and, consequently, its waveform is smooth. Figure 4.2.4 b shows the same situation as in Figure 4.2.4 a, except that the exciter has been modelled. Exciter parameters are as shown in Table A2.2 (Appendix II), and variable names are as in Figure 3.4.2.

In its attempt to control the terminal voltage, the exciter brings the machine field current right down to zero. Because of the modelling, intermittent current still flows in the field circuit (which has no reverse current capability, modelled by a large reverse field resistance). Some voltage chatter shows up on the field voltage waveform, which is probably more a numerical phenomenon than reality. Anyway, its magnitude is negligibly small, well within exciter ceiling voltages of +5 and -3.5 times nominal field voltage.

This section shows how important it is to include different kinds of VAR sources. The total VARs entering a generating plant may be from other machines or from reactances (capacitors or filters). It is not adequate to lump all these VAR sources into one equivalent capacitance because though they all cause the same equivalent steady state response, i.e., initial value of field current and so on, they all behave differently during transients. Manitoba Hydro's Northern Collector system is one example of this sort, in which VARs entering the machine are the sum total of ac filter generated VARs and VARs from the other generating plant, minus the VAR consumption of the dc rectifiers.

4.2.3 Effect of VARs due to ac filters

This situation can result if a generating plant connected to an HVDC rectifier station experiences tripping of some of its machines, after being left connected to the ac harmonic absorbing filters present on the rectifier bus as shown in Figure 4.2.5. For steady state VAR calculation purposes, these filters (which are tuned to harmonic frequencies such as the 5th, 7th, 11th, 13th, etc.) are treated as capacitor loads, because at fundamental frequency their impedance is purely capacitive. However, the machine-filter oscillations are quite different from the machine-capacitor oscillations of section 2.6.

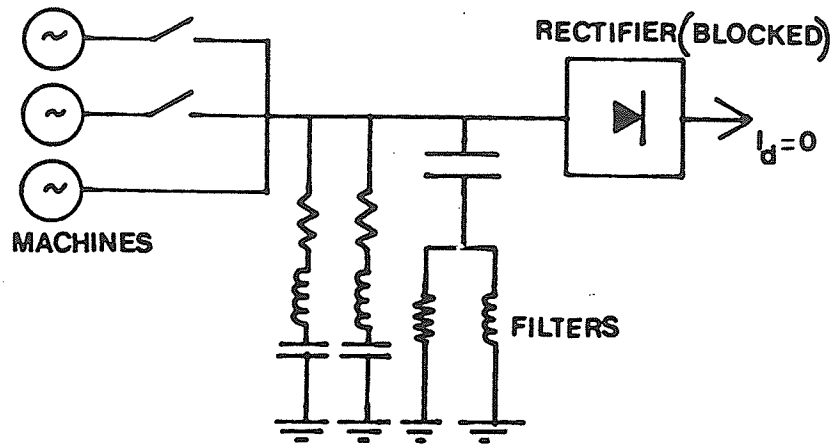


Figure 4.2.5: Machines isolated onto ac filters.

This can be explained by means of Figure 4.2.6 which shows a typical impedance plot for a 5th and 7th filter. Superposed on it is the machine subtransient inductance's impedance as a function of frequency. As can be noticed, there can now be two resonant frequencies f_1 and f_2 , instead of the one in the case of a pure capacitor, and hence four frequencies ($f_1 \pm f_0$, $f_2 \pm f_0$ with $f_0 =$ fundamental frequency) in the field circuit, as from the arguments of section 2.6.

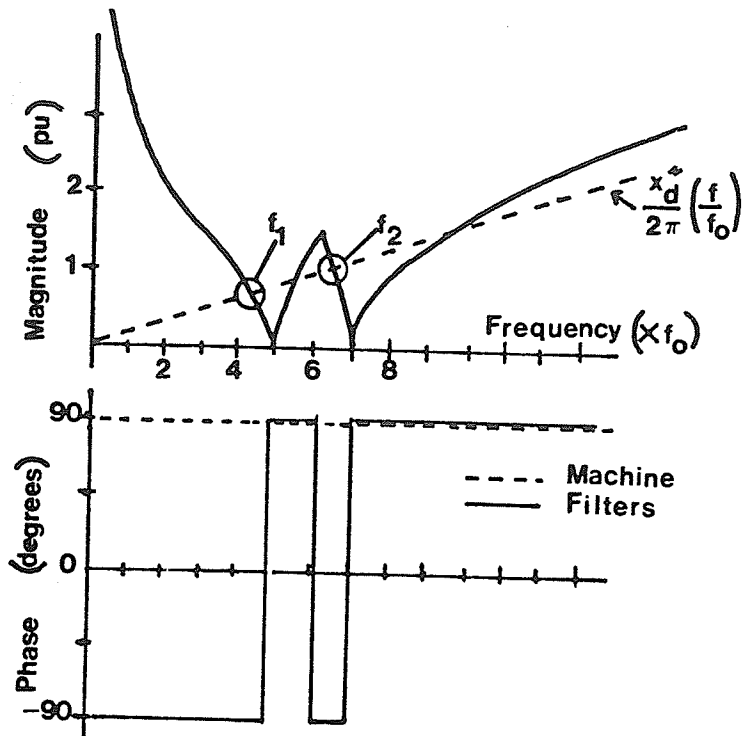


Figure 4.2.6: Typical impedance plots of machine and filter with 5th and 7th filter.

Figure 4.2.7 shows the field current, voltage and terminal voltage for the case of Figure 4.2.5, with two out of three machines tripping when connected to 5th, 7th, 11th and 13th filters constituting a total of 0.88 pu MVAR at fundamental frequency. (The machine data is as given in Table 2.1, for the Kettle machines, but with $X_{md} = 0.94$ and not 1.0).

The presence of different frequencies in the field overvoltage (as compared to Figure 2.4.1) can be seen. The peak overvoltage magnitude is also different from that of Figure 2.4.1, which models a somewhat identical situation. The presence of higher frequencies in the field current response may cause rapid rates of rise of the field overvoltage, which may be too fast for the exciter overvoltage arrester, thereby resulting in a possible exciter thyristor breakdown.

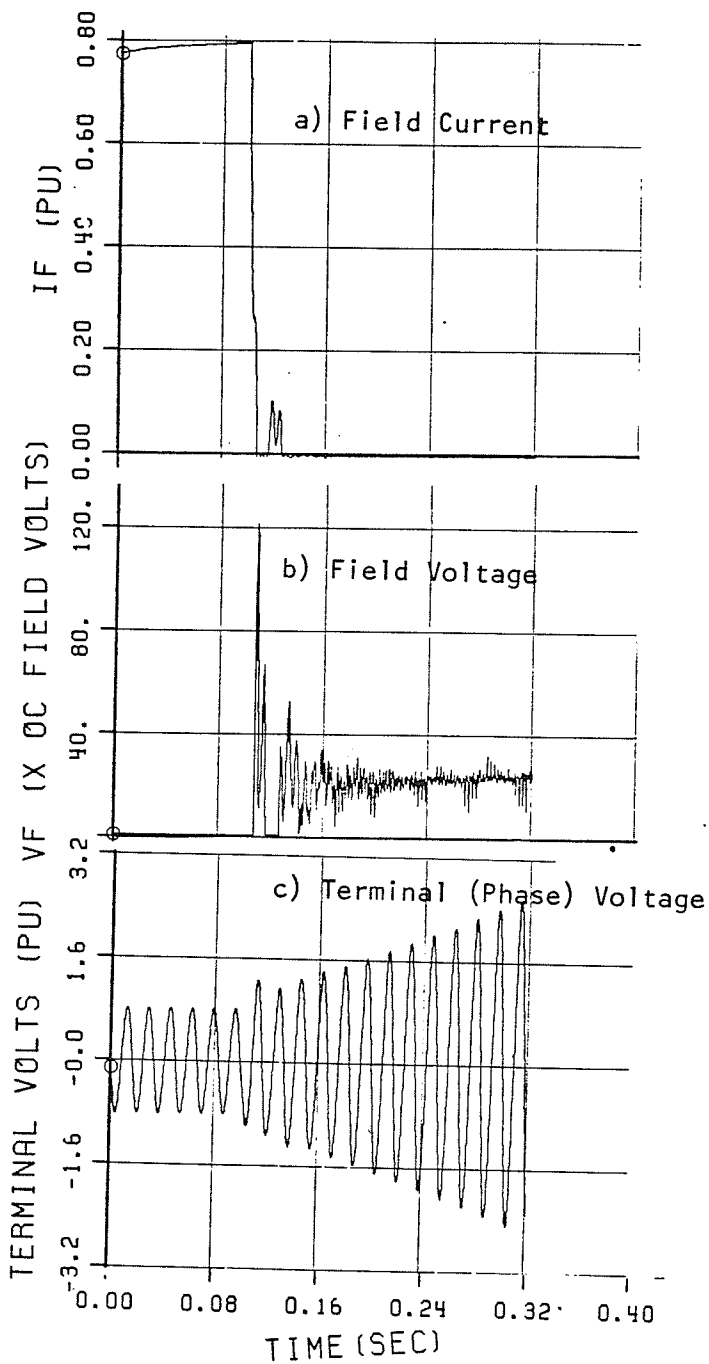


Figure 4.2.7: 2 out of 3 Machines Tripping when Connected to 0.88 pu Filter Load Comprising of 5th, 7th, 11th and 13th Harmonic Filters

Thus, once again, this exercise shows that for proper simulation of exciter overvoltage, it is necessary to model the ac system completely, and not as an equivalent capacitor.

4.3 Machines Connected to dc Converters

In this section, the contents of section 4.2.3 are expanded further. The effect of a dc load rejection is studied, as is the effect of the machine transformers that always isolate the machines from the system. Also, the effect of a machine breaker opening phase by phase is looked at. The conclusions of this section show that the actual modelling of the dc converter gives different results from when it is modelled as an R-L load, and so does the effect of the phase by phase opening of the machine breaker, when compared with an instantaneous switching action. Star-Star and Star-delta transformers on the machine terminals, however, do not cause significant differences in the field current response. In this section the modelling is fairly complete, with the machine saturation and exciter dynamics included. Exciter data as in Table A2.2, Appendix II.

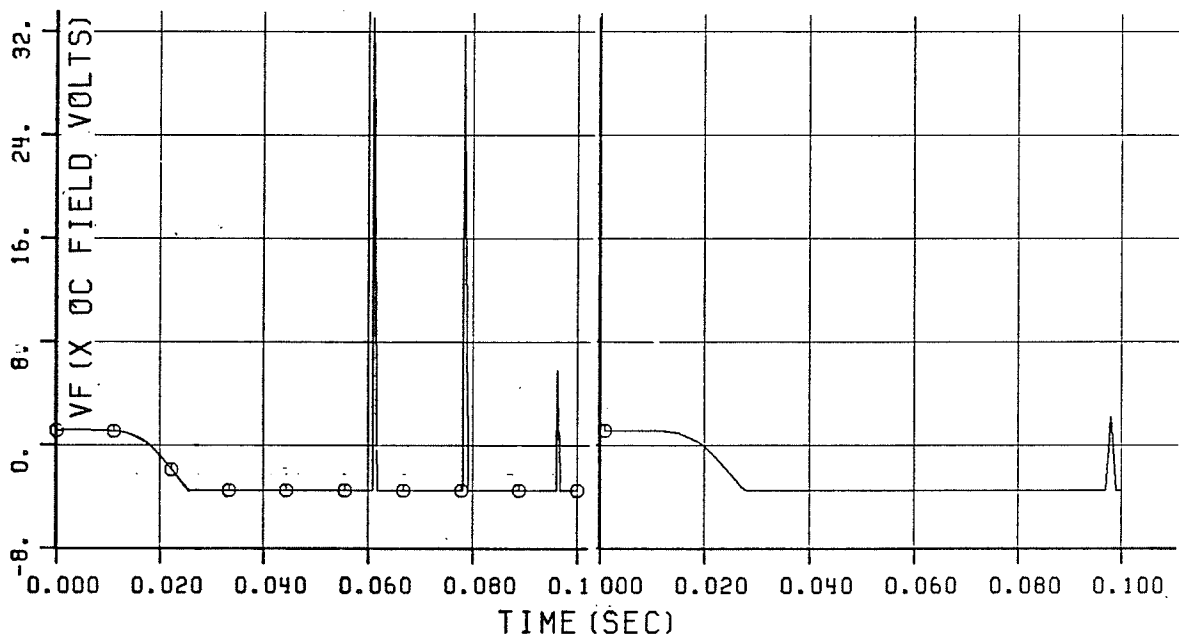
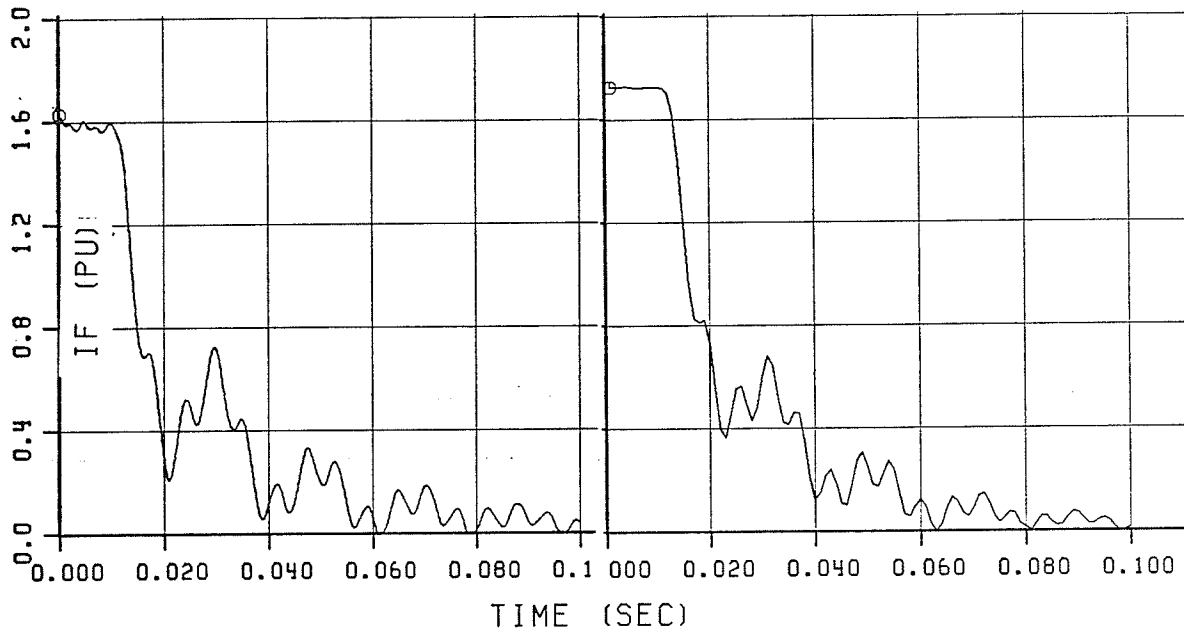
4.3.1 Comparison of actual dc load rejection with R-L load type dc load approximation

When operating in the steady state, the HVDC converter behaves as a real plus reactive power load, as far as power transfers at the fundamental frequency are concerned, and hence may be modelled as an R-L load. However, the dynamic behaviour of the converter under transients is quite different from the dynamic behaviour of a parallel R-L load, due to the different dc control strategies in use. Also,

more importantly, the actual dc converter is a source of harmonics and hence the ac filters at the converter bus are loaded with these harmonics even in the steady state. Thus the filter initial conditions just before the commencement of the transient are quite different from those that would be observed with the converter replaced by an R-L load. (In which case the initial loading is purely due to fundamental frequency voltage, there being no source of harmonics.)

For the purpose of comparison, the system was set up as in Figure 4.2.5, except with only one ac machine, and with full dc converter modelling (as in Section 3.5). The equivalent fundamental frequency loading of the converter was 104 MW and 66 MVAR.

Figure 4.3.1 a shows the corresponding field current and field voltage responses. (In this case, the MVARs are not exactly sufficient to self-excite the machine, but are quite close to this point.) Note the spikes of overvoltage in the exciter output voltage. A similar load using a parallel R-L load representation for the converter is shown in Figure 4.3.1 b. The slight difference in field current prefault value is due to the fact that the parallel load turned out to be $104 + j73$ MVA instead of $104 + j66$ MVA. The field current in this case is seen to contain the same frequencies as in Figure 4.3.1 a, but the magnitude of the harmonics is less. Consequently, the field current makes fewer negative transitions, and the corresponding field voltage has fewer overvoltage spikes. (The field voltages in this case show the sudden negative swing after the dc rejection because of the exciters going into the inverter mode on account of the sudden terminal voltage rise.)



a) Bipole Load of $(104 + j66)$ MVA b) R-L Load of $(104+j72)$ MVA.

Figure 4.3.1: Comparison of Waveforms for Full Bridge Modelling and Equivalent R-L Load Approximation

4.3.2 Inclusion of delta-star transformers

Most synchronous machines are connected to the ac system which they feed, through a delta-star step-up transformer, in order to step the generated voltage (around 13.8 kV, typically), to the system voltage (i.e., 138 kV, etc.). The delta winding is on the side of the machine, and eliminates the flow of any zero sequence currents in the machine windings. Any machine-system oscillation of the type discussed this far, must now take place through this transformer, which would introduce a phase shift. This section examines the effect of such a winding which is always present in the actual situation. A comparison is therefore made between the two cases shown in the single line diagram of Figure 4.3.2. The machine data is as in the previous cases. The filters are also as in the case of Figure 4.3.1, but have been scaled to supply a total MVAR of 1.2 pu, at unity pu voltage and frequency, which is not quite enough to self-excite one machine, but just about.

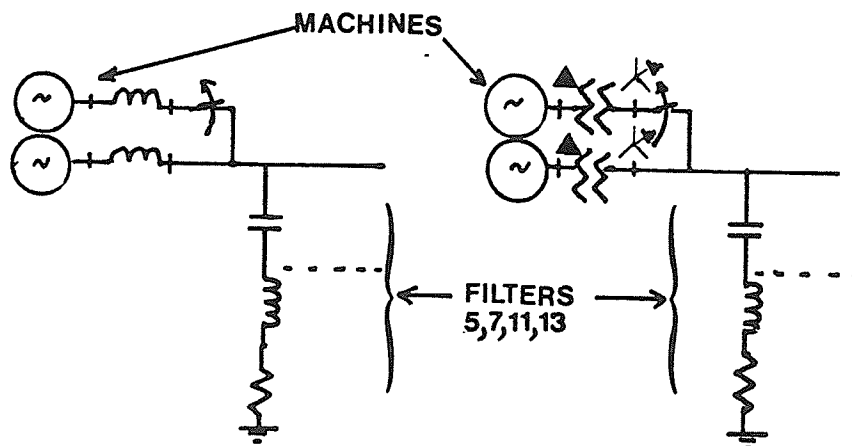
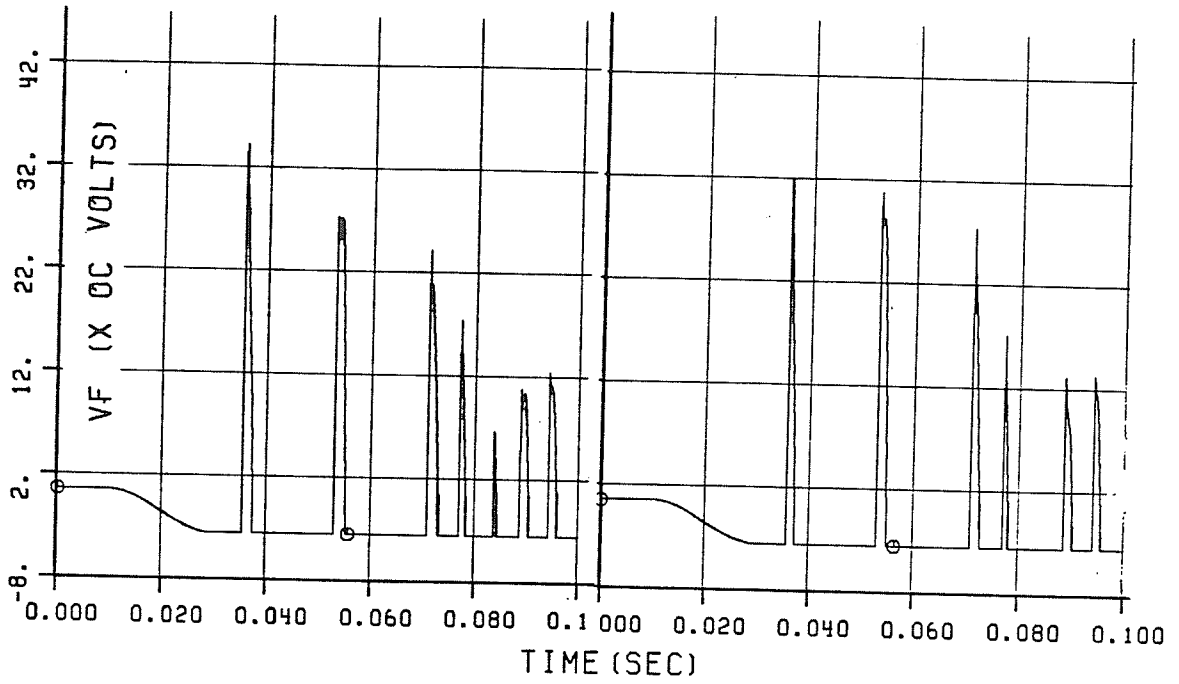


Figure 4.3.2: To study the effect of Δ -Y transformer windings.

In the analysis of Section 2.6, it was seen that the rotor transients are due to positive and negative sequence oscillations between the terminal capacitive impedance, and the machine's subtransient reactance. It is important to notice that there is no zero sequence component in these oscillations, and so they should not be affected by the delta-star winding introduced, which affects only the zero sequence. The field current and exciter voltage plots of Figures 4.3.3 a and b bear this out. The difference between the two responses is very marginal. Thus, in studies dealing with rotor transients, the transformer may be simplified by including it as a series inductance equal to the value of its leakage impedance. This inductance can even be incorporated directly into machine data, in the form of an increased machine leakage reactance. This is, however, true only if transformer saturation is not being considered. But in many cases, it may not be necessary to include saturation of the transformer for studies of rotor overvoltage, which occurs essentially in the first few cycles following a trip, in which case the terminal voltage of the machine may not have risen high enough to cause a substantial transformer saturation current.

4.3.3 Inclusion of the proper opening of the machine breaker

In the studies carried out so far, it was assumed that when one out of two machines tripped, this happened instantaneously. This could then be simulated by just scaling the number of machines down from 2 to 1 in the machine subroutine (section 3.3.2). In reality, however, the machine to trip is removed from the system phase by phase, because the current in all three phases does not cease to flow simultaneously. It was important to see how well this approximation of



(a)

(b)

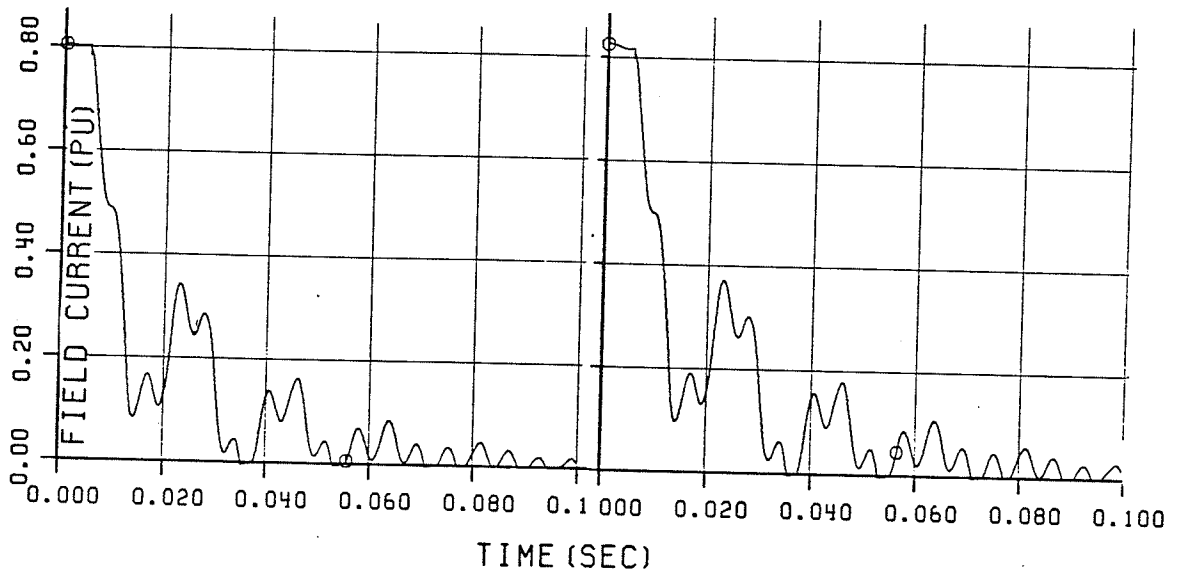


Figure 4.3.3: 1 out of 2 Machines (on 1.2 pu of 5th, 7th, 11th and 13th Harmonic Filter Loading) Trips

a) Δ -Y Machine Transformer not Modelled

b) Δ -Y Machine Transformer Modelled

instantaneous opening matched with a phase by phase opening because with the approximation only one machine with changeable scaling factor (to simulate tripping) is adequate, and saves computer effort. The situation of Figure 4.3.2 was again simulated, but this time with two calls to the machine model and with breaker opening logic, which set the impedance in each breaker phase to infinity only when the current through the phase went to zero. The field voltage and current waveforms were as in Figure 4.3.4, and showed about a 20% increase in peak overvoltage in the field. Thus, it appears that for a complete simulation, the system should be modelled as it actually exists, that is, with two machines and a breaker.

Discussed in the following chapter is a situation which actually occurred on Manitoba Hydro's Northern Collector System. In that simulation, the approximation has been used, because the overhead required in the repeated modelling of each machine was considered high. After all, only an estimate of the field voltage was required, and a 20% error seemed to be acceptable for the purpose. The transformers, however, were modelled in detail, because they did not significantly increase problem complexity. Also, the breaker opening at current zero represents an extreme case. In actuality, the breaker would be considered open somewhere in between the instant of trip initiation and current zero.

4.4 Chapter Summary

Looked at in this chapter were realistic capacitive loads, and comparisons were made with the idealized capacitor loads of Chapter

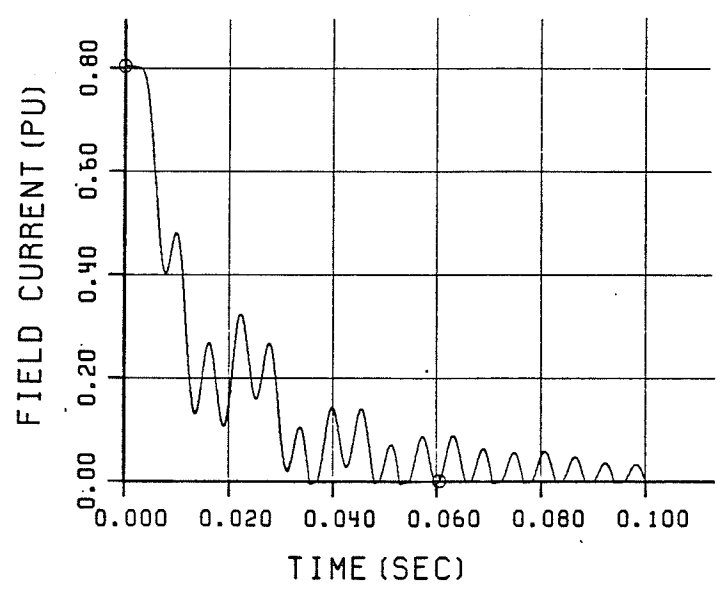
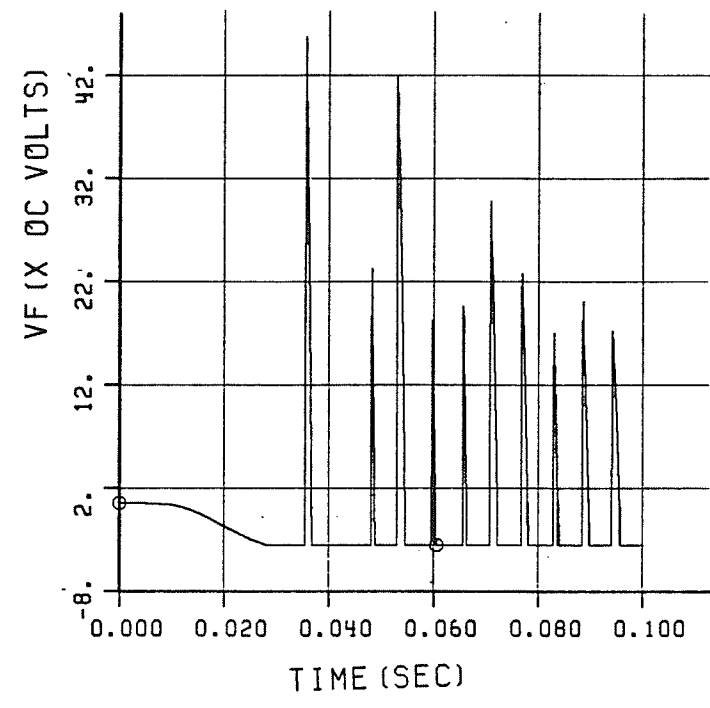


Figure 4.3.4: Waveforms with Machine Breaker Opening Phase by Phase
 (Data as for Figure 4.3.3)

2. The importance of complete modelling of these capacitive loads (especially for VARs entering one machine from another) was identified. The case of machines connected to an HVDC converter and filters was investigated, and the need for dc modelling in order to properly simulate the prefault ac filter conditions seen to be necessary. Also compared was the effect of programming approximations to the real case of machines connected to Star-delta transformers and breakers. The overvoltage in the case of the breaker being modelled (as opposed to the case of an instantaneous trip) was found to be somewhat higher than in the approximate case.

In the next Chapter is considered the case of an actual field overvoltage situation that took place on Manitoba Hydro's system. The case includes all the factors considered in this Chapter taken together in that the VARs were primarily from ac filters and other machines, and the load was due to an HVDC converter.

CHAPTER 5

Simulation of an Actual Disturbance

5.1 Introduction

A particularly severe case of excitation system overvoltage in Manitoba Hydro's Northern Collector System occurred on September 30, 1978. A brief description of this case was given in Chapter 1. Of particular interest is the fact that the reactive power (VARs) into the machines with damaged exciters were from other machines, as well as from filters, both these cases having been discussed independently in Chapter 4. The simulation also shows some overvoltage due to a sudden load rejection due to the blocking of the dc rectifiers.

The sequence of events appears to have been as follows [7] (some of these events have been reconstructed, because the different time recorders in the system were not in synchronism, and thus time events recorded in different time recorders cannot be accurately related).

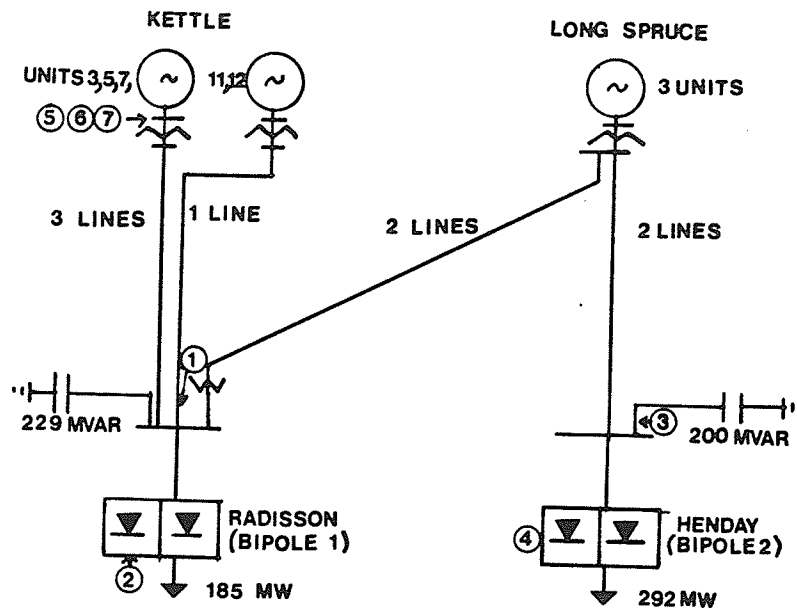


Figure 5.1.1: Manitoba Hydro Collector System on September 30, 1978, 09:22 hrs.

Initial Condition:

At 09:22 hrs, the system found itself in the configuration of Figure 5.1.1, with five machines at the Kettle station and three at the Long Spruce station. Two dc bipoles were on at Radisson and Henday each taking in 185 and 292 MW of power respectively, and operating in 12 pulse operation. In addition, the 5th, 7th, 11th and 13th harmonic filters at Radisson were supplying a total reactive power of 229 MVAR and the high pass filter at Henday was supplying 200 MVAR. In this condition, each of the Kettle machines was loaded to approximately 34 MW and 64 MVAR (capacitive) and the Long Spruce machines to about 103 MW and 49.41 MVAR (inductive) respectively. Thus there was a net reactive power flow from the Long Spruce machines to the Kettle

machines. This is not a normal operating condition, but the system was cast into this situation on account of some prior disturbances.

Event 1 (time = - 1.7 sec)

Due to the fact that the line connecting Kettle units 11, 12 to Radisson carried the current of both these units (unlike the lines connected to units 3, 5, 7 which carried only one machine each), it tripped due to overcurrent relay operation. This event has been labelled 1 in Figure 5.1.1.

Event 2 (time = 0.15 sec)

The converter at Radisson blocked due to commutation arcbuck, and thus there was a load rejection of 185 MW in the Collector System (see event labelled 2 in Figure 5.1.1).

Event 3 (time = 2.1 sec)

There was an overvoltage in the Collector System due to this load rejection, which tripped the 200 MVAR filter at Henday.

Event 4 (time = 2.215 sec)

By an intertripping arrangement on the protection system at Henday, the converter at Henday (Bipole 2) blocked.

Events 5, 6, and 7 (time = 2.28 sec, 2.33 sec, and 2.38 sec)

In the duration between Events 3 and 4, the three units at Kettle were still absorbing a large quantity of reactive power and suffered a drop in terminal voltage due to the tripping of the filter. There are loss-of-field relays on these units, which are essentially impedance relays with undervoltage supervision. That is, they take the machine off-line if they detect excessive VARs going into the machines, and a simultaneous drop in voltage, which is precisely what happened between Events 3 and 4, which after a delay tripped the three machines after the end of Event 4.

Thus, the Kettle machines began to trip in succession, because of the operation of these relays. As at the instant of tripping, they were absorbing a considerable amount of reactive power, they suffered an overvoltage in their field circuit, and thus had damaged exciters. As the machines to trip later were more heavily loaded with reactive power than the ones that tripped earlier, the amount of exciter damage was observed to be in direct proportion to the sequence of tripping.

Units 3 and 7 exciters showed damage to smaller circuits, and signs of arrester flashover. Unit 5 had 12 out of 84 [8] thyristors fail in the short circuited mode, resulting in a complete short circuit on the exciter's dc bus. It is believed that failure of one string of thyristors in the short circuited mode could have protected the rest in parallel with it from being damaged. The Unit 5 exciter also showed evidence of arrester flashover and had 35 of 60 plates damaged.

5.2 Modelling Details

To analyze this disturbance, MH-EMTDC (Chapter 3) was used. As was shown in Chapter 3, it was important to model both the HVDC converter and the associated filters in detail. Figure 5.2.1 shows the single-line schematic layout for the system model utilized in this study. In order to model the speed effects properly, a governor model of the sort mentioned in Section 3.4 was utilized.

Tables A2.1 to A2.6 of Appendix II give the data used in the simulation, and refer to Figure 5.2.1.

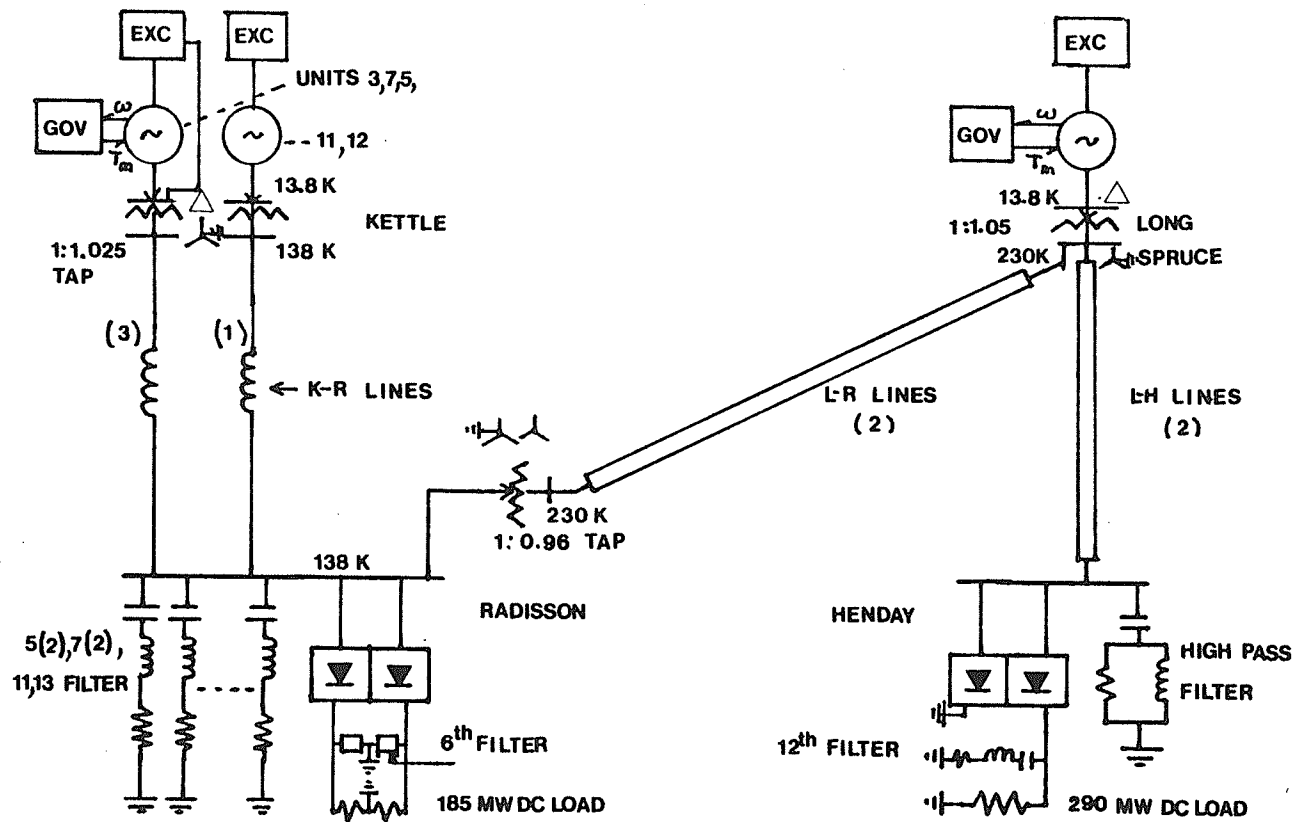


Figure 5.2.1 : Collector System Single Line Diagram as Used in Study.

The first step in the simulation was to obtain the initial machine angles, terminal voltages and tap changer ratios from a load flow. These were then 'plugged' into the transients model, and the system started up using the starting up procedure described in section 3.3.3. Once the dc converter voltages had built up, the dc converters were deblocked, and the system allowed to reach the steady state. At this point, the machine speed, which was fixed at a value of $2 \times \pi \times 60$ rad/sec (electrical) is controlled by the machine inertia and governor system so that the mechanical dynamics are now represented.

One of the checks that a transient solution program is working properly is that it should yield the same steady state values as the load flow. Figure 5.2.2 shows the real and reactive powers calculated from the load flow, and from the predisturbance stabilized transient solution. Agreement is close. The slight differences arise because the reactive power consumption of the rectifiers depends on the firing angles on the valves. These are exactly represented in the transient EMTDC solution but not in the load flow. Also, the machine initial angles were calculated (using the method in section 3.3.3), neglecting saturation, and may be slightly off from the values with saturation included.

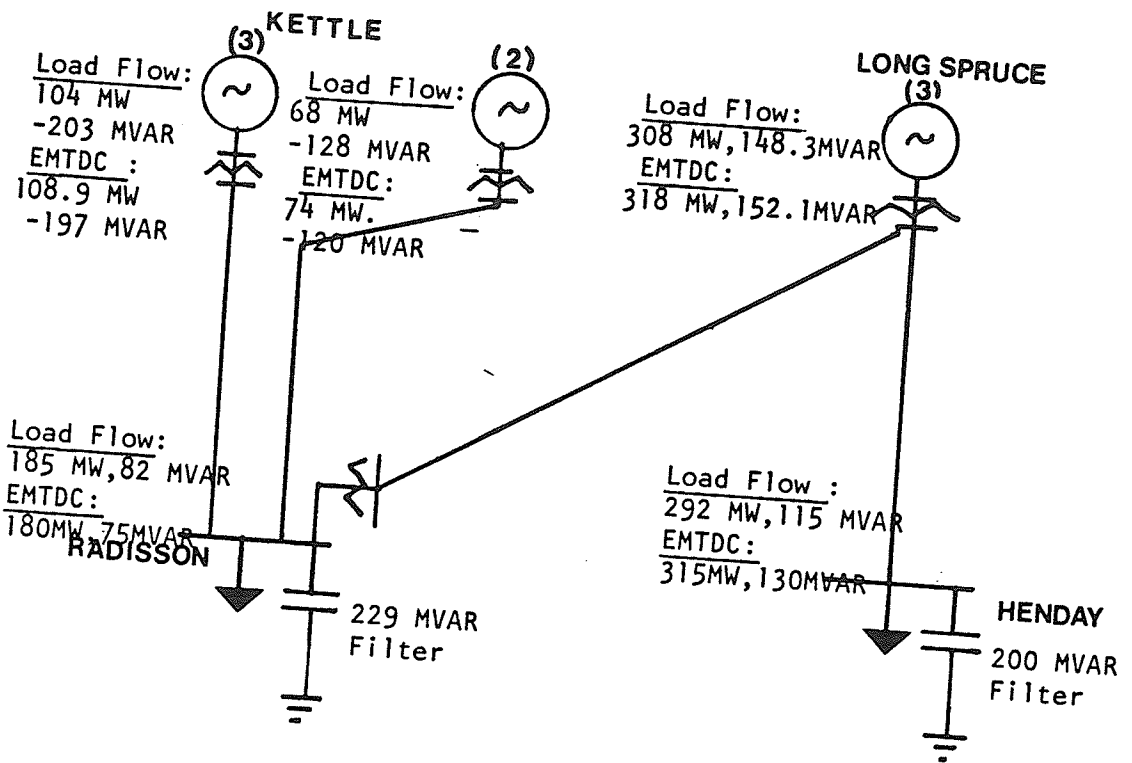


Figure 5.2.2: Comparison of Load Flow and EMTDC Steady State solutions.

5.3 The Simulation Results

The sequence of events described in Section 5.1 was simulated, and presented here are the results from Event 2 onwards (dc load rejection at Radisson), because that is what caused the field current to go to zero for the first time.

Event 2 occurred at 0.1 second in the simulations of Figure 5.3.1, which show the Kettle and Long Spruce field currents, the exciter voltage at Kettle, the terminal voltage (r.m.s.) of the Kettle

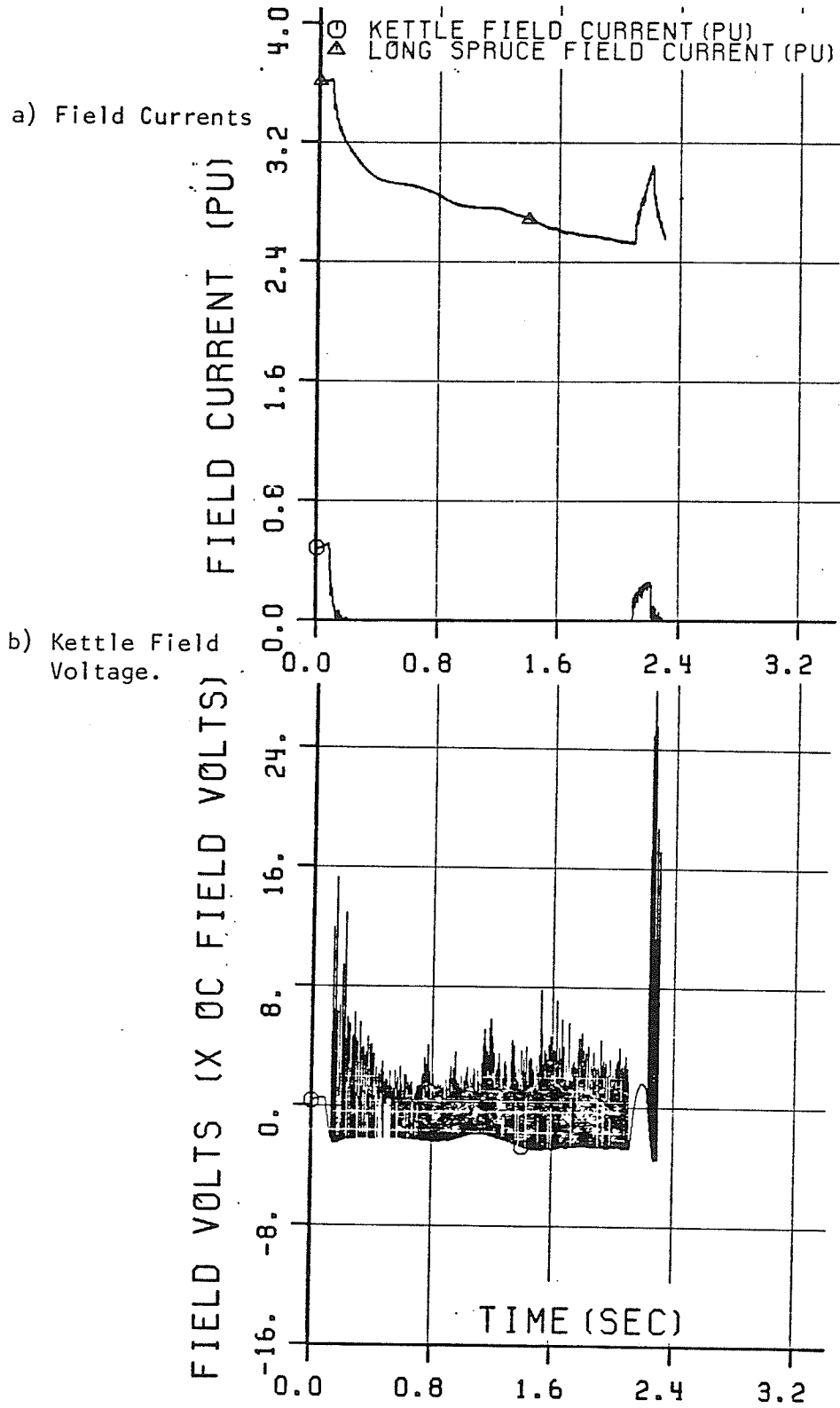
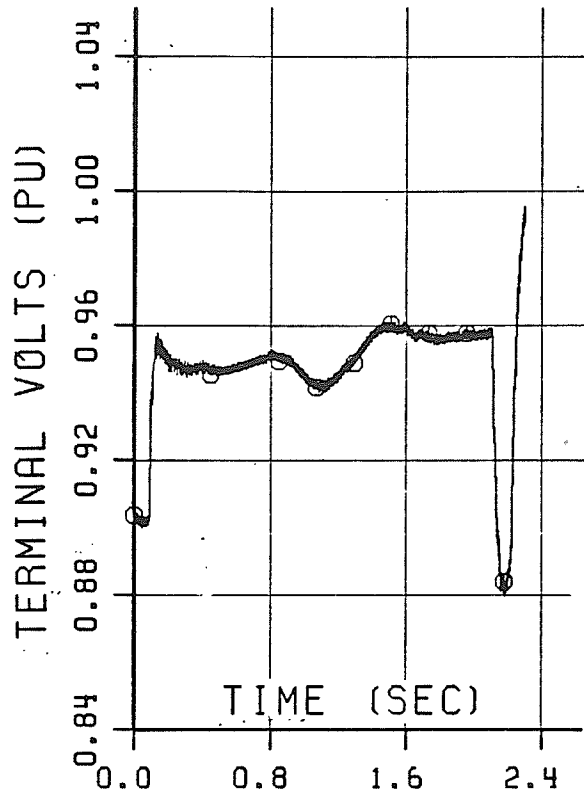
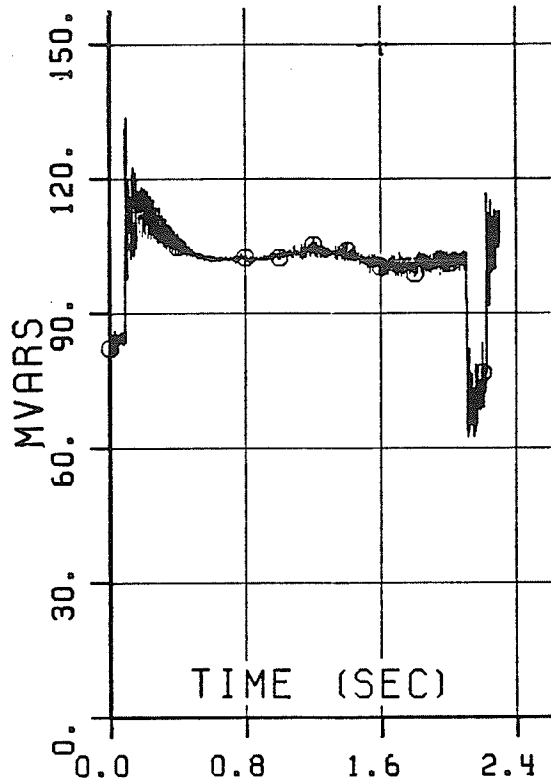


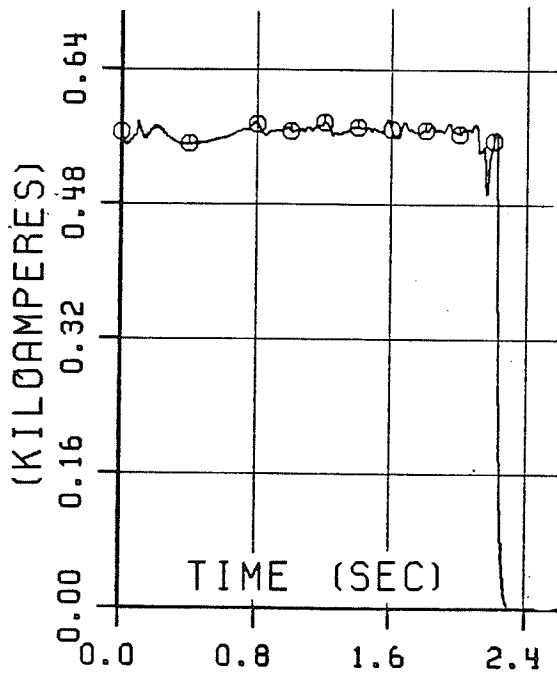
Figure 5.3.1 : Waveforms for the Simulation of Events 1-4.



c) Kettle Terminal Voltage.



d) Kettle MVAR s/Machine.



e) Bipole 2 dc Current.

Figure 5.3.1 : Simulations of Events 1-4 (...Contd.)

machines, the reactive power per Kettle machine, and the dc current at Henday in Figures a, b, c, d and e respectively. The 180 MW load rejection causes both field currents to go down, and the terminal voltage to go up. The megavars into the machines at Kettle also increased. The simulation shows that as a result of exciter action, the field current reached zero and there is evidence of some overvoltage in the field due to this transient. The magnitude of this overvoltage is, however, only about 15 times open circuit field voltage at the maximum, and thus not expected to cause any exciter thyristor damage. From this time onwards to time = 2.1 seconds, there is some chatter in the field voltage shown in Figure 5.3.1 b, as the field current hovered around the zero mark, but this too is (as it should be) small in magnitude.

As the Kettle machine field current had reached zero, the exciter had no further controlling effect on controlling terminal voltage (as seen in Figure 5.3.1 c), and thus partially, the system voltage (which was still somewhat controlled by the Long Spruce machines). This voltage thus gradually increased with the system frequency which increased due to the load rejection. There was thus overvoltage at Henday (dc converter bus), and the protection scheme removed the 200 MVAR high pass filter off that bus (Event 3). This occurred at 2.1 seconds in Figure 5.3.1. The sudden decrease in MVARs caused dips in the Kettle machine voltage (to 0.88 pu) and an increase in the machine field currents. The Kettle field current again went positive (Figure 5.3.1 a) and the exciter resumed smooth normal operation as seen in

Figure 5.3.1 b. The dc current experienced a momentary dip (Figure 5.3.1 e) as the voltage at Henday dipped.

Automatic intertripping caused the dc converter at Henday to block, and thus cause a 100 percent load rejection on the ac collector system (Event 4). This occurred 110 msec after Event 3. At time = 2.21 second, the blocking of the converter can be evidenced in Figure 5.3.1 e which shows the dc current going to zero. This load rejection had a similar, but far severer effect on the collector system than the earlier load rejection at Radisson at time = 0.1 second. Voltages and megavars went up (Figure 5.3.1 c and d), and field currents went down (Figure 5.3.1 a), and the Kettle field current, in fact hit zero. The resulting overvoltage in the field is seen in Figure 5.3.1 b.

As mentioned in Section 5.1, the dip in voltage between Events 3 and 4 caused the loss of field relays in the Kettle machines to operate, but because of the delay in the protection circuit, the machines were actually removed from the system about 70 msec after Event 4. The undervoltage setting on the loss of field relays was 0.83 pu on Kettle machines 7 and 3, and 0.80 pu on Unit 5. The simulation (Figure 5.3.1) shows a voltage dip to only 0.88 pu, but there may be some error in this. (Also, the system frequency was about 63 Hz because of the load rejection at 0.1 second, which may have slightly raised this threshold.) But it is interesting to note that this protection operated only in Units 7 and 3, which had the 0.83 pu setting and not on Unit 5. These units tripped at $t = 2.28$ and $t = 2.33$ seconds respectively (Events 5 and 6). Figure 5.3.2 a and b shows these events more clearly. The time origin for Figure 5.3.2 is 2.1 sec., so that

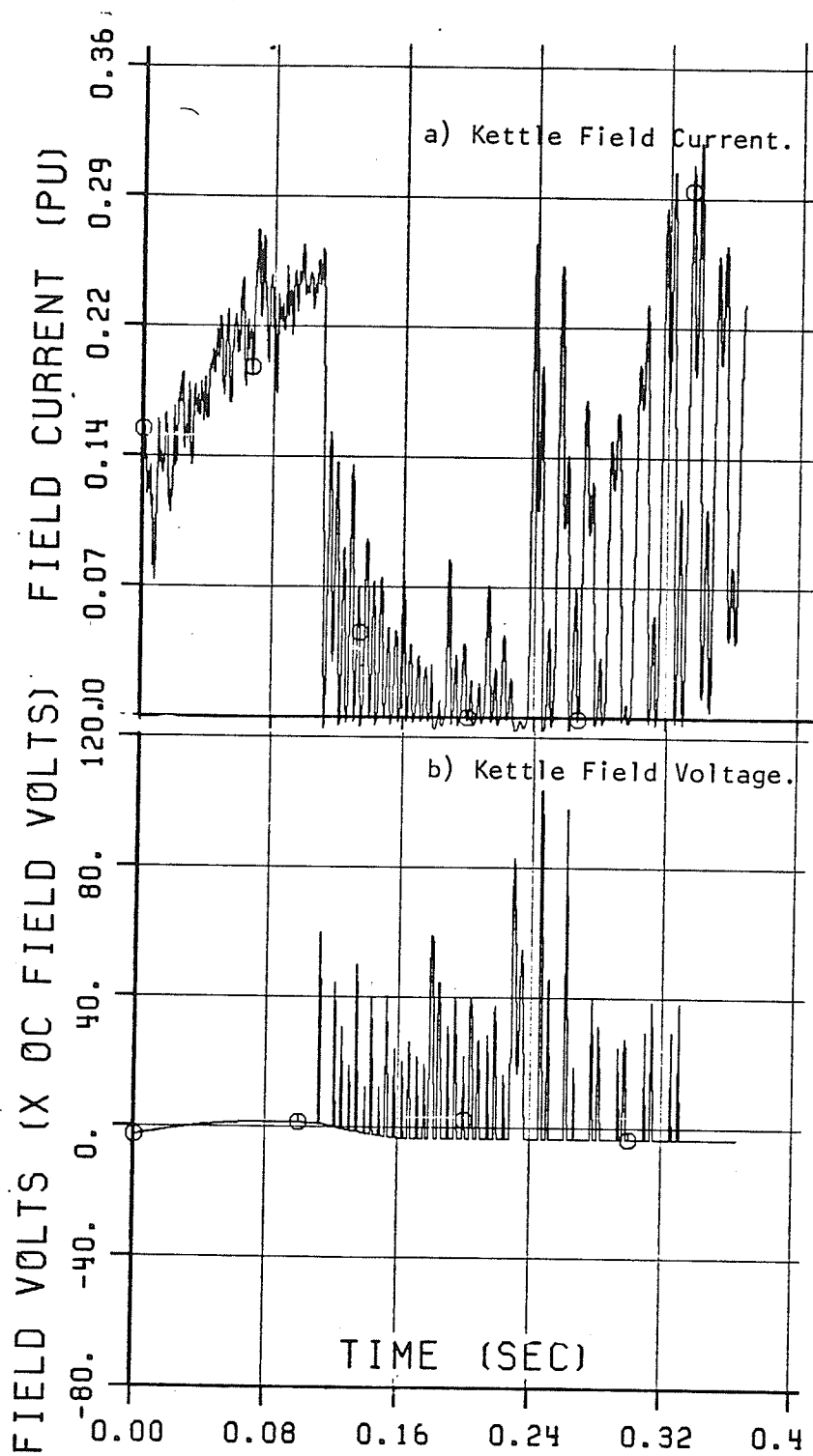


Figure 5.3.2: Waveforms for the Simulation of Events 4-6

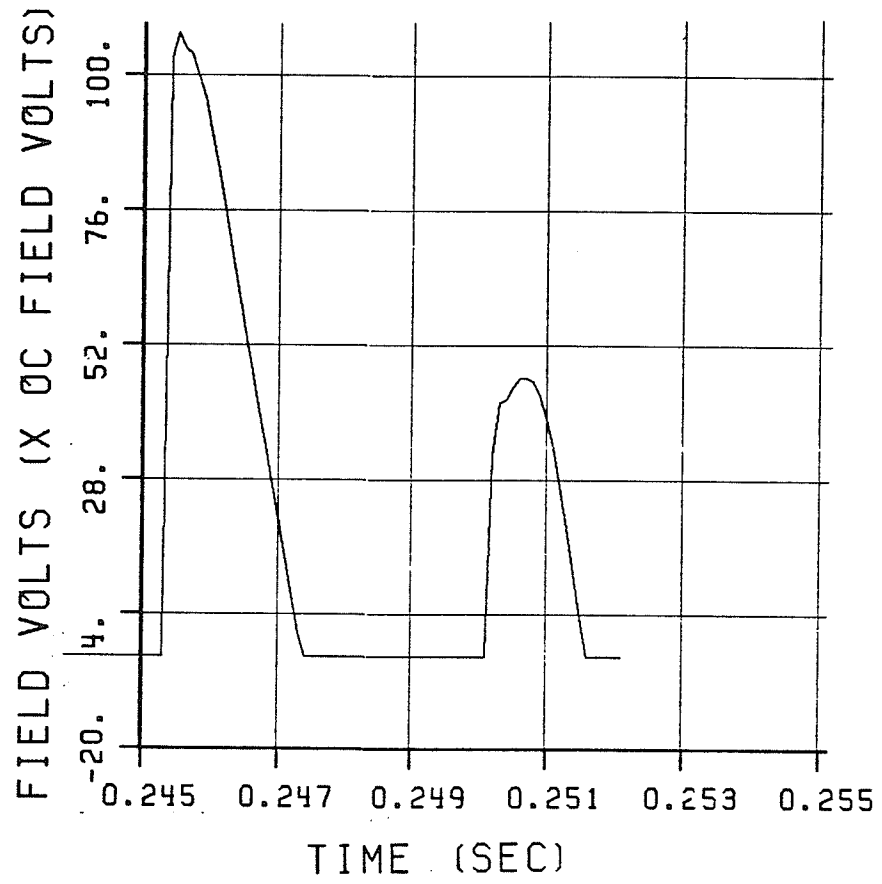


Figure 5.3.3: Expanded Plot of Highest Overvoltage

Events 4, 5 and 6 occur at times 0.11, 0.18 and 0.23 seconds respectively, with respect to this new time origin.

Peak overvoltages of about 60 times open circuit field voltage were caused by load rejection at 0.11 sec, and machine tripping at 0.18 seconds (of course, Unit 7 only saw the first of these). The field current and voltage picture of Figure 5.3.2 is really that of Unit 5, the last unit to trip. However, the response for the other two are the same, until they are tripped off. Tripping of Unit 3 at $t = 0.23$ sec in Figure 5.3.2 caused a severe overvoltage in the Unit 5 exciter of a peak of about 110 times nominal open circuit field voltage. This overvoltage caused the Unit 5 exciter to have thyristor failure, which essentially short circuited the ac side of the exciter, and caused the unit to be removed from line by exciter overcurrent relay operation (Event 7). An expanded view of the most severe overvoltage is shown in Figure 5.3.3 where the steep initial wavefront should be noted. This rate of rise is about 1 (o.c. field volts)/ μ sec or about 120 V/ μ sec.

This simulation explains why the severity of damage in Units 3 and 7 was less than that in Unit 5, mainly because Unit 5 had a far severer field overvoltage. Unit 5 was the only one that suffered thyristor damage, the other two showed signs of arrestor flashover only. It is expected that in Unit 5, the arrestor flashed over too late to save the thyristors on account of the speed with which the overvoltage occurred.

5.4 Chapter Summary

In Chapter 4, the effect of various types of load rejections and reactive power loadings on field circuit transients was discussed. This Chapter explains an actual disturbance that took place in Manitoba Hydro's Northern Collector System based on the investigations of Chapter 4. MVAR loading on the Kettle machines was due to filters and the Long Spruce machines. Overvoltage stresses were due to load rejections (Event 4) and machine tripping (Events 5 and 6).

In the next Chapter are discussed ways of minimizing exciter overvoltage stress, so that failures of this type may be avoided. It must be emphasized that such an event is a rare event because the system is not normally operated in a fashion that may result in a field current negative transition. The event of September 30, 1978 was the result of a unique contingency.

CHAPTER 6

Protection Methods

6.1 Introduction

It has been shown in Chapters 2, 4 and 5 that the overvoltages in the field circuit associated with machines tripping on capacitive (or filter) loads, are of substantial magnitudes, and have extremely rapid rates of rise. In this chapter, a representative situation such as the one shown in Figure 4.2.4 (Chapter 4), but with only two machines of the Kettle Generator type isolated onto a pair of 5th and one each of the 7th, 11th and 13th filters (see Appendix II, Table 2.5 for data) has been considered. One of the machines is then made to trip, and thus the entire (132 MVAR) filter load is felt by the other machine, which sees an overvoltage in its field on account of the field current transition to zero. Figures 6.1.1 a and b show the field current and voltage responses for this case. (Note the diminishing field overvoltage with time, on account of the machine saturating as its terminal voltage [Figure 6.1.1 c] rises). Figure 6.1.1 d shows an expanded time plot of the first two overvoltage peaks, the first of which has a near vertical rise, and a magnitude of about 100 times the nominal field voltage needed to achieve unity terminal voltage.

In the subsequent sections it shall be shown that the reverse resistance of the exciter circuit has a bearing on this overvoltage, which decreases both in magnitude and rate of rise, with decreasing reverse resistance. This is also typical of other types of field overvoltages caused by line-to-line or line-to-ground short circuits [9, 12, 7] or pole slipping [9, 10, 13]. Thus protection strategies

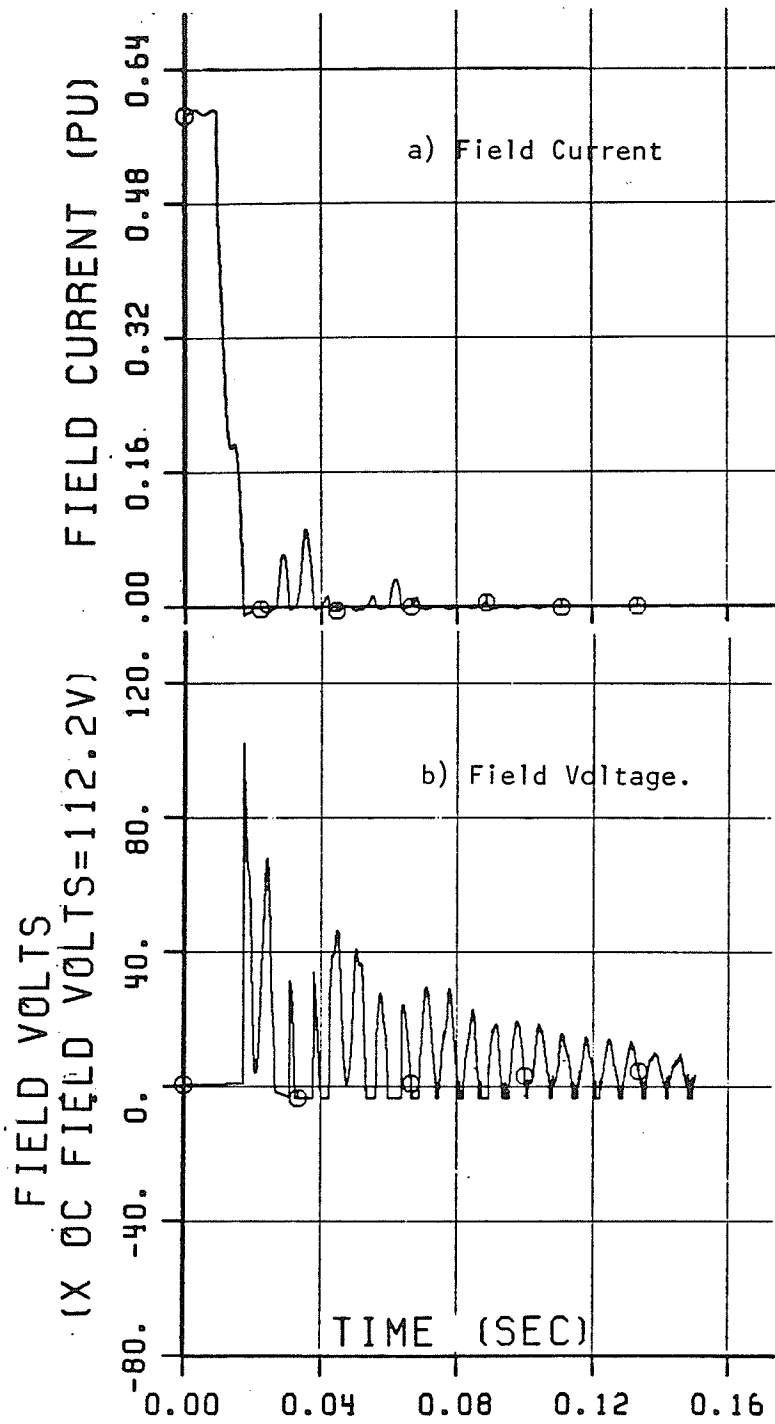


Figure 6.1.1 : 1 out of 2 Kettle Machines Tripping on 132 MVAR Filter Load.

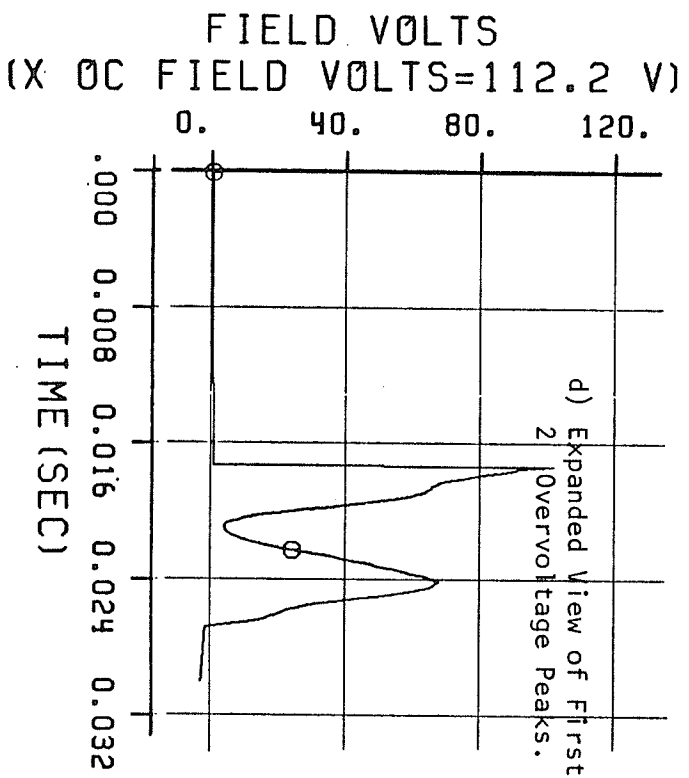
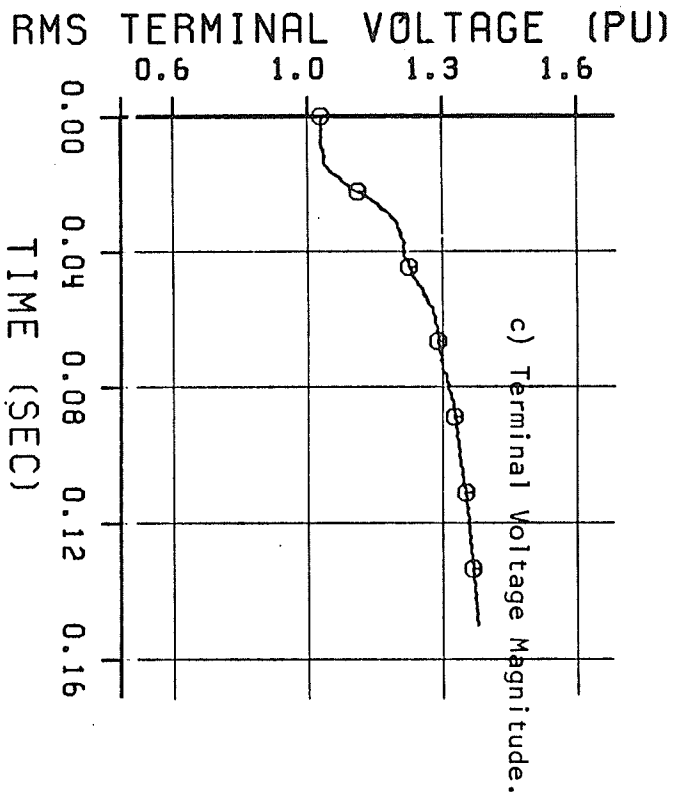


Figure 6.1.1 : (...Continued:)

similar to the ones discussed in the above references [9, 12] should be applicable here. These consist of either having such low reverse resistance in the field circuit as to prevent the overvoltage in the first place, or to have an alternative reverse current path through a solid state switch to provide a low resistance path for the reverse current.

The former of these causes considerable power loss in the protection circuit (thus necessitating forced cooling), and the latter is amenable to pulse triggering of the bypass switch which could result in a short-circuiting of the exciter. Another possible method is to have a very fast acting surge arrestor, which breaks down quickly enough to prevent the rapidly rising voltage from appearing across the thyristors. The need for fast arrestor response can be alleviated somewhat by decreasing the rate of rise of the overvoltage by placing a reverse resistance in the field, which is not small enough to cause excessive loss as in the first method listed above.

The final protection choice, of course, rests with the designer, who would weigh the pros and cons of each of the above schemes and select one.

6.2 Desired Speed of Response of the Surge Arrestor

A surge arrestor model was developed and placed at the machine's field circuit terminals, to see how soon the arrestor had to operate in order to protect the exciter thyristors. Figure 6.2.1 shows a functional diagram of the surge arrestor model. The model consists of a dual slope V-I characteristic, one of higher slope (RREV)

representing the normal (high) arrester resistance, which breaks over after threshold voltage (E_1) into a characteristic of lower slope (R_2), signifying a breakdown of the arrester. The lower slope characteristic can be offset vertically by changing the voltage (E_2) in Figure 6.2.1.

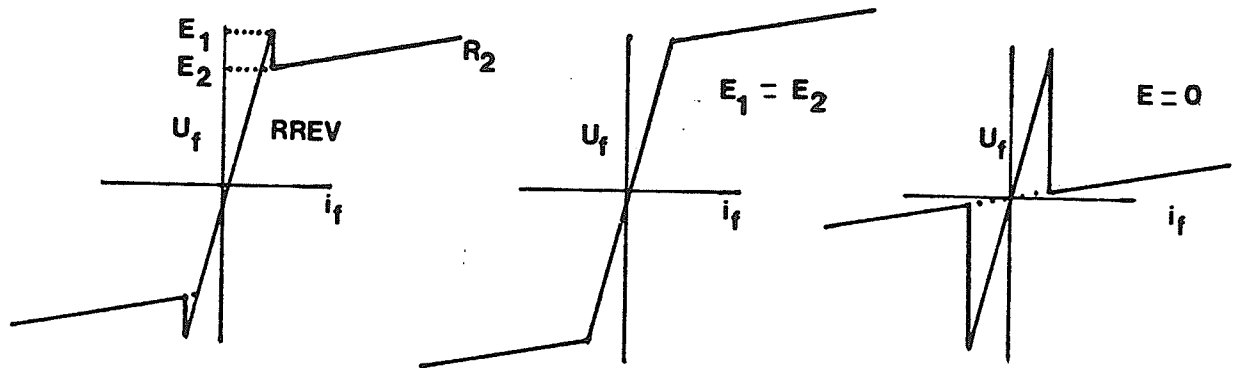


Figure 6.2.1: Surge Arrester Model.

A delay is built in, so that the transition from RREV to R_2 takes place with a pre-selected specified delay. Characteristics such as in Figure 6.2.1 b (representing a solid state surge suppressor [35]) or as in Figure 6.2.1 c (representing a low resistance introduced via a solid state switch, such as described in Section 6.1), may be modelled, merely by proper selection of E_1 and E_2 .

Figures 6.2.2 a and b show the field voltage responses for the case of Figure 6.1.1, but with the arrester modelled, with $RREV = 10,000 R_f$, $R_2 = R_f$, $E_1 = E_2 = 15$ times open circuit field voltage. Here R_f is the normal (forward direction) field resistance. Comparisons can be made between Figure 6.1.1 d and Figures 6.2.2 a and b, as

they all show field voltages in the various cases. It can be seen that the peak overvoltage is unaffected by an arrester which breaks down in 100 μ sec, and even in the case of an arrester one with a 25 μ sec delay, there is still an overvoltage peak of about 35 times the open circuit field voltage. Thus, it would appear that for an arrester to protect the thyristors from overvoltage, its time of response should be faster than 25 microseconds.

This modelling of a sudden breakdown at a pre-specified time after the overvoltage is an approximation to the real phenomenon. In surge suppressors, the current builds up to its steady state response to the overvoltage continuously, with a time constant. Zinc oxide arrestors, used for much higher overvoltages, have a time constant in the order of 10 μ sec [36] (variable, depending on actual overvoltage). Selenium suppressors, which have been used in many cases, are slower. The response speed of 25 μ sec desired above may thus possibly be achieved with the right arrester. However, sometimes protection against capacitor induced field stresses may be required on generators already installed (such as at Manitoba Hydro), and a patch up solution (without installing another arrester) may be wanted. The time of 25 μ sec response is not too fast for solid state arrestors, as far as the breakdown phenomenon are concerned. However, lead inductance effects may increase the time considerably because they introduce a delay in the current. The following sections deal with this problem, and address means of providing protection by alternative means.

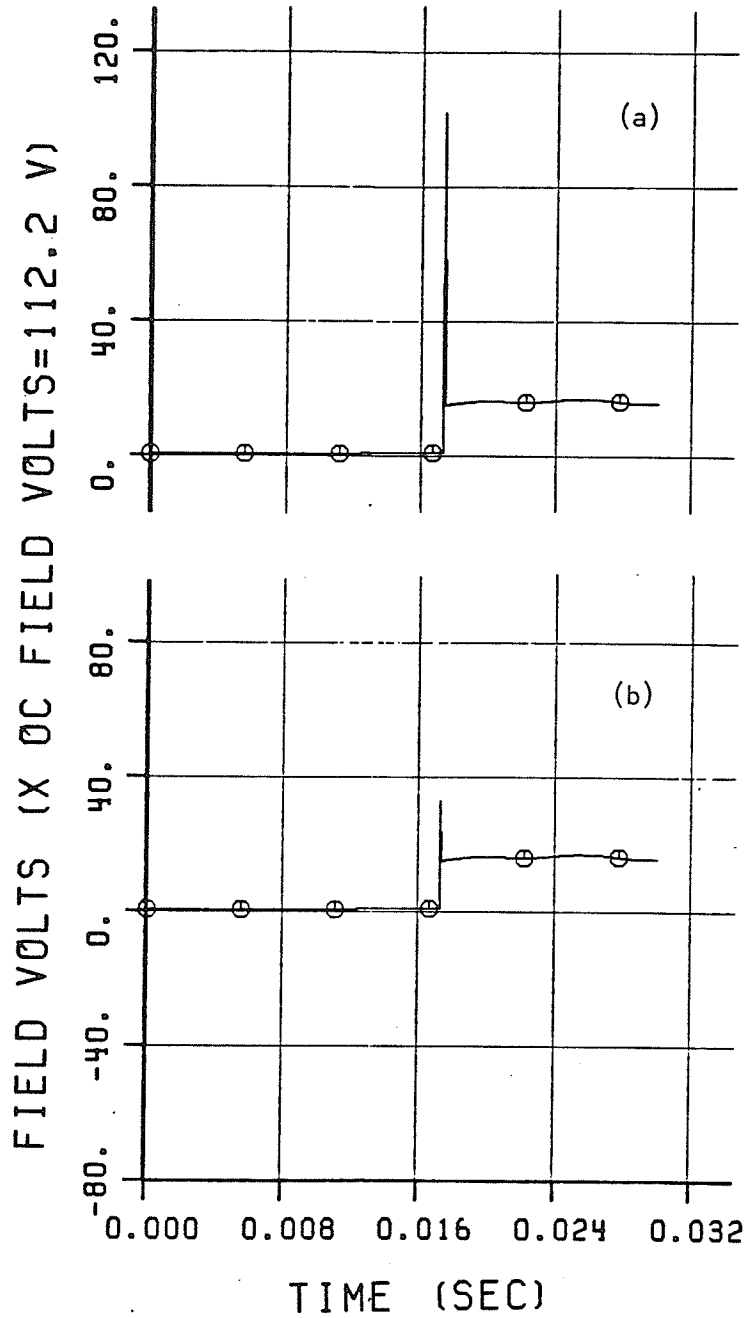


Figure 6.2.2: Effect of Delay in Arrester Operation

a) 100 μ s delay

b) 50 μ s delay

6.3 Effect of Different Reverse Resistances

As the reverse resistance in the field is decreased, the overvoltage decreases too. The first two overvoltage peaks of Figure 6.1.1 d were re-simulated using different values of field reverse resistance. Figure 6.3.1 shows these peaks for a reverse resistance to normal field resistance (R_{REV}/R_f) ratio, varying in decades from 10 to 10,000. As can be seen, for $R_{REV}/R_f = 10$, there is hardly any overvoltage (maximum of $4 \times$ o.c. field volts) and $R_{REV}/R_f = 100$ gives a maximum of about 21 times the open circuit field voltage.

Another factor to be noticed is that the rate of rise of overvoltage is also markedly affected. Comparisons of the $R_{REV}/R_f = 10,000$ and $R_{REV}/R_f = 1000$ waveforms show that the two waveforms are very close as time progresses, but the initial rate of rise is very different.

This substantial variation in overvoltage magnitude is also observed in other kinds of field overvoltages, such as those due to unsymmetrical short-circuits [9,12], and pole slipping [9,10]. This variation would, at first glance, suggest that one of the ways to combat this overvoltage is to place a shunt resistance of about 10 times the forward resistance across the slip rings. But, taking the example of the Kettle Generator (see Appendix II, Table A2.1), in which $R_f = 0.17 \Omega$, the required reverse resistance for a ratio of 10, would be 1.7Ω . The field voltage for producing 1 pu terminal voltage is 112.2 V, and on a large inductive load, could be as large as twice this value. This would mean a power dissipation of about 30 kW in this resistor! With $R_{REV}/R_f = 100$, the power loss for the above case would

be 3 kW, which can be handled without a complicated cooling system. (This power loss can be fractionally reduced by connecting a diode in series with the reverse shunt resistance [9], which allows only unidirectional current in this resistor, and thereby prevents loss when the 6 pulse exciter voltage goes partially negative, such as is the case at higher exciter firing angles.) However, the peak voltage is still about 22 times the open-circuit field voltage, which may be above the peak inverse voltage rating for the exciter thyristors. In any case, merely having a lower reverse resistance is one protection alternative, if the cooling requirements do not prove to be excessive.

6.4 Other Protection Methods

One of the ways to prevent the excessive power loss in a small reverse resistance is to have it switched into the system automatically, when the field voltage begins to rise and threaten thyristor damage. This may be achieved by an arrangement such as in Figure 6.4.1.

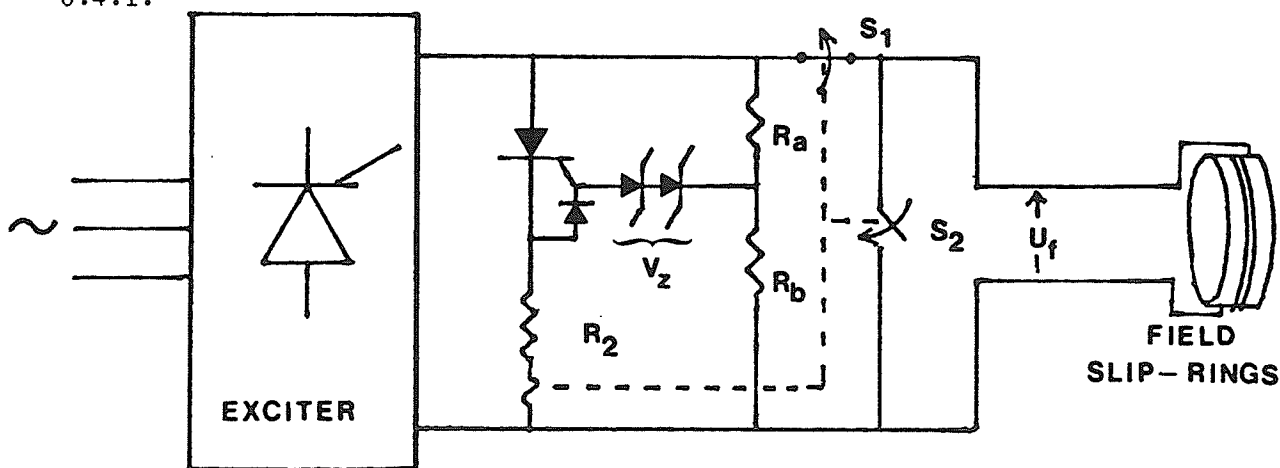


Figure 6.4.1: Possible Automatic Switching Scheme.

In this case, the lower reverse resistance (R_2) is switched in only when the voltage V_0 exceeds the Zener diode threshold voltage

V_z , that is, when the field voltage exceeds U_{f_0} where

$$U_{f_0} = V_z \left(\frac{R_A + R_B}{R_A} \right) \quad \dots 6.4.1$$

If the current in R_2 exists for a long period of time, it operates the ganged switches S_1 and S_2 which short circuit the field, and remove the exciter from the machine. R_A and R_B are chosen to be very large, so that their losses are negligible. This type of scheme, again, has been suggested by Canay [12] for prevention of exciter damage from unsymmetrical terminal short circuits, and is sometimes called a 'crowbar' circuit. Figure 6.4.2 shows waveforms of such an operation with the 'crowbar' switched on at $15 \times$ o.c. field volts.

Another possible way to prevent exciter damage is to slow down the rate of rise of overvoltages by shunting the field with a not too small value of reverse resistance. From Figure 6.3.1, we see that an R_{REV}/R_f ratio of 1000 decreases the slope quite a bit. This R_{REV}/R_f ratio would give a continuous (worst case) power dissipation in the reverse resistance of about 300 W, which is quite acceptable from the cooling point of view. The surge arrester across the field, then, may have adequate time to breakdown and prevent damage to the thyristors.

The case considered in Section 6.1 (132 MVAR load on two machines) is reexamined here, but with a reverse resistance of 1000 times the field resistance. Figure 6.4.3 shows field voltage waveforms for the arrester breaking down in 100 and 50 microseconds respectively.

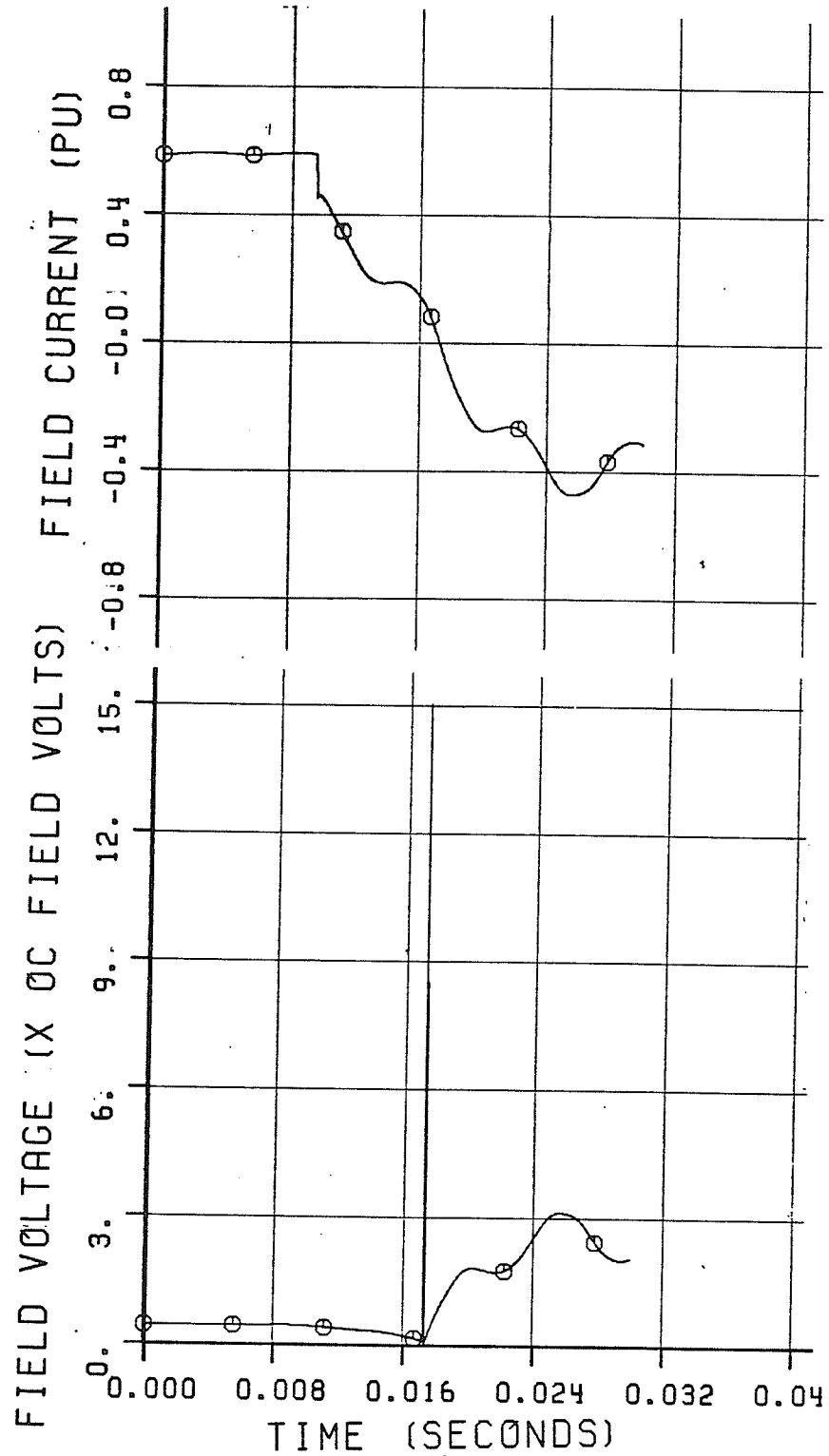


Figure 6.4.2 : Field Current & Voltage Waveforms for $R_2=R_f$ Switched on at $15 \times O.C.$ Field Volts. (With Delay= $10 \mu s$)

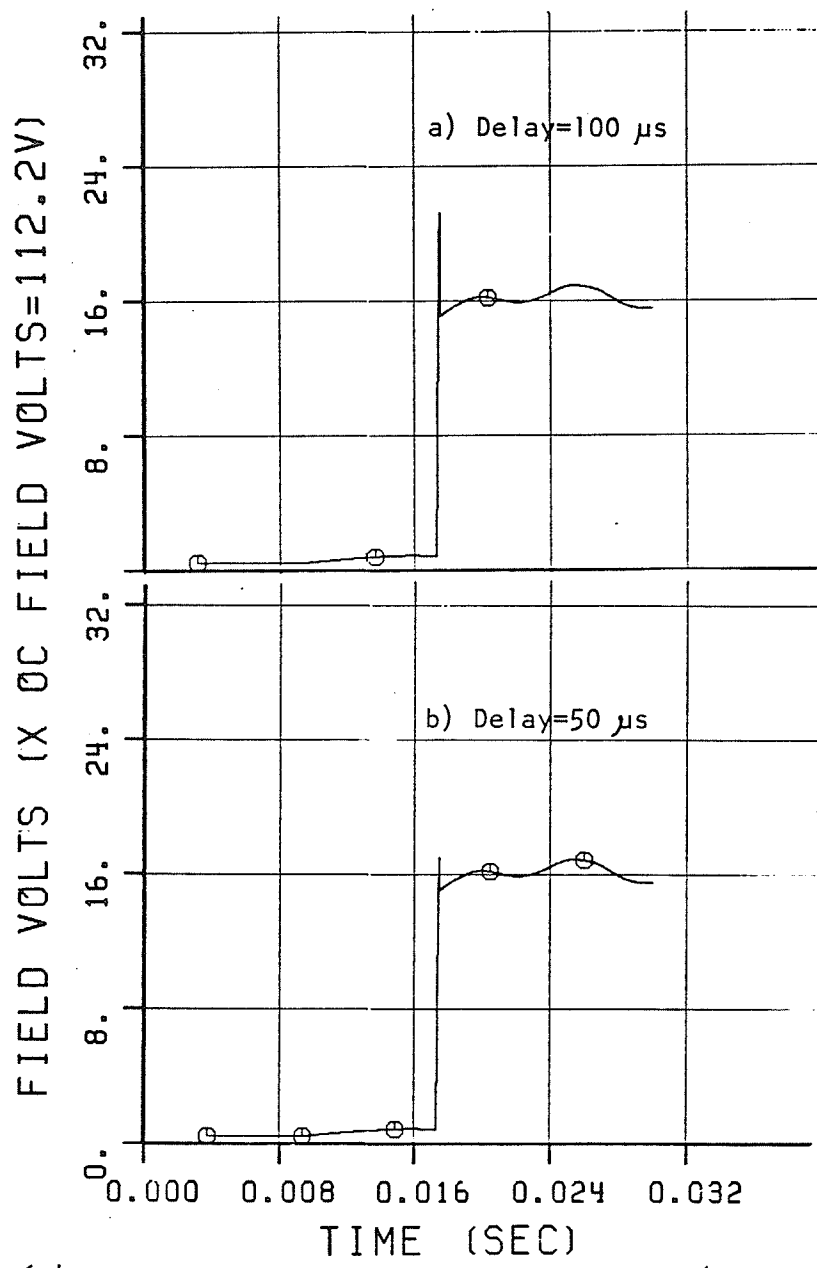


Figure 6.4.3 : RREV=1000 x RF, Arrestor Operation(with delay) at 15 x O.C. Field Volts.

A surge arrester breakdown threshold of 15 times the open circuit field voltage has been assumed, with a peak inverse rating of 20 times the open circuit field voltage on the exciter thyristors. The switched on resistance R_2 is equal to R_f . It can be seen that a breakdown delay of 50 μ sec is sufficient to prevent damage. The allowed delay would be even larger if a slightly smaller ratio of reverse to forward resistance were used. This would allow for the existing (slower) arrester to be adequate for protecting against the overvoltage.

Although the above method does not have the drawback of spurious turn-on, as in the case of the 'crowbar' circuit, it relies on arrester operation for thyristor protection and thus increases arrester duty.

6.5 Chapter Summary

In this chapter, a candidate situation of field overvoltage for the case of the tripping of one machine out of a pair, connected to a 132 MVAR filter load, has been considered.

It has been pointed out that the arrester operation speeds in excess of a maximum of 25 microseconds delay are necessary to protect the exciter thyristors from damage, if no reverse resistance is used.

The considerable decrease in the exciter overvoltage stress, both in magnitude and rate of rise, with decreasing reverse resistance suggests a number of protection schemes, which are listed below:

(i) Utilizing a reverse resistance of low value, permanently connected in parallel with the field slip rings: This scheme is

robust, but results in a large power loss, which necessitates a correspondingly large cooling system.

(ii) Utilizing a 'crowbar' circuit: This has the advantage of minimum steady-state losses, but has the danger of a spurious turn-on and limited duration operation.

(iii) Utilizing a reverse resistance to slow down the rate of rise of overvoltage so that it can be handled by the arrester: This method does not have the false turn-on drawback of method (ii) above, but results in repeated surge-arrester operation.

The first two of these methods have been suggested as protection schemes for protecting the exciter thyristors against pole slipping or unsymmetrical short-circuit induced field overvoltages. As demonstrated here, they will work equally well in the case of capacitor induced voltages.

The third method of reducing the rate of rise of overvoltage so that even an arrester with slow response time can prevent exciter damage, appears to be the simplest and may be used on the existing (slower) arresters.

When a new plant is constructed, an analysis of such transients may help in deciding whether to use a fast arrester, if available, or any of the three above methods.

CHAPTER 7

Conclusions and Recommendations

7.1 Conclusions

The main aim of this thesis has been to explain the cause and the nature of overvoltages in the field circuits of machines that are required to pick up a capacitive load suddenly. To tackle this problem, however, detailed simulation on a digital computer was necessary, because there was no recourse to major experimentation on the actual system. Thus efficient modelling, particularly of the synchronous machine, and its interfacing with an electromagnetics transients program, are also considered to be contributions of this thesis.

The major conclusions, in itemized form, are now stated below:

1. It was found that the machine-terminal capacitance oscillatory circuit causes transients of the field current. If the exciter has no reverse current capability (as is the case with most present day solid state exciters), and if these transients try to make the field current go transiently negative, high overvoltages result in the field circuit. These overvoltages can damage the thyristors of the exciter system, unless adequate protection is provided.
2. Simulations were first carried out on a machine model connected to a simplified ac system in which the capacitive load was represented by a lumped capacitance element. The field transients were found to be violent in

the case of the machines remaining on line connected to a pure capacitance after other identical machines at the same bus had tripped off. The overvoltages were particularly severe when the machine thus left behind was in or near a potential self-excited condition. Transients in the case of a machine picking up reactive power because of a resistive-inductive load rejection, were not so severe.

3. In the case of an exciter (without surge arrestor), the damage to its thyristors actually introduces a reverse current capability. This prevents rapid rate of rise of the machine terminal voltage, which would have otherwise been the case of a machine left at the onset of self-excitation due to the sudden tripping of its neighbouring machines at the same plant. (This would have been the case with the last machine to trip when an entire plant is tripped.) This is commensurate with observations by others, that reverse field current capability prevents rapid self-excitation.
4. A simplified mathematical analysis to explain the magnitudes, frequencies and time constants of these field transients was carried out, and agreed reasonably well with the results of detailed simulations.
5. The inability of the exciter to control field current under such conditions, on account of an extended time constant was demonstrated by simulation and experimentation.

6. A detailed machine model for use with Manitoba Hydro's EMTDC electromagnetic transients simulation program was developed. The machine was modelled as a voltage dependent current source which computed the currents to be injected into the ac system by utilizing the values of terminal voltages in the previous time steps. A novel method of interfacing this program with EMTDC was developed, in which the nodes of connection of the machine to the ac system were also connected to ground with a resistance. The current error introduced by this resistance was compensated for by slightly modifying the machine injected currents. This scheme was found to greatly enhance the numerical stability of the model, and also allowed more than one machine to be connected at the same bus. In this way, the machine model constructed here was without the drawbacks of other comparable models.
7. The effect of realistic capacitive loads on the transients in the field was simulated. In particular, it was shown that a filter load, a capacitor load, or an unterminated long line load were potential producers of exciter overvoltages, but that if the reactive power into the machine were purely from another machine, there was no danger of exciter overvoltage. Also the frequencies (and hence rates of rise of exciter voltage) in the field current depended a great deal on the type of capacitive load.

8. When investigating the field overvoltages due to an HVDC converter, it was found necessary to model the dc converter as a thyristor bridge. This would change the initial conditions on the filters, and hence increase the severity of the field transient, when compared to the case of the dc converter modelled as an equivalent R-L load.
9. In the case of machine tripping, the effect of phase by phase opening of the breaker was simulated, and found to increase the severity of the field transient. Also, as expected, there was little effect on the field transient due to the star-delta machine transformer. This was because the field transients are only due to positive and negative sequence terminal currents (though not at fundamental frequency), which pass unhindered through the star-delta connected transformer.
10. An actual case of such exciter overvoltages, brought on by machines tripping when connected to filters, was simulated. The simulated situation actually occurred on September 30, 1978 in the Northern Collector System of Manitoba Hydro's HVDC system. The case involved field transients due to dc load rejections, and also due to machine tripping. The reactive power going into the damaged machines came from two sources: filters, and another generating station, and hence involved the superposition of some of the transients discussed in point 7 above. The severity of the actual damage was in line with that predicted by the simulation.

11. An approximate model of a field surge suppressor was utilized in order to recommend protection methods for the exciter thyristors. Though the mechanism of the suppressor operation modelled is somewhat different from that of the actual suppressor (in that unlike the actual suppressor, the suppressor is suddenly made to act after a pre-specified delay after the occurrence of overvoltage), it nevertheless gives a good idea of the time constant required for the suppressor. If a suppressor with sufficient speed were unavailable, it was shown that overvoltages could be reduced by reducing the field resistance either permanently, or transiently by solid state switching. Both these methods have been discussed before in literature for exciter stresses due to other causes such as line-to-line short-circuits or pole slipping. They were found to apply here equally well.

Another simple method was proposed, in which the rate of rise of the overvoltage was reduced by a suitably small field reverse resistance, so that a slower arrester could react before thyristor damage occurred.

12. The field overvoltage and exciter transients were demonstrated utilizing a 15 kVA laboratory machine. The situation was also simulated using the program, and agreement was excellent, which was an additional check on the efficacy of the machine model.

7.2 Recommendations for Further Work

As this thesis was primarily an investigative thesis (as opposed to a developmental one), there are not many recommendations for further research as far as the phenomenon of capacitor induced transients are concerned. Further work can be carried out though into the proper scheme for protection against such exciter stresses - an area that was not exhaustively covered in Chapter 6 of this thesis.

The machine model used was very adequate for the present study. However, additional coils on axes or additional inertias and shaft stiffnesses may be easily incorporated, if needed for other studies.

APPENDIX I

The Per Unit System used for Synchronous Machines

1.1 The System

There appear to be two main reasons for the use of a per-unit system, and they are as follows.

1. That the values of similar quantities for a large number of greatly differing machines (or systems) have the same orders of magnitude when expressed in the per-unit system. These values are typically of the order of unity.
2. Turns ratios between windings on the same axis can be made to disappear, resulting in simpler equations for the mutual coupling between coils. For example, the expression for the net magnetizing (mutual) flux in the d axis of a synchronous machine is:

$$\psi_{md} = L_{md} (i_d + i_f + i_{kd}) \quad \dots \text{A 1.1}$$

where i_d , i_f , i_{kd} are the three currents in the three coils in the d axis circuit that are mutually coupled, and ψ_{md} is the mutual flux linking all three.

In the per-unit system used here, the rms values of line-neutral voltages and line currents on the stator side are chosen as the bases for the per-unit voltages and currents. This is the system followed by Adkins [20].

Also, when base voltages and currents are applied to the machine, base power flows into the machine (motor convention), and hence the per-unit expression for power becomes:

$$P_{(\text{pu})} = \frac{1}{3} (v_a i_a + v_b i_b + v_c i_c) \quad \dots \text{A 1.2}$$

When transformed to dqo axis quantities, by the dqo transformation (shown here for voltages),

$$\begin{pmatrix} u_d \\ u_q \\ u_0 \end{pmatrix} = \frac{2}{3} \begin{pmatrix} \cos \theta & \cos(\theta - 2\pi/3) & \cos(\theta - 4\pi/3) \\ \sin \theta & \sin(\theta - 2\pi/3) & \sin(\theta - 4\pi/3) \\ 1 & 1 & 1 \end{pmatrix} \begin{pmatrix} v_a \\ v_b \\ v_c \end{pmatrix} \quad \text{A 1.3}$$

the equation for power becomes:

$$P_{(\text{pu})} = \frac{1}{2} (u_d i_d + u_q i_q) + u_0 i_0 .$$

Unlike in other per-unit systems [21], the angular speed of the machine is not expressed in per-unit, but in radians/sec. (This is tantamount to assuming one second as the per-unit base for time.) Hence, the machine equations that result (listed as equations 3.3.1 and 3.3.2 in Chapter 3) have, for the ω multiplier term, the nominal value of 377 radians/sec. Also, 1 pu torque is defined as that produced by 1 pu input power at synchronous speed, and so in the steady state synchronous speed operation, the power and torque are equal in value. In steady state operation at speed ω , Torque = Power $\times (\omega/\omega_0)$.

The machine mechanical dynamics equations are expressed in terms of the per-unit inertia constant, which is the ratio of the stored energy in the rotor to the rated machine KVA. The mechanical dynamic equation may be written as:

$$T = J \frac{d\omega}{dt} \quad \dots \text{ A 1.4}$$

where T and J are the per unit torque and moment of inertia. At synchronous speed, the energy stored in the rotor is $\frac{1}{2} J \omega_0$ (in per unit), so that

$$H = \frac{1}{2} J \omega_0 \quad \dots \text{ A 1.5}$$

Thus $J = \frac{2H}{\omega_0}$, and equation A 1.4 becomes

$$T = \frac{2H}{\omega_0} \frac{d\omega}{dt} \quad (\text{in per unit}) \quad \dots \text{ A 1.6}$$

A damping term expressing damping in pu MW loss/pu frequency deviation may also be added so that the damping torque corresponds to:

$$T_d = D \frac{(\omega - \omega_0)}{\omega_0} \quad \dots \text{ A 1.7}$$

Equations A 1.6 and A 1.7 have been used in writing Equation 3.3.7 of Chapter 3.

Field Quantities

In the steady state open circuit operation, the voltage induced in the d axis is zero, and the terminal voltage is that generated on the q axis by relative motion of the q axis and the d axis field.

Thus,

$$v_{oc} = \frac{u_q}{\sqrt{2}} = \frac{\omega}{\sqrt{2}} \psi_d$$

$$\frac{\omega L_{md}}{\sqrt{2}} i_f = \frac{x_{md}}{\sqrt{2}} i_f \quad \dots \text{ A 1.8}$$

Here i_f is the field current. Because the machine is open circuited, $i_d = 0$, and because it is in steady state, $i_{kd} = 0$ (amortisseur current). Thus the d axis flux, ψ_d , is produced solely by the field current. The $\sqrt{2}$ term comes in because of the 2/3 constant in the dqo transformation (Equation A 1.3), and the fact that $v_a = \sqrt{2} V_{rms} \cos(\omega t)$, etc.

Thus, if i_{fo} is the field current required to produce unity terminal voltage on open circuit

$$1 = \frac{x_{md}}{\sqrt{2}} i_{fo}$$

$$\text{or } i_{fo} = \frac{\sqrt{2}}{x_{md}} \quad \dots \text{ A 1.9}$$

The actual value (in amperes) of this field current (say i_{fo} (actual)) is known, so that the field base current

$$i_{fb} = \frac{x_{md}}{\sqrt{2}} i_{fo} \text{ (actual)} \quad \dots \text{ A 1.10}$$

By MVA balance between the phase a stator circuit and field circuit bases, we have

$$i_{sb} \cdot v_{sb} = i_{fb} \cdot v_{fb} \quad \dots \text{ A 1.11}$$

where the left-hand side stands for stator base quantities, and the right hand for field base quantities. Thus

$$\begin{aligned} v_{fb} &= \frac{i_{sb} \cdot v_{sb}}{i_{fb}} = \frac{1}{3} \frac{(\text{VA}) \text{ base}}{i_{fb}} \\ &= \frac{1}{3} \cdot \frac{x_{md}}{\sqrt{2}} \left(\frac{\text{VA base}}{i_{fo} \text{ (actual)}} \right) \quad \dots \text{ A 1.12} \end{aligned}$$

The quantity in brackets is usually very large because it is the ratio of the rated volt-amperes of the machine to the field amperes needed to produce 1 pu terminal volts. Thus, the nominal values of field voltage expressed in per-unit turn out to be very small. This is the reason why most of the field voltage plots in the thesis are not on a pu field volts scale, but on a scale which uses the value of field voltage required to produce unity open circuit terminal voltage (i_{fo} (actual) $\times r_f$ (ohms)) as base.

APPENDIX II

Data Used in Various Simulations

Given below is a list of machine, exciter, governor and system characteristics that were used in the various simulations.

A2.1 Manitoba Hydro System

TABLE A2.1: Machine Data Used in Simulation.

	<u>Kettle</u>	<u>Long Spruce</u>
MVA	120	115
Voltage	13.8 kV	13.8 kV
x_a *	0.17 (pu) ₁	0.14 (pu)
x_{md}	0.936 (pu)	0.61 (pu)
x_{kf}	0.002 (pu)	0.0 (pu)
x_{kd}	0.122 (pu)	0.048 (pu)
x_f	0.152 (pu)	0.162 (pu)
x_{mq}	0.472 (pu)	0.36 (pu)
x_{kq}	0.0835 (pu)	0.131 (pu)
k_a	0.0037 (pu)	0.0064 (pu)
k_{Rd}	0.0035 (pu)	0.0144 (pu)
k_{Rq}	0.0035 (pu)	0.0521 (pu)
k_f	0.0007 (pu)	0.00026 (pu)
H	3.42 (pu)	3.44 (pu)

* $x_{md} = 1$ in Chapters 1 to 3, and up to Section 4.2.1 in Chapter 4.

TABLE A2.2: Exciter Data (see Model in Section 3.4).

	<u>Kettle</u>	<u>Long Spruce</u>
T_A	1.43 sec	0.1 sec
T_B	7.04 sec	0.1 sec
K	289.0	117.0
T_E	0.012 sec	0.06 sec
E_{MAX}	5.0 × o.c. field volts	6.0 × o.c. field volts
E_{MIN}	-3.5 × o.c. field volts	-5.0 × o.c. field volts

TABLE A2.5: Filter Data.

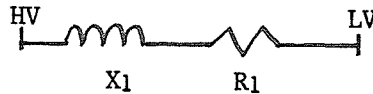
Filter:	R(Ω)	L(mH)	C(μ f) (per phase all)
5 th (each)	1.08	61.4	4.58
7 th (each)	1.52	61.4	2.337
11 th	0.75	15.2	3.84
13 th	0.89	15.2	2.749
High Pass (at Henday)	134.0	4.9	10.0
6 th (dc, Radisson)	8.84	391.0	0.5
12 th (dc, Henday)	7.94	122.2	0.4

(for circuit details, see Figure 5.2)

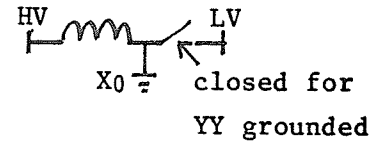
Table A2.6: Transformer Data.

Transformer	HV side	LV side	MVA	R %	X ₁ %	X ₀ %
Kettle (machine, each)	141.45	13.8	125	0.403	10.3	9.34
Long Spruce (machine, each)	235.75	13.8	100	0.17	6.89	5.83
Radisson	230	13.8	200	0.0	8.2	6.7

(all impedances on our MVA and LV side base)
where:



Positive Network Sequence



Negative Network Sequence

TABLE A2.3: Governor Data (See Model in Section 3.4).

	<u>Kettle</u>	<u>Long Spruce</u>
K_I	0.0	0.0
K_P	1.0	1.0
K_A	0.461	0.03
T_1	∞ (sec)	0.3 (sec)
T_2	6.0 (sec)	200.0 (sec)
T_3	∞ (sec)	2.0 (sec)
T_4	0.02 (sec)	0.07 (sec)
T_5	0.9 (sec)	1.28 (sec)
T_R	0.266 (sec)	6.1 (sec)
T_{MAX}	1.0	1.0
r	0.394	0.36
R	0.04	0.04
$\pm V_{GMAX}$	0.22	0.172
MAXGATE	1.0	1.0
MINGATE	-0.05	-0.05

TABLE A2.4: Transmission Line Impedances.

<u>Line:</u>	R_{11}	X_{11}	B_{11}	R_{00}	X_{00}	B_{00}	(all Ω/km)
L-R	-0.047	0.487	3.386	0.361	1.475	2.26	(each line)
L-H	0.047	0.49	3.38	0.375	1.53	2.26	(each line)
K-R	modelled as a reactance of $r + j\omega\ell$, where $r = 0.109 \Omega$, $\ell = 0.003\text{H}$						(each line)

R_{11} , X_{11} , B_{11} are the line positive sequence resistance, series reactance and shunt susceptance per kilometer. R_{00} , etc., are the corresponding zero sequence quantities.

TABLE A2.7: Laboratory Machine Data.

A 2.2 The Laboratory Machine

KVA	15	kVA	
Voltage	208 V	ℓ - ℓ	(rated)
x_a	0.052	(pu)	
x_{md}	0.610	(pu)	
x_{kf}	0.0	(pu)	
x_{kd}	0.1413	(pu)	
x_f	0.0736	(pu)	
x_{mq}	0.26	(pu)	
x_{kq}	0.260	(pu)	
r_a	0.042	(pu)	(includes contact resistance)
r_{kd}	0.3378	(pu)	
r_{kq}	0.207	(pu)	
r_f	0.0042	(pu)	
Inertia:	Assumed infinite		

REFERENCES

1. deMello, F.P., Leuzinger, L.M. and Mills, R.J.: "Load Rejection Overvoltages as Affected by Excitation System Control," IEEE Trans. PAS-94, No. 2, March/April 1981, pp. 280-287.
2. Concordia, C.: "Two Reaction Theory of Synchronous Machines with Balanced Terminal Impedences," AIEE Trans., Vol. 56, September 1937, pp. 1124-1127.
3. Rustebakke, H.M., and Concordia, C.: "Self Excited Oscillations in a Transmission System Using Series Capacitors," IEEE Trans. PAS-80, No. 7, September/October 1970, pp. 1504-1512.
4. Concordia, C. and Carter, G.K.: "Negative Damping of Electrical Machinery," AIEE Trans. Vol. 60, March 1941, pp. 116-119.
5. Butler, J.W. and Concordia, C.: "Series Capacitor Application Problems," AIEE Trans. Vol 56, August 1937, pp. 975-988.
6. Memo from R.W. Haywood to D.W. Gunter, (Manitoba Hydro Internal Report): "System Disturbance, September 30, 1978," Interim Report, November 11, 1978.
7. System Performance (Manitoba Hydro Internal Report): "Kettle Exciter Failure on September 30, 1978."
8. Memo from B. Manning to R.B. Gibson (Manitoba Hydro Internal Report): "Kettle G.S. Damage on Unit 5 Static Exciter," October 10, 1978.
9. Goto, M., Isono, A. and Okuda, K.: "Transient Behaviour of Synchronous Machines with Shunt Connected Thyristor Exciter under System Faults," IEEE Trans. PAS-71, pp. 2218-2227.
10. Rao, K.V.N. and Adkins, B.: "Peak Inverse Voltages in the Rectifier Excitation Systems of Synchronous Machines," IEEE Trans. PAS-93, pp. 1685-1692.
11. deMello, F.P. and Hannet, L.M.: "Validation of Synchronous Machine Models and Derivation of Model Parameters from Tests," IEEE Trans. PAS-100, February 1981, pp. 662-672.
12. Canay, I.M. and Simond, J.J.: "Overvoltages in the Field Circuit," Brown Boveri Review, September 1980, pp. 516-523.
13. Malik, O.P.: "Overvoltages Across the Reactifying Bridge of Brushless Excitation System Under Asynchronous Operation," Paper A-77 003-7, IEEE PES Winter Meeting, Los Angeles, California, 1978.
14. Woodford, D.A., Gole, A.M. and Menzies, R.W.: "Digital Simulation of DC Links and AC Machines," Paper No. 825M480-2, IEEE PAS Summer Meeting, San Francisco, California, July 1982.

15. Lauw, H.K. and Scott Meyer, W.: "Universal Machine Modelling for the Representation of Rotating Electric Machinery in an Electro-Magnetics Transients Program," IEEE Trans. PAS, Vol. PAS-101, No. 6, June 1982.
16. Saito, O., Mukae, H. and Murotani, K.: "Suppression of Self Excited Oscillations in Series Compensated Transmission Lines by Excitation Control of Synchronous Machines," IEEE Trans. PAS-94, No. 5, September/October 1975, pp. 1777-1778.
17. Peneder, F.: "Significance of Generator Excitation in Power System and Power Station Operation," Brown Boveri Review, June 1980, pp. 20-21.
18. deMello, F.P. and Hannet, L.N.: "Large Scale Generators for Power Systems," IEEE Trans. PAS-100, No. 5, May 1981, pp. 2610-2618.
19. Crary, S.B.: "Two Reaction Theory of Synchronous Machines," AIEE Trans., Vol. 56, 1937, pp. 27-31.
20. Harley, R.G. and Adkins, B.: General Theory of AC Machines, Chapman and Hall, London, 1975.
21. Concordia, C.: Synchronous Machines, John Wiley and Sons, London, 1951.
22. Elgerd, O.: Electric Energy System Theory, McGraw Hill, New York, 1971.
23. Stevenson, W.O.: Elements of Power Systems Analysis, McGraw Hill, New York, 1962.
24. Dommel, H.W.: "Digital Computer Solution of Electromagnetic Transients in Single- and Multi-phase Networks," IEEE Trans. PAS, Vol. PAS-88, No. 4, April 1969, pp. 388-399.
25. I.B.M.: System/360 Continuous System Modelling Program, IBM Publication H20-0367-2.
26. Tinney, W.F.: "Compensation Theorem for Network Solutions by Optimally Ordered Triangular Factorization," IEEE Trans. PAS, Vol. PAS-91, No. 1, January/February 1972.
27. Canay, I.M.: "Causes of Discrepancies on Calculation of Rotor Quantities and Exact Equivalent Diagrams of the Synchronous Machine," IEEE Trans. PAS-88, No. 7, July 1969, pp. 1114-1120.
28. Ogata, K.: Modern Control Engineering, Prentice-Hall, Inc., Englewood Cliffs, New Jersey, 1970.
29. Gross, G and Hall, M.C.: "Synchronous Machine and Torsional Dynamics Simulation in the Computation of Electromagnetic Transients," IEEE Trans. PAS, Vol. PAS-97, July/August 1978.

30. Brandwajn, V. and Dommel, H.W.: "A New Method for Interfacing Generator Models with an Electromagnetic Transients Program," 1977 PICA Conference Proceedings, pp. 260, 265.
31. Ainsworth, J.D.: "The Phase Locked Oscillator - A New Control System for Controlled Static Converters," IEEE Trans. on PAS, PAS-87, No. 3, March 1968.
32. Adamson, L and Hingorani, N.G.: High Voltage Direct Current Transmission, Garraway, 1960.
33. Jasmin, G., Leroux, A. and Bowles, J.P.: "Electronic Simulation of a Hydro-generator with Static Excitation," IEEE PAS Winter Meeting, Atlanta, Georgia, February 1981, Paper 81WM183-3.
34. Thio, C.V.: "AC-DC Integration Aspects and Operational Behaviour of the Nelson River HVDC System," Paper presented to CIGRE Study Committee 14 (HVDC Lines), Rio de Janeiro, Brazil, August 25-26, 1981.
35. Eggert, H.: "Selenium Surge Suppressor for the Protection of Voltage Sensitive Components," Siemens Review 28, No. 3, 1971, pp. 128-131.
36. Tominaga, S., Shibuyu, Y. Fuziwara, Y. and Netta, T.: "Electrical Properties for Zinc Oxide Valve Element for a Surge Arrestor," IEEE Summer Meeting, Los Angeles, California, Paper A78595-1.